Draft version January 19, 2023
Typeset using LaTeX twocolumn style in AASTeX63

Science with the Ultraviolet Explorer (UVEX)

S. R. Kulkarni,[1] Fiona A. Harrison,[1] Brian W. Grefenstette,[1] Hannah P. Earnshaw,[1] Igor Andreoni,[2]
Danielle A. Berg,[3] Joshua S. Bloom,[4] S. Bradley Cenko,[5] Ryan Chornock,[4] Jessie L. Christiansen,[6]
Michael W. Coughlin,[7] Alexander Wuollet Criswell,[8] Behnam Darvish,[1] Kaustav K. Das,[1] Kishalay De,[9]
Luc Dessart,[10] Don Dixon,[11] Bas Dorsman,[12] Kareem El-Badry,[13] Christopher Evans,[14] K. E. Saavik Ford,[15]
Christoffer Fremling,[1] Boris T. Gänsicke,[16] Suvi Gezari,[17] Y. Götberg,[18] Gregory M. Green,[19]
Matthew J. Graham,[1] Marianne Heida,[20] Anna Y. Q. Ho,[21] Amruta D. Jaodand,[1]
Christopher M. Johns-Krull,[22] Mansi M. Kasliwal,[1] Margaret Lazzarini,[1] Wenbin Lu,[23] Raffaella Margutti,[4]
D. Christopher Martin,[1] Daniel Charles Masters,[6] Barry McKernan,[15] Yaël Nazé,[24] Samaya M. Nissanke,[12]
B. Parazin,[25] Daniel A. Perley,[26] E. Sterl Phinney,[1] Anthony L. Piro,[18] G. Raaijmakers,[12] Gregor Rauw,[24]
Antonio C. Rodriguez,[1] Hugues Sana,[27] Peter Senchyna,[18] Leo P. Singer,[28] Jessica J. Spake,[29]
Keivan G. Stassun,[30] Daniel Stern,[31] Harry I. Teplitz,[6] Daniel R. Weisz,[4] and Yuhan Yao[1]

[1]*Division of Physics, Mathematics, and Astronomy, California Institute of Technology, Pasadena, CA 91125, USA*
[2]*Joint Space-Science Institute, University of Maryland, College Park, MD 20742, USA*
[3]*Department of Astronomy, The University of Texas at Austin, 2515 Speedway, Stop C1400, Austin, TX 78712, USA*
[4]*Department of Astronomy, University of California, Berkeley, CA 94720-3411, USA*
[5]*Astrophysics Science Division, NASA Goddard Space Flight Center, 8800 Greenbelt Road, Greenbelt, MD 20771, USA*
[6]*IPAC, California Institute of Technology, Pasadena, CA 91125, USA*
[7]*School of Physics and Astronomy, University of Minnesota, Minneapolis, MN 55455, USA*
[8]*University of Minnesota, Minneapolis, MN 55455, USA*
[9]*MIT-Kavli Institute for Astrophysics and Space Research, 77 Massachusetts Ave., Cambridge, MA 02139, USA*
[10]*Institut d'Astrophysique de Paris, CNRS-Sorbonne Université, 98 bis boulevard Arago, F-75014 Paris, France*
[11]*Vanderbilt University, Nashville, TN 37235, USA*
[12]*GRAPPA, University of Amsterdam, Science Park 904, 1098 XH Amsterdam, Netherlands*
[13]*Center for Astrophysics | Harvard & Smithsonian, 60 Garden Street, Cambridge, MA 02138, USA*
[14]*UK Astronomy Technology Centre, Royal Observatory, Blackford Hill, Edinburgh, EH9 3HJ, UK*
[15]*Department of Science, CUNY Borough of Manhattan Community College, 199 Chambers Street, New York, NY 10007, USA*
[16]*Department of Physics, University of Warwick, Coventry, CV4 7AL, UK*
[17]*Space Telescope Science Institute, 3700 San Martin Drive, Baltimore, MD 21218, USA*
[18]*The Observatories of the Carnegie Institution for Science, 813 Santa Barbara St., CA 91101, USA*
[19]*Max Planck Institute for Astronomy, D-69117 Heidelberg, Germany*
[20]*ESO, Karl-Schwarzschild-Str 2, 85748 Garching b. München, Germany*
[21]*Miller Institute for Basic Research in Science, 468 Donner Lab, Berkeley, CA 94720, USA*
[22]*Department of Physics & Astronomy, Rice University, 6100 Main St., Houston, TX, USA*
[23]*Department of Astrophysical Sciences, Princeton University, Princeton, NJ 08544, USA*
[24]*Groupe d'Astrophysique des Hautes Energies, STAR, Université de Liège, Quartier Agora (B5c, Institut d'Astrophysique et de Géophysique), Allée du 6 Août 19c, B-4000 Sart Tilman, Liège, Belgium*
[25]*Northeastern University, Boston, MA 02115, USA*
[26]*Astrophysics Research Institute, Liverpool John Moores University, IC2, Liverpool Science Park, Liverpool L3 5RF, UK*
[27]*Institute of Astronomy, KU Leuven, Celestijnlaan 200D, 3001 Leuven, Belgium*
[28]*Astroparticle Physics Laboratory, NASA Goddard Space Flight Center, Code 661, Greenbelt, MD 20771, USA*
[29]*Division of Geological and Planetary Sciences, California Institute of Technology, Pasadena, CA 91125, USA*
[30]*Department of Physics and Astronomy, Vanderbilt University, Nashville, TN 37235, USA*
[31]*Jet Propulsion Laboratory, California Institute of Technology, 4800 Oak Grove Drive, Pasadena, CA 91109, USA*

ABSTRACT

Corresponding author: S.R. Kulkarni
srk@astro.caltech.edu

arXiv:2111.15608v3 [astro-ph.GA] 18 Jan 2023

UVEX is a proposed medium class Explorer mission designed to provide crucial missing capabilities that will address objectives central to a broad range of modern astrophysics. The *UVEX* design has two co-aligned wide-field imagers operating in the FUV and NUV and a powerful broad band medium resolution spectrometer. In its two-year baseline mission, *UVEX* will perform a multi-cadence synoptic all-sky survey 50/100 times deeper than *GALEX* in the near/far ultraviolet, cadenced surveys of the Large and Small Magellanic Clouds, rapid target of opportunity follow-up, as well as spectroscopic followup of samples of stars and galaxies. The science program is built around three pillars. First, *UVEX* will explore the low-mass, low-metallicity galaxy frontier through imaging and spectroscopic surveys that will probe key aspects of the evolution of galaxies by understanding how star formation and stellar evolution at low metallicities affect the growth and evolution of low-metallicity, low-mass galaxies in the local universe. Such galaxies contain half the mass in the local universe, and are analogs for the first galaxies, but observed at distances that make them accessible to detailed study. Second, *UVEX* will explore the dynamic universe through time-domain surveys and prompt spectroscopic followup capability will probe the environments, energetics, and emission processes in the early aftermaths of gravitational wave-discovered compact object mergers, discover hot, fast UV transients, and diagnose the early stages of stellar explosions. Finally, *UVEX* will become a key community resource by leaving a large all-sky legacy data set, enabling a wide range of scientific studies and filling a gap in the new generation of wide-field, sensitive optical and infrared surveys provided by the Rubin, *Euclid*, and *Roman* observatories. This paper discusses the scientific potential of *UVEX*, and the broad scientific program.

Keywords: surveys — ultraviolet: galaxies — ultraviolet: stars — ultraviolet: general — instrumentation: photometers — instrumentation: spectrographs

1. INTRODUCTION

The Pathways to Discovery in Astronomy and Astrophysics for the 2020's report (Astro2020, The National Academies Press 2021) broadly considers the scientific landscape for the coming decades, identifying the areas of New Windows on the Dynamic Universe, and Unveiling the Drivers of Galaxy Growth as priorities motivating future investments. Astro2020 emphasizes the New Windows area because of the tremendous opportunities in multi-messenger astronomy enabled by the opening of the gravitational wave (GW) and particle windows, and the upcoming power of cadenced wide-field surveys with the Vera C. Rubin Observatory for finding explosive and time varying phenomena. Astro2020 also emphasizes the Galaxy Growth area, recognizing the power of the Atacama Large Millimeter/submillimeter Array (ALMA) and *James Webb Space Telescope* (*JWST*) to observe the seeds of galaxy growth in the early Universe, and of Rubin, the *Nancy Grace Roman Space Telescope* and *Euclid* surveys for transforming our understanding of how galaxies and their contents grow and evolve over cosmic time.

Wide-field imaging and spectroscopy in the near- and far-ultraviolet (UV) bands are essential capabilities for addressing these priority science themes and for a rich and broad range of astrophysical studies. Wide-area surveys and followup spectroscopy are central for uncovering and understanding the predominantly low-mass galaxy population in the local universe, identifying local low-metallicity analogs of the seed galaxies in the early Universe that are being studied by *JWST*. Finding the low-mass, low-metallicity galaxy population will significantly advance our understanding of star formation and evolution in such environments, providing templates for understanding measurements in the early Universe. Deep, wide-area UV surveys are an essential complement to Rubin, *Euclid*, and *Roman* for breaking fundamental degeneracies in photometric distance measurements, and for determining star formation rates for faint galaxies in the local universe.

In the time domain, the majority of explosive phenomena peak in the UV at early times, with this emission probing the hot initial phases of the expanding shocks and/or ejecta. Hot gas is rich in UV resonant line transitions, and early UV spectroscopy can measure elemental composition in the regions close to the progenitor. UV observations are therefore unique for both identifying transients in early phases through imaging, and diagnosing the aftermaths via photometry and spectroscopy. With a wealth of time-domain facilities operating in the coming decade, rapid UV followup of triggers from the collaboration of the Laser Interferometer Gravitational-Wave Observatory, Virgo, and Kamioka Gravitational Wave Detector (LIGO/Virgo/KAGRA), Rubin, the Deep Synoptic Array-110, the Square Kilometer Array (SKA), and more will open an entirely new
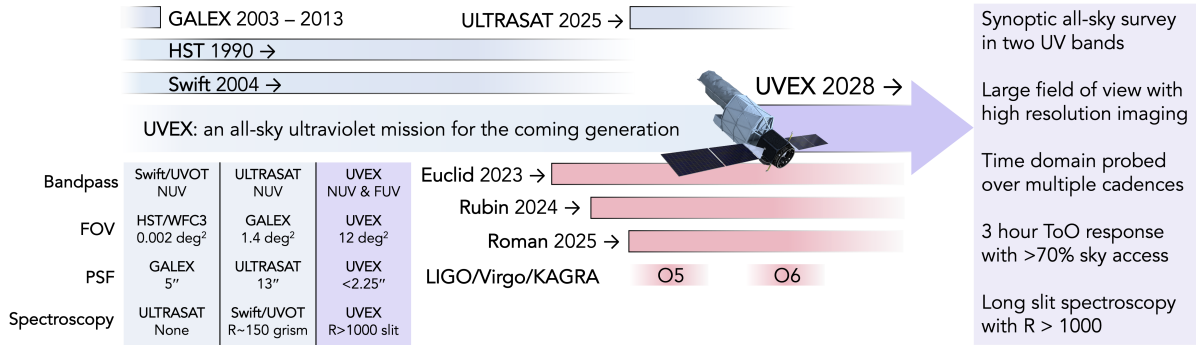
Figure 1. The timeline of *UVEX* in relation to other UV missions and the upcoming generation of multi-wavelength, multi-messenger facilities that *UVEX* will complement with its coverage of the dynamic UV sky.

view on the dynamic universe. Considering the legacies of the *Hubble Space Telescope* (*HST*) and the *Galaxy Evolution Explorer* (*GALEX*), it is clear that UV observations are also broadly central to astrophysical studies of comets, planets, stars, galaxies, AGN, compact objects, as well as dust and gas in the Milky Way and beyond.

Figure 1 shows a timeline of existing or approved missions in relation to *UVEX* and illustrates the key advances *UVEX* will make in UV capabilities, as well as the suite of multi-wavelength and multi-messenger facilities for which *UVEX* will provide necessary complementary UV data. No existing or upcoming mission[1] will have the deep, broadband (NUV and FUV) synoptic UV imaging, broadband spectroscopy, and rapid response target of opportunity (ToO) followup capabilities required to address many priority questions in astrophysics in the coming decades. While *HST* continues to provide deep imaging and spectroscopy, it is over a narrow field of view (FOV) and with typical ToO turnaround times of two weeks, far too slow to study the relatively short-lived (few day-long) hot UV emission from early explosive stages. Further, *HST* is an aging observatory whose longevity is uncertain. The *Neil Gehrels Swift Observatory* (*Swift*) UVOT instrument (Gehrels et al. 2004) has rapid turnaround capability, but covers only the NUV band, with limited FOV, sensitivity and spectral resolution. The upcoming *Ultraviolet Transient Astronomical Satellite* (*ULTRASAT*, Sagiv et al. 2014) is designed for wide-field NUV imaging for transient identification, as well as followup of GW counterparts and other explosive phenomena, but lacks the depth, FUV coverage, spatial resolution, and spectroscopy to address many of the goals and objectives of the galaxy growth and dynamic universe themes.
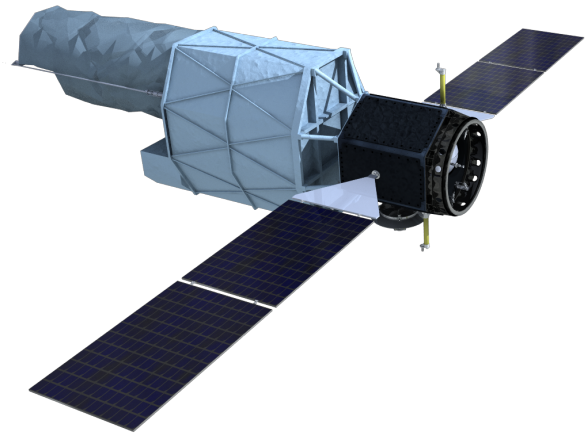
[1] Here we include only missions that are adopted and/or are in development.

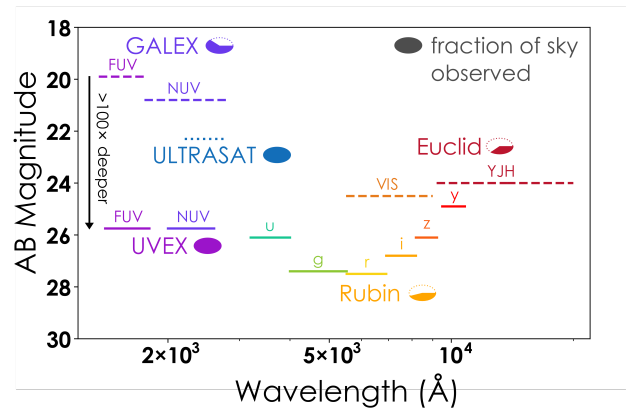**Figure 2.** A render of the proposed *UVEX* telescope.

Figure 3. *UVEX* will provide deep, two-band UV data to complement planned deep, wide-field ($> 10,000 \deg^2$) optical and near-IR surveys by Rubin and *Euclid*.

In this paper we describe the *Ultraviolet Explorer (UVEX)*, illustrated in Figure 2, a proposed Medium-Class Explorer (MIDEX) mission that is designed to provide crucial missing capabilities to address key elements

of the Galaxy Growth and Dynamic Universe priority decadal science themes. *UVEX* will explore the low-mass and low-metallicity galaxy frontier, and will also provide a new view of the dynamic universe through cadenced wide-field NUV and FUV imaging for transient detection, as well as rapid photometric and spectroscopic followup of transients reported by other observatories. By performing a deep (50/100 times fainter than *GALEX* in NUV/FUV) synoptic all-sky survey, *UVEX* will be an essential complement to the Rubin Observatory and *Euclid* mission (Figure 3). *UVEX* will leave a legacy archive that will enable a rich range of community science investigations for decades to come.

We focus this paper on describing the *UVEX* primary scientific goals and objectives; a followup paper will describe the details of the instrument and mission designs. Section 2 provides a brief overview of the *UVEX* design, including the mission design, the optical telescope array, and the UV instrument module. Section 3 describes the three primary science pillars: exploring the low-mass, low-metallicity galaxy frontier, providing a new window on the dynamic Universe, and contributing the missing piece to a legacy of deep, multi-wavelength, synoptic all-sky surveys. Finally, Section 4 describes a sample of the rich range of science beyond the primary mission that can be be pursued by the community using the *UVEX* archive.

2. UVEX DESIGN OVERVIEW

UVEX is designed for wide-field imaging simultaneously in FUV and NUV imaging bands, and for moderate resolution long-slit spectroscopy covering a broad FUV to NUV bandpass. Table 1 provides the observatory's top level design parameters. The FOV is large, and the design and orbit provide for a large field of regard (FoR) for high instantaneous sky accessibility. The instrument leverages modern high quantum efficiency CMOS detectors and coatings to achieve high sensitivity, eliminating the bright source constraints that precluded *GALEX* from surveying the Galactic Plane and Magellanic clouds. Placed into a *TESS*-like lunar resonance orbit, *UVEX* achieves low and stable background and high observing efficiency. With frequent ground station contacts, *UVEX* has low data latency (data is transmitted every 6 hours) and rapid response to ToOs (average response time is three hours).

2.1. *UVEX Instrument*

Detector and coating technologies have advanced significantly over the last two decades. The development of backside-illuminated silicon solid state detectors (Nikzad et al. 1995; Hoenk 2009) enables dramatic improvements in quantum efficiency over the microchannel

Table 1. *UVEX* Mission Parameters

UVEX	Design
Imaging FOV	$3.5° \times 3.5°$
Image quality (HPD)	$\leq 2.25''$
FUV imaging bandpass	1390–1900 Å
NUV imaging bandpass	2030–2700 Å
Spectroscopy band/resolution	1150–2650 Å, $R \geq 1000$
Photometric sensitivity	>24.5 AB (SNR 5, 900 s) [a]
Sky survey depth	>25.8 FUV and NUV
Instantaneous sky accessibility	$> 70\%$
Average ToO response	<3 hrs
Data latency	<6.5 hrs
Orbit	elliptical $17R_e \times 15R_e$
Orbital period	13.7 days
Sun exclusion angle	$45°$
Baseline mission duration	2 years
Target launch date	Fall 2028

[a] for a point source in an extragalactic field with average background

plate detectors employed by *HST*, *GALEX*, and *Swift*. Solid state detectors also do not suffer from damage due to illumination by bright sources, enabling observations of the Galactic Plane and Magellanic Clouds, which have a high density of bright stars. By employing new detector and coating technologies, *UVEX* achieves significantly improved sensitivity compared to *GALEX* with a relatively modest aperture consistent with a MIDEX-scale mission.

UVEX has a single instrument consisting of an UV-optimized optical telescope array (OTA) and the UV Instrument Module (UVIM). The OTA employs a standard all-reflective three-mirror anastigmat design, with an effective aperture of 75 cm. At the UVIM entrance, a dichroic splits the light into FUV and NUV channels that are simultaneously imaged by two focal planes, each of which is composed of a 3×3 array of $4k \times 4k$ CMOS detectors. Light for the long-slit spectrograph avoids the dichroic, passes through the slit, and is then dispersed by a grating onto a single CMOS detector. All the detectors and their modular readout electronics are identical except for individualized coatings for out-of-band light suppression. All imaging and spectroscopic data are compressed onboard and then sent to the ground once every six hours for scientific analysis.

The OTA provides a field-averaged point spread function (PSF) with half-power diameter (HPD) $<2.25''$ across the $3.5° \times 3.5°$ FOV. This is Nyquist sampled
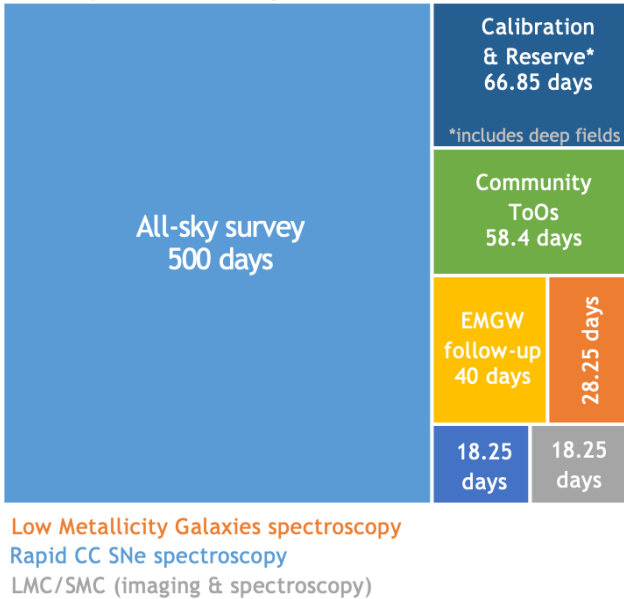
730 days of science operations

Figure 4. The anticipated distribution of *UVEX* observing time during the two-year baseline mission.

by the $1''$ pixels. A standard 900-s dwell consists of $3 \times$ 300-s imaging exposures, with each exposure read out in a high dynamic range (HDR) mode to avoid saturation on bright sources. The use of CMOS devices enables a shutterless rolling readout and a exposure duty cycle of 99%.

The dichroic beamsplitter enables simultaneous imaging in both the FUV (1390–1900 Å) and NUV (2030–2700 Å) bands. Bandpass filters (Hennessy et al. 2021) suppress the out-of-band background associated with zodiacal light and geocoronal Lyα emission (e.g., Colina et al. 1996; Leinert et al. 1998; Murthy et al. 2014). The aperture for the long-slit spectrograph is offset from the imaging field so that light bypasses the dichroic and is transmitted through a $1°$ long slit. The width of the fixed slit varies along its length, with apertures ranging from $2''$ to $16''$. A grating disperses the light, with resulting spectral resolution ranging from $R \sim 1600$ at 1150 Å to $R \sim 3500$ at 2750 Å (for the portion of the slit with $2''$ width).

3. THE UVEX BASELINE SCIENCE PROGRAM

Three scientific 'pillars' provide the primary scientific motivation for *UVEX*, and define the primary requirements for the baseline mission design and observing program: (I) Exploring the low-mass, low-metallicity galaxy frontier; (II) Providing new views on the dynamic universe; and (III) Leaving a broad legacy of modern, deep synoptic surveys adding to the panchromatic richness of 21st century astrophysics.

During its two-year baseline mission, *UVEX* will undertake a deep, synoptic all-sky survey, as well as targeted, cadenced observations of the Large and Small Magellanic Clouds, spectroscopic followup of selected samples of stars and low-mass, low-metallicity galaxies, and ToO followup of GW events, supernovae, and transient events both discovered by *UVEX* and triggered by the community, many of which will be discovered by other facilities (Figure 4). These observations serve to fulfill the *UVEX* top level mission requirements, and will also provide a rich data set that will be promptly made available to the community for a wide variety of investigations.

In the sections below we describe the primary scientific pillars, as well as examples of the broad range of science that can be undertaken by the community using archival observations from the baseline mission. In Section 4 we describe additional scientific observations that could be pursued in an extended mission phase through Guest Observer (GO) observations.

3.1. *Pillar 1: The Low-Mass, Low-Metallicity Galaxy Frontier*

Our knowledge of galaxies and galaxy halos is based largely on studies of those with masses comparable to or larger than the Milky Way ($M \sim 5 \times 10^{10} M_\odot$). However, the properties of these galaxies (e.g., Solar metallicity, dusty) are not well-matched to the low-mass ($M \sim 10^5 - 10^9 M_\odot$), low-metallicity (1–50% solar) systems that dominate the hot, metal-poor early universe, are thought to power cosmic reionization ($6 \lesssim z \lesssim 20$), and are believed to be the majority of galaxies in the local universe. Although low-mass, low-metallicity (LMLZ) systems are central to a broad range of astrophysics, they are among the least explored galaxy frontier, because only a small fraction of the large expected LMLZ galaxy population is known at any redshift and the birth, evolution, and death of stars at low metallicities is poorly understood.

A definitive study of local LMLZ galaxies is key to understanding the processes of galaxy formation, stellar evolution and death, and the formation of compact objects in metal-poor environments. UV heating and radiation pressure from massive metal-poor stars and the explosive deaths of metal-poor single and binary stars regulate star formation in ways that are different from the Milky Way (Dessart et al. 2017) and may be responsible for initial mass function (IMF) variations and bursty, chaotic star formation in many known LMLZ systems (Meurer et al. 2009a; Lee et al. 2009, Weisz et al. 2012). With reduced opacities, low-metallicity stars can grow to and maintain larger masses and sizes,
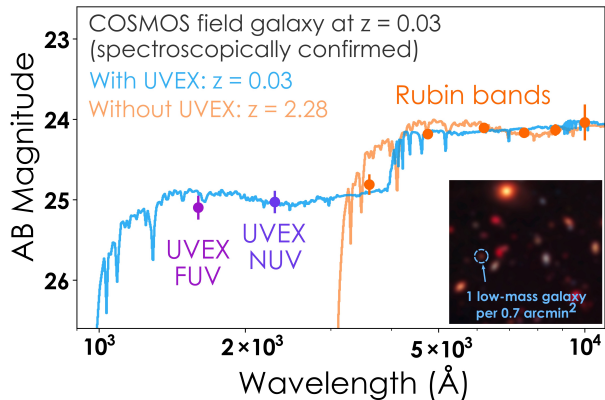
Figure 5. *UVEX* imaging picks out low-mass, $z < 0.3$ galaxies by providing the crucial UV photometry needed to differentiate the Balmer break for a low-redshift system (blue) from the Lyman break in far more numerous high-redshift galaxies (orange).

and many more interact in binary systems (Sana et al. 2012; Krumholz 2014). In close binaries, lower-opacity winds reduce mass loss rates (e.g., Smith 2014) which leads to significant, but poorly understood changes to stellar evolution such as fewer red supergiants (Weisz et al. 2012), enhanced production of single and binary black holes (Sana et al. 2012), and a broader diversity of supernova (SN) types.

Deep *UVEX* all-sky imaging, undertaken during the baseline mission, along with upcoming O/IR surveys (e.g., Rubin, *Euclid*), will help uncover millions of nearby ($D \leq 100$ Mpc; $z \leq 0.03$) LMLZ galaxies that are predicted to exist and measure their basic properties (e.g., mass, age, star formation rate, dust). Targeted *UVEX* spectroscopy of the youngest, strongest star-forming LMLZ systems will provide crucial rest-frame UV nebular emission templates needed to interpret observations of the first galaxies in the early Universe. The unique and powerful capabilities of *UVEX* will define the LMLZ frontier for decades to come.

3.1.1. *Finding the Low-Mass Galaxy Population in the Local Universe*

With an all-sky survey $\geq 50\times$ deeper than *GALEX*, *UVEX* will find the missing local population of LMLZ galaxies. Key questions that will be addressed include: Where are the local LMLZ galaxies located? What are their properties? How do these properties vary with environment?

Our current census of the nearby LMLZ galaxies is highly incomplete. Within 100 Mpc ($z \leq 0.03$), theoretical matching of stellar and dark matter halo masses predicts the existence of ∼10–200 million LMLZ galaxies. Yet only ∼20,000 LMLZ galaxies are known in this

volume (Karachentsev & Kaisina 2019; Tully et al. 2016, Tully et al. 2019), far fewer than even the most conservative theoretical estimates.

Finding local LMLZ galaxies is challenging. They are intrinsically faint and spread across the sky, tracing the local cosmic web from low-density filaments and voids to high-density groups and clusters. Their properties appear to vary with environment: star-forming and gas-rich galaxies dominate the field, while groups and clusters host more diverse populations. But these conclusions are based on small, incomplete samples.

Mapping the nearby LMLZ population requires a wide-area, sensitive UV imaging survey. Degeneracies in age/metallicity/dust/redshift mean that optical/infrared (O/IR) colors (e.g., from Rubin, *Euclid*) alone cannot distinguish local LMLZ galaxies from more massive higher-redshift ($z > 2$) interlopers (Figure 5). Due to redshift and intergalactic gas absorption, massive background galaxies have little flux in rest-frame UV bands, whereas local LMLZ field galaxies have little dust and are predominantly star-forming (e.g., Geha et al. 2012, Lee et al. 2009), making them UV bright. Moreover, joint analysis of *GALEX*+SDSS data shows that the UV is essential for measuring basic properties (e.g., mass, age, star formation rate) of nearby LMLZ galaxies (Salim et al. 2016).

UVEX will identify millions of LMLZ galaxies within 100 Mpc down to $M_* \sim 10^6 M_\odot$ when combined with optical imaging from Rubin and Northern-hemisphere counterparts (e.g., UNIONS, DESI Legacy Survey). Due to the lack of deep, wide-field observations, we base the expected numbers that *UVEX* will find on theoretical models, which come with large uncertainties (e.g., Garrison-Kimmel et al. 2017). We estimate the total number of low-mass galaxies ($M_* \sim 10^6 - 10^9 M_\odot$) within 100 Mpc using two different stellar halo mass relationships (SHMs; e.g., Behroozi et al. 2013, Conroy et al. 2015) that bracket the accepted range of low-mass galaxy formation models and current empirical constraints ($M_\star \propto M_{\rm halo}^\alpha$, where $\alpha \sim 1.6 - 3.1$; e.g., Garrison-Kimmel et al. 2017). These relations predict between $\sim 1.5 \times 10^7$ and $\sim 3 \times 10^8$ luminous $M_* > 10^6 M_\odot$ galaxies within 100 Mpc. The lowest-mass galaxies dominate the population by number due to the steepness of the SHM relationship.

The number of dark matter halos predicted by SHMs agrees well with large-volume N-body simulations at slightly higher masses (Elahi et al. 2018), which unfortunately cannot be used directly for our estimates because no simulations include large enough volumes and low enough halo mass ranges. Local galaxies with $M_* < 10^6 \ M_\odot$ are often quenched in groups due to

environmental effects or reionization in the early Universe. However, most local galaxies with $M_* > 10^6 \, M_\odot$ are known to be star-forming. For slightly higher mass galaxies ($M_* > 10^7 M_\odot$), Geha et al. (2012) estimates that only 0.06% of field galaxies and 24% of galaxies associated with groups lack recent star formation. Smaller, less complete samples of low-mass galaxies within 10 Mpc yield similar estimates (e.g., Karachentsev et al. 2013). Conservatively, we assume that ∼1/3 of galaxies with $M_* > 10^6 \, M_\odot$ are quenched and thus undetectable in the UV due to a lack of massive stars. In total, our estimate is that there are 10–200 million star-forming galaxies with $M_* > 10^6 M_\odot$ within 100 Mpc, in good agreement with estimates from other approaches aimed at finding low-mass galaxies (e.g., via transients; Conroy et al. 2015). *UVEX*, through its all-sky survey, is designed to detect all such galaxies in the extragalactic sky.

A large sample is essential for anchoring the SHM relation, providing the 3D maps of the low-mass, low-density Universe (probing poorly surveyed filaments and voids), enabling the first large-scale study of how the lowest-mass halos evolve as a function of environment, and finding the most extreme examples (lowest metallicity and youngest) for followup (e.g., Nuza et al. 2014). For example, if low mass galaxies continue to form, the probability of finding one within 10 Myr of formation is ∼10 Myr/10 Gyr, or 1/1000. Thus we require a very large sample to isolate the rarest and most interesting forming galaxies.

Adequately sampling rare LMLZ galaxies, and studying large-scale cosmic structures requires surveying the entire extragalactic sky (i.e., 20,000 deg^2). A typical $10^6 \, M_\odot$ star-forming galaxy has $M(UV) = -10 \, \mathrm{mag}$ (AB). Detecting such galaxies to 100 Mpc, and constraining star formation rates requires SNR $\geq$ 5 to a depth of $m_{UV} = 25$ in both FUV and NUV. We estimated this minimum luminosity by drawing on *GALEX* studies of star-forming dwarfs in the Local Volume (e.g., Lee et al. 2011). Pairing UV luminosities from Lee et al. (2011) with UV+optical stellar masses from Weisz et al. (2012), we find that an actievly star-forming galaxy with $M_* \sim 10^6 M_\odot$ has a typical UV luminosity of M_{FUV} of –13 mag, which includes Milky Way foreground and internal extinction corrections (Lee et al. 2011; Weisz et al. 2012). Then, as shown in Weisz et al. (2012), due to long duty cycles and the bursty nature of star formation, galaxies with $M_* < 10^7 M_\odot$ spend $\approx$ 80–90% of their time in post-burst states (i.e., with little or no Hα and reduced UV luminosities) that can make star-forming galaxies with $M_* = 10^6 M_\odot$ as faint as $M_{FUV} = -10$ mag. Thus, in order to capture a large, unbiased sample of low-mass, star-forming galaxies (i.e., not just the brightest, most active systems), *UVEX* must reach this sensitivity limit over the extragalactic sky.

We estimate the metallicity range (1–50% $Z_\odot$) for our LMLZ sample based on the well-established relationship between gas-phase metallicity and stellar mass (see Berg et al. 2016 for an example), the latter of which is estimated as described above.

Figure 3 shows the estimated depth of the *UVEX* all-sky UV survey (in a typical high-latitude extragalactic field), highlighting both its generational improvement enabling it to explore the low-mass nearby galaxy population, and its complementarity to modern wide-area O/IR surveys. *UVEX* reaches 4–5 mag fainter than the *GALEX* wide area surveys over the entire extragalactic sky. *GALEX* reached $m_{UV} \sim 25$ over only 80 deg^2, far too small an area to obtain a global census of low-mass systems (Nuza et al. 2014). The *HST* FOV is far too small to undertake the needed survey. Many LMLZ galaxies are too faint ($m > 24$) for optical spectroscopy, while because of the bursty star formation histories narrow-band imaging (e.g., Hα) is a less reliable tracer of star-formation in many LMLZ galaxies compared to the UV.

There is, and will continue to be, rich complementary data to *UVEX* for characterizing and studying the large local LMLZ population. As previously mentioned, wide area O/IR surveys (e.g., Rubin, UNIONS) will immediately help *UVEX* with the first steps in making fundamental progress on discovery and characterization (e.g., masses, star formation rates [SFRs], distances). Beyond the optical and IR regime, there is a wealth of multi-wavelength data that will further enhance the science delivered by *UVEX*. For example, *UVEX* imaging when paired with H I and Hα will provide new insight into the process by which gas is turned into stars at low metallicities. Pathfinder examples of such science have already been shown using *GALEX*, but the number of systems are small (e.g., Donovan Meyer et al. 2015). When combined with H I (e.g., from ALFALFA, SKA and its pathfinders), *UVEX* SFRs will provide new insight into the star formation process in regimes in which H I dominates over H II, regimes in which standard relations (e.g., Kennicutt-Schmidt) are not applicable (e.g. Krumholz 2014). The process of converting gas into stars at such low metallicities, and how it may be affected by surrounding environments (e.g., groups vs voids; Nuza et al. 2014), is poorly understood observationally and theoretically. Similarly, the millions of LMLZ galaxies discovered by *UVEX* will enable followup observations of rare objects (as in Salzer et al. 2020). When combined with existing and planned datasets in

the optical, near-IR and radio, *UVEX* will enable fundamental and transformative progress in a variety of areas, such as measuring the stellar mass function and reducing the 2 dex uncertainty in the SHM (e.g., Garrison-Kimmel et al. 2017), exploring claims of systematic variations in the high-mass IMF (e.g. Krumholz 2014; Lee et al. 2009; Weisz et al. 2012), quantifying the bursty nature of star formation and its duty cycle (e.g. Meurer et al. 2009a), determining galaxy-wide dust properties at low metallicities (e.g. Salim et al. 2018), identifying rare classes of LMLZ systems (e.g., various analogs to higher-redshift systems such as green peas, extreme bursting systems, rare massive star populations; Ravindranath et al. 2020; Senchyna et al. 2017; Izotov et al. 2019a), and much more as highlighted in Section 4.3.

3.1.2. *Nebular Emission in the Lowest Mass, Lowest Metallicity Systems*

UVEX will diagnose LMLZ galaxies dominated by radiation from hot stars, and polluted by early generations of SN. This is essential to the quest to understand the first galaxies at high redshift. Key questions that will be addressed include: What is the radiation environment created by the first generation of stars? What are the feedback processes in high-z star forming regions at very low metallicity?

What we learn from ALMA, *JWST*, and the ELTs about the first galaxies and their stars will come from integrated nebular emission lines. Emission lines are powerful diagnostics of the baryonic processes that shape galaxy evolution (e.g., star-formation history, SN feedback, ionizing radiation field). However, interpreting emission lines from the first galaxies is challenging due to a lack of local anchors. The extremely low metallicities, strong radiation fields, and high star formation rates of the first galaxies are not captured in typical nearby calibration samples of resolved stars (e.g., Milky Way, SMC) or integrated light observations of most nearby low-metallicity dwarf galaxies.

To understand the extreme environments of high-redshift galaxies we need integrated spectral templates of extremely low-metallicity, strongly star-forming, young, nearby galaxies. These spectra will anchor the stellar population synthesis models used to interpret observations of primordial galaxies. Rest-frame UV spectra are particularly urgent, as they contain several key diagnostic nebular lines, such as He II $\lambda1640$, O III] $\lambda\lambda1661, 1666$, Si III] $\lambda\lambda1883, 1892$, and C III] $\lambda\lambda1907, 1909$, all of which are being detected in high-redshift observations. The most powerful constraints include the C/O ratio (sensitive to the star formation history, SN feedback, gas-phase metallicity, and age of the current bust of star formation) and the C III]/O III]

vs. C IV/He II diagnostic (sensitive to the shape of the ionizing spectrum).

HST has opened this field by obtaining UV spectra of several dozen local, strongly star-forming, modestly low-metallicity systems. However, progress with *HST* in understanding the lowest-metallicity and youngest galaxies is fundamentally limited by several factors. For one, only a very small number of systems at metallicities below $\sim 5\%$ $Z_\odot$ ($12 + \log O/H < 7.35$: in the regime of extremely metal-poor galaxies; XMPs) with light-weighted effective ages < 10 Myr are known (Figure 6). This is a product of severe observational biases: most XMPs known were discovered in SDSS spectroscopy, which was broadly restricted to only the brightest galaxies in continuum magnitudes. And second, *HST* UV spectroscopic throughput is limiting: the available detector/grating combinations on *HST*/STIS and COS have throughputs that fall precipitously redwards of ~ 1950 Å, limiting studies to a handful of the brightest and lowest-redshift LMLZ systems. In contrast, *UVEX* is optimized for sensitivity and resolution across the range from 1500–2000 Å, making it ideal for acquiring the sorely lacking UV spectra in low-redshift LMLZ galaxies.

UVEX will revolutionize this area: the all-sky survey will reveal substantial numbers of new metal-poor and young LMLZ galaxies. We estimate the total number of galaxies with $10^6 M_\odot < M_\star < 10^7 M_\odot$ and low metallicities $12+\log(O/H) < 7.35$ (e.g., Berg et al. 2016) within 100 Mpc to be $\sim 9 \times 10^6$ to 240×10^6, using the same SHM relations as in Section 3.1.1. Of these, $\sim 0.4\%$ are expected to be dominated by young stars that are just entering a burst phase (i.e., ensuring the light-weighted ages will be < 10 Myr; Stark 2016, Williams et al. 2018, Meurer et al. 2009b, Tweed et al. 2018). This suggests that *UVEX* will discover 2.8×10^4 to 5.2×10^5 galaxies in the largely unexplored region of parameter space illustrated in Figure 6. There are ~ 10 such systems currently known from the SDSS in this area of parameter space, which is likely a lower limit due to various selection effects in detecting and characterizing SDSS galaxies and the known high degree of incompleteness in SDSS for galaxies with $M_\star < 10^7 M_\odot$ (e.g., Geha et al. 2012).

As part of the baseline mission, *UVEX* will take spectra of 100 strongly star-forming low-mass galaxies over a range of metallicity and age. The improved sensitivity of the spectrograph onboard *UVEX* has the potential to increase the nearby LMLZ spectroscopic sample by orders-of-magnitude, providing a platform for fundamental progress in the study of such young systems that are our best analogs to the chemically-young systems of the early Universe (e.g., Stark 2016, Williams et al.
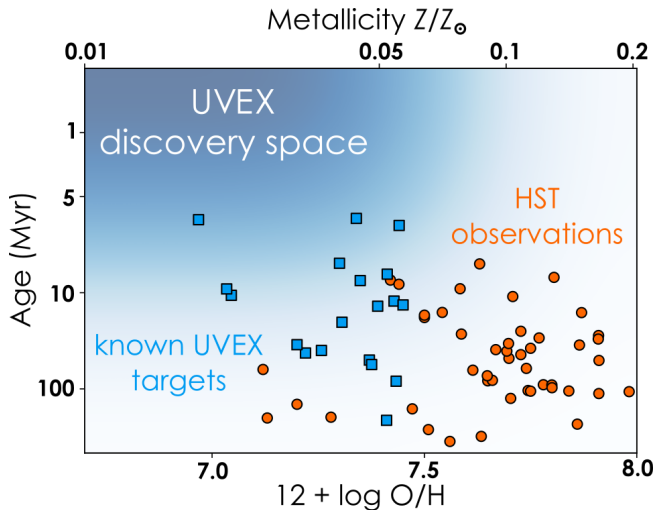
Figure 6. *UVEX* will obtain spectra of the lowest-metallicity galaxies in the local universe. Orange dots are measurements from *HST*, blue squares indicate the known sample selected for *UVEX* followup. *HST* can still make some progress in the lighter shaded blue regions but probing the darker blue region requires *UVEX*.
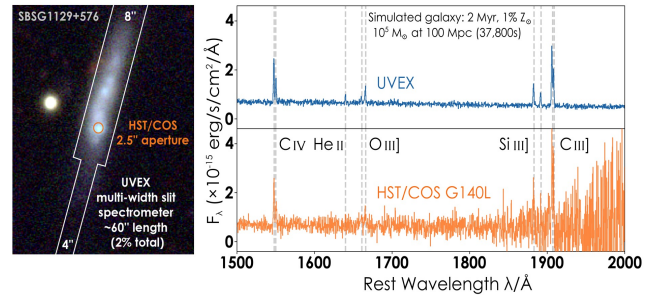

Figure 7. The *UVEX* spectrograph is optimized for observing nebular emission lines over the crucial wavelength range of 1500–2000Å. (Left) A *gri* image of a local extremely metal-poor galaxy showing *HST*/COS and *UVEX* spectroscopic apertures. (Right) A simulated *UVEX* spectrum of a ∼1% $Z_\odot$ low-mass galaxy at 100 Mpc compared to *HST*/COS for similar integration times.

2018, Endsley et al. 2021). Twenty very low-metallicity galaxies too faint for *HST* but accessible to *UVEX* have already been identified (Berg et al. 2019; Izotov et al. 2019a,b; Senchyna & Stark 2019a; see Figure 6). New systems will be selected from the first year of *UVEX* imaging based on UV-optical spectral energy distributions (SEDs), good proxies for age, metallicity, and dust (Senchyna et al. 2019b), and confirmed with follow-up optical spectroscopy. *UVEX* exposure time calculator (ETC) simulations indicate 2–80 ksec exposures for the existing sample of 20. Exposures for the *UVEX* sample will be at the lower end of this range as bright systems will be prioritized. We provide more details (e.g., extinction, targeted excitation states) on the sample and calculations for the UV line measurements in Appendix A.

3.1.3. *The Magellanic Clouds: A Laboratory for Low-Metallicity Stars*

Massive star evolution is key for understanding galaxy evolution, and mass loss and multiplicity are key for understanding massive stars. Mass loss from stellar winds in massive single and binary stars are driven by high energy radiation pressure which is uniquely observed through absorption line spectroscopy of resonance lines in the UV – only stars with the very highest mass loss rates exhibit wind features in the optical (Hillier 2020). Metallicity is a key parameter in wind-driven mass loss due to the strong metallicity dependence of wind opacity (Vink & Sander 2021). However, at fixed metallicity and spectral type, there is significant variation in wind properties. These variations are currently not under-

stood and may reflect variation in the past history and current evolutionary stage of the objects, including possible consequences of the presence of a nearby companion and/or prior interaction. Indeed, the binary fraction increases with stellar mass while interactions between close binaries are more common at lower metallicities as stars can grow to larger sizes (Moe et al. 2019).

Binary interactions have dramatic evolutionary consequences. A third of all massive stars are expected to lose their hydrogen-rich envelopes via mass transfer or common envelope ejection (Sana et al. 2012; de Mink et al. 2014; Moe et al. 2019), leaving hot and compact helium cores exposed (i.e., a stripped star). As prolific sources of ionizing radiation, low-metallicity stripped stars helped power cosmic reionization (Stanway et al. 2016; Götberg et al. 2019, 2020b; Secunda et al. 2020). Binary stripped stars are thought to be precursors to many merging compact objects (e.g., merging neutron stars [NSs]; Tauris et al. 2017; Vigna-Gómez et al. 2020; Ye et al. 2020); while extremely compact stripped binaries may themselves be sources of GWs detectable with the *Laser Interferometer Space Antenna* (*LISA*) (Götberg et al. 2020b; Nelemans et al. 2004; Wu et al. 2020). However, our knowledge of stripped stellar systems is essentially unconstrained by data. Only a handful candidate stripped stars have been identified so far, most of them in the form of an sub-dwarf O star (sdO) paired with a rapidly rotating Be star (Thaller et al. 1995; Peters et al. 2008, 2013; Wang et al. 2017, 2021). Some objects have been caught soon after the mass transfer before the stripped star has reached thermal equilibrium and is still bloated and cooler than its sdO counterpart (Shenar et al. 2020; Bodensteiner et al. 2020; Frost et al. 2022). In many cases, these systems cannot be sufficiently characterized from the optical to
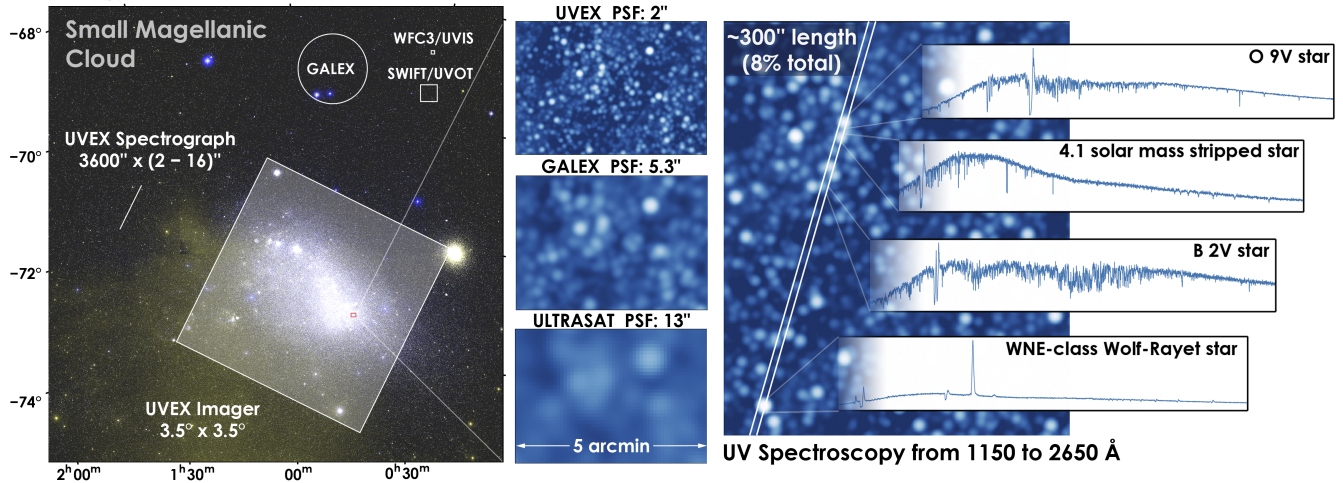
Figure 8. The *UVEX* survey of the Magellanic Clouds illustrated. (Left) The *UVEX* field of view overlaid on an optical image of SMC. Select other UV facility footprints are shown for comparison. At 12 deg², *UVEX* will be able to image the main bodies of the LMC and SMC in just seven pointings. *UVEX* will visit the LMC and SMC weekly over its prime mission to obtain deep and cadenced imaging as well as spectroscopy for > 1000 hot stellar systems. (Middle) A simulated image in a central portion of the SMC illustrating the spatial resolving power of *UVEX*. The PSF of *UVEX* ensures it will be able to resolve stars in all but the most crowded regions; a dramatic improvement over other UV facilities. (Right) Simulated *UVEX* spectroscopy for a handful of objects that *UVEX* will observe during its prime mission. The SNR and spectral resolution of *UVEX* are comparable to *HST*/COS G140L.

constrain evolutionary models, while stripped stars descending from truly massive stars have remain elusive.

Understanding how massive single and binary stars, and their descendants, shape galaxy evolution requires us to understand how their wind properties change with metallicity. Current models are insufficiently constrained so that the way forward relies on observations of large samples at lower metallicities. Fortunately, nature has provided us with nearby, sub-solar metallicity laboratories that are close enough to be spatially resolved: the LMC ([Fe/H] = –0.5) and SMC ([Fe/H] = –1.0) (McConnachie 2012).

By exploiting these nearest low-metallicity laboratories where individual stars can be resolved (see Figure 8 and Figure 9), *UVEX* will probe the mass-loss driven evolution of hot and massive stars as a function of metallicity and binarity across the Hertzsprung-Russell (H-R) diagram. As part of the baseline mission, *UVEX* will (i) perform deep, cadenced imaging of the LMC and SMC, making a near-complete census of hot and stripped stars and (ii) obtain UV spectra of 100 *UVEX*-identified stripped and 1,000 hot (O and B) single and binary stars, measuring wind velocities using the blue edge of P-Cygni profiles (Crowther et al. 2016). Binarity will be determined from *UVEX* cadenced imaging and/or ground-based optical surveys (Sana et al. 2013; Cioni et al. 2019). Key questions *UVEX* will address: How does mass loss from hot, massive stars depend on
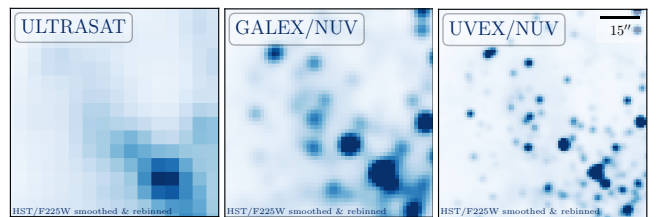
Figure 9. The spatial resolution of *UVEX* compared to select UV facilities. This *HST* UV image on the outskirts of 30 Doradus (from program GO-11360) has been convolved with the PSF of each facility. This stellar field is unresolved by *ULTRASAT*, marginally resolved by *GALEX*, and resolved by *UVEX*. As other regions in the LMC and SMC are less crowded, *UVEX* will reveal the detailed distribution of stars without being significantly affected by crowding throughout most of the LMC and SMC.

their properties? What are the demographics of stripped stars, and what influences their formation?

A *UVEX* survey of the LMC/SMC will transform our understanding of hot single and binary stars. *UVEX* imaging will discover and characterize thousands of hot stars, from single stars on the main sequence (MS) to rare binary stars in various post-MS evolutionary stages (e.g., stripped stars), efficiently identified via photometric techniques (e.g., UV excess, Götberg et al. 2018). Cadenced UVEX imaging will identify and characterize eclipsing hot, massive systems, and systems containing a stripped star (Figure 10). *UVEX* absorption line spectroscopy (e.g., CIV, NV, HeII) will measure termi-

nal wind velocities and mass loss rates for single, binary, and stripped stars across the H-R diagram (Figures 11,12,13).

Only *UVEX* has the required sensitivity, resolution and FOV to identify populations of hot and stripped stars. With its $\sim 2''$ PSF, *UVEX* will resolve individual stars in all but the most crowded star formation regions (e.g., 30 Doradus) in the LMC and SMC (Figure 9). Second, its exquisite sensitivity enables very deep imaging. Separating the lowest mass stripped stars (0.37 $M_\odot$) from the main sequence via the color excess method requires a color precision of $NUV - g \leq 0.1$ (Götberg et al. 2018) at $m_{NUV} = 25$. Moderately deep optical imaging with DECam (Nidever et al. 2017) will enable the identification of intermediate and massive stripped stars. When combined with deep Rubin imaging, *UVEX* will uncover stripped stars of all possible masses in the LMC and SMC. Though extinction in the LMC and SMC is modest (e.g., Zaritsky et al. 2004), the addition of the FUV band will help to mitigate mild degeneracies between temperature and extinction. By comparison, the *GALEX* and *Swift* imaging surveys are too shallow; *hst*'s FOV is too small. In the LMC/SMC the *HST* FOV will contain 0.3 stripped stars, while a single *UVEX* field at similar depth will contain 1400 (Götberg et al. 2019). By design, the *HST* Ultraviolet Legacy Library of Young Stars as Essential Standards (ULLYSES) spectroscopic survey only includes a handful of close binaries in the LMC and SMC, covering a small range of the H-R diagram (Roman-Duval et al. 2020). Further context for the uniqueness of *UVEX* imaging and spectroscopic measurements in the Magellanic clouds, and the relationship between ULLYSES and other surveys is provided in Appendix B, while details of our expected spectroscopic exposure times are presented in Appendix C.

3.2. *Pillar 2: New Views of the Dynamic Universe*

The coming decade will be a golden era in time-domain and multi-messenger astronomy. Rubin in the O/IR and the Square Kilometer Array (SKA) in the radio will join an existing, vibrant suite of panchromatic wide-field observatories that will identify hundreds of thousands of variable and transient events, opening tremendous discovery space. *UVEX* will be a unique and powerful tool in this exciting new era: it will explore the GW window opened by major upgrades to the LIGO/Virgo sensitivity that will be online by 2028; it will perform the first rapid UV spectroscopic observations of infant SNe; and it will, through a community-driven ToO program, provide the first deep rapid UV

spectroscopic followup capability, opening a new window on the dynamic universe.

3.2.1. *The Gravitational Wave Frontier*

UVEX will probe the physics of compact object mergers, as well as the nature and energetics of the material ejected in NS mergers. Key questions that *UVEX* will address include: What mechanism powers the early UV emission from NS-NS mergers? What are the properties (mass, com-position, velocity) of the early ejecta? How rapidly does the remnant collapse to a black hole?

When two NSs, or a NS and black hole (BH) merge, the NS will be tidally distorted, and ejected material can produce an electromagnetic (EM) counterpart. Indeed, on August 17, 2017, LIGO detected its first binary NS (BNS) merger, GW170817 (Abbott et al. 2016), at a surprisingly close distance of 40 Mpc. EM radiation was subsequently observed across the spectrum, from gamma-rays to radio waves. An astounding number of scientific results came from the single BNS GW170817 event: detection of a short gamma-ray burst (GRB) 1.7s after the merger (Goldstein et al. 2017) confirmed the connection between short GRBs and NS mergers (Paczynski 1986; Eichler et al. 1989); the optical localization (Coulter et al. 2017) and host redshift measurement yielded an independent determination of the Hubble constant (Abbott et al. 2017c); the fading UV/O/IR light indicated the presence of a moon-mass worth of neutron-rich ejecta that generated heavy elements, indicating NS mergers are a long-sought source of r-process material (Cowperthwaite et al. 2017; Drout et al. 2017; Arcavi et al. 2017; Tanvir et al. 2017; Kasliwal et al. 2017); and the late-rising X-ray and radio light indicated that a relativistic jet was produced but viewed $\sim 20°$ off axis (Troja et al. 2017; Alexander et al. 2017; Margutti et al. 2017; Haggard et al. 2017; Mooley et al. 2018; Hallinan et al. 2017).

A striking feature of the EM emission from GW170817 was the prominent UV "blue bump" detected by *Swift* UVOT follow-up beginning 0.6 days after the event (Evans et al. 2017). This emission was bright ($\sim 10^{42}$ erg s^{-1}), blue (peaking at 10,000 K), and had a high velocity ($\geq 0.2c$) (Shappee et al. 2017). The origin of this emission is hotly debated (Arcavi 2018), and understanding it holds the key to understanding fundamental issues, including the amount, composition, and velocity distribution of the first ejecta, the NS mass ratio, and the question of how quickly the merger remnant collapsed to form a BH, which can be used to constrain the equation of state (EOS) of exotic, ultra-dense matter (Piro et al. 2017). One idea is that the blue emission was radioactively powered, referred to as a "blue kilonova"
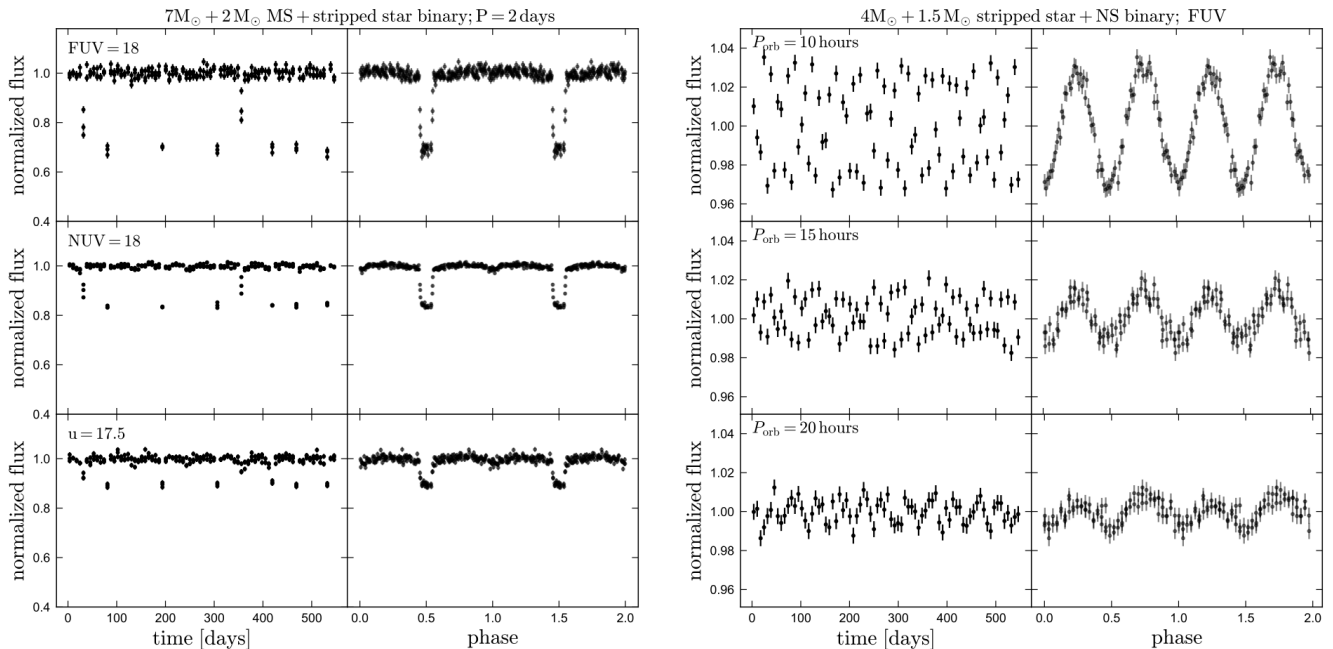
Figure 10. Predicted light curves for two types of binaries containing stripped stars detectable with *UVEX* time-series photometry in the Magellanic Clouds. Left two panels show an eclipsing binary containing a $7M_\odot$ main-sequence star and a $2M_\odot$ stripped star. Deep eclipses are apparent in the UV, where the stripped star contributes almost half of the total light. Shallower eclipses are apparent in the optical (e.g. Rubin/LSST *u*-band), but these would be misinterpreted as being due to a normal main-sequence companion without the UV data. Right panels show a $4M_\odot$ stripped star with a neutron star companion at different orbital periods in the FUV; the predicted variability is due to a combination of ellipsoidal variability and Doppler beaming. Such a system will evolve to become a binary neutron star.

(BKN) (Metzger et al. 2010), with the blue colors implying an ejecta composition dominated by relatively light r-process elements (e.g., Se, Br, Kr). The source of the ejecta could be neutrino-driven winds from an accretion disk (Kasen et al. 2015; Metzger et al. 2008) or material squeezed from the interface of the colliding stars. However, challenges exist with both models (Fernández et al. 2019; Sekiguchi et al. 2015). The composition and mass of the ejecta constrain the NS mass ratio and EOS.

The merger of a NS and BH offers another potential, but less certain, opportunity to probe extreme physics, BH formation, and relativistic phenomena. LIGO reported detections of the first NS-BH mergers in its O3 observing run (Gottlieb et al. 2018). However, either the mass ratio was too large for EM emission, or poor GW spatial localizations precluded meaningful EM counterpart constraints. If there is a large amount of debris (Bhattacharya et al. 2019), UV observations combined with the GW signal will afford better constraints on the BH mass and spin distribution (Duez et al. 2010; Özel et al. 2010). Many of the same processes inferred in GW170817 may be present in a NS-BH merger, and early-time UV detections or strong limits on the EM flux are the best way to probe these processes (Metzger et al. 2015; Bulla et al. 2019).

The future for probing EM emission from GW events is bright over the next decade (Figure 1). The LIGO/Virgo/KAGRA GW interferometers are currently executing a major upgrade (termed A+) that will come online in the fifth observing run (O5) in 2025–26. The sixth observing run (O6) is planned to last 18–24 months beginning in 2028 with LIGO India added, dramatically improving the number of well-localized BNS events. In O4 to O5 to O6, the expected rate of BNS mergers localized to $<100\,\mathrm{deg}^2$ increases from 7 to 47 to 117 per year (Abbott et al. 2017c, 2021). *UVEX* will follow up a sample of ≥ 20 NS mergers with localizations $<100\,\mathrm{deg}^2$ within hours of the event, which requires it to detect events as far away as 250 Mpc (for details on the simulations that give rise to these numbers, see Section 4.7). Given the *UVEX* sensitivity, it will reach events to 850 Mpc in NUV and 450 Mpc in FUV for either BKN or shock models. For these events, *UVEX* will obtain high-quality two-band light curves (Figure 14).

For achieving the scientific goals enumerated above, only *UVEX* provides the envisioned capabilities. Two-band measurements extending to the FUV are crucial to understanding the early explosive stages, when the emission peaks in the *UVEX* FUV band. Quantitative constraints on emission models require a significant

C IV 1548−51
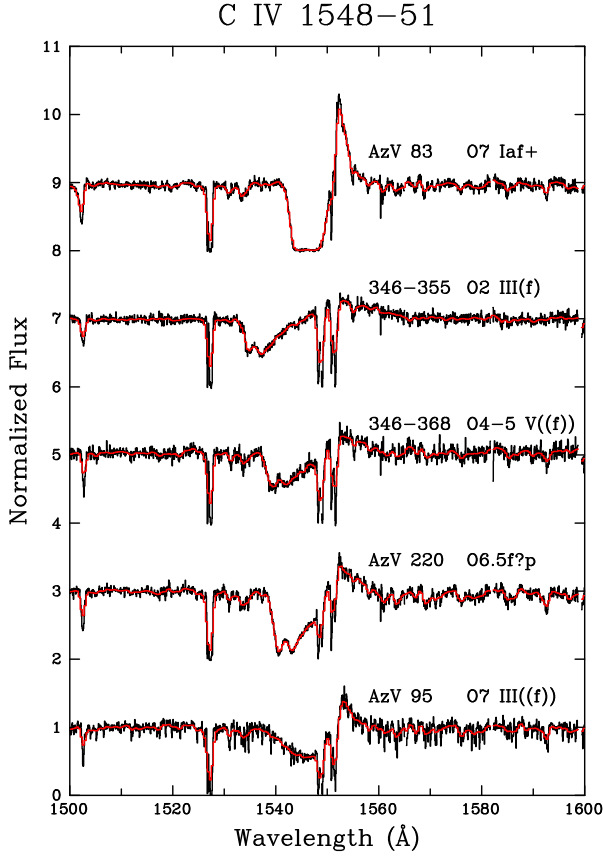
Figure 11. Example spectra showing the C IV doublet in O-type stars in the SMC. STIS/E140M observations (Walborn et al. 2000) are shown in black. The same spectra smoothed to *UVEX* resolution are shown in red. Because key features of the UV resonance lines (e.g., terminal velocities, peak intensities) are so prominent, they are preserved at the resolution of *UVEX*. The low metallicity of the SMC means these wind features are among the weakest and least pronounced. The UV line fidelity is equally well-preserved for stronger winds typically found in the higher metallicity LMC (Crowther et al. 2016).

sample of events to probe viewing angle differences and spectral information to remove degeneracies in models. While *HST* has the sensitivity, its FOV is too small and it does not respond fast enough. While *Swift* has rapid response, its FOV and sensitivity are insufficient to find the UV counterparts at early times (GW170817 was first detected in the optical band). *ULTRASAT* will have a larger FOV and rapid response in NUV but lacks the needed two-band coverage extending into the FUV. *ULTRASAT* is also much less sensitive than *UVEX*, corresponding to an event rate ∼7 times less than *UVEX*, without considering sensitivity losses from host Galaxy contamination due to *ULTRASAT*'s coarser (13″) PSF.
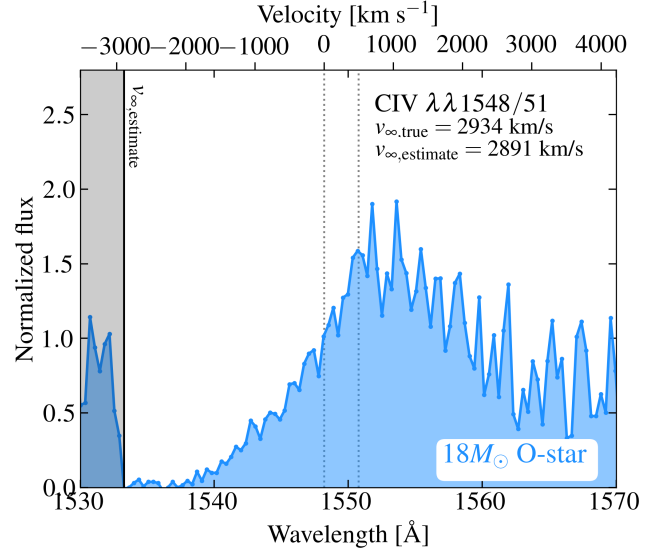
Figure 12. The simulated *UVEX* spectrum ($SNR = 10$ at the C IV doublet) of a typical LMC metallicity O-star spectrum with an average wind velocity, zoomed in on the C IV resonance line. By fitting for the blue edge of the C IV P-Cygni profile, we recover the wind velocity to within a few percent. *UVEX* will enable the accurate determination of massive star wind speeds for 1000 hot, massive single and binary stars in the LMC and SMC.
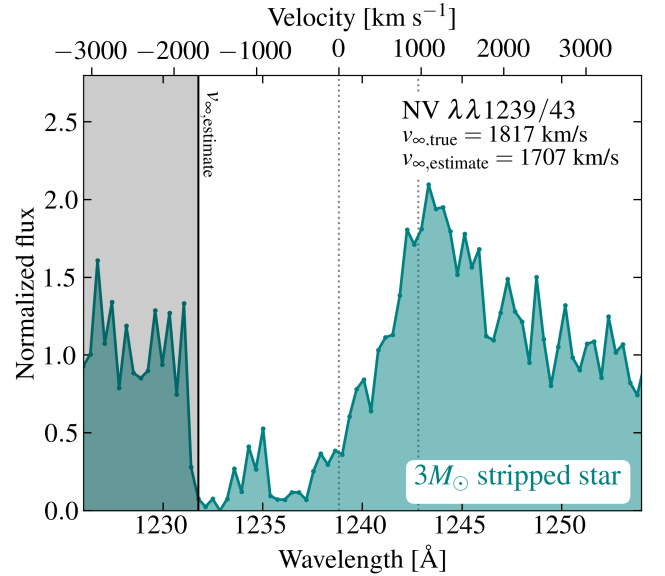
Figure 13. The simulated *UVEX* spectrum ($SNR = 5$ at the N V doublet) of a $3M_\odot$ stripped star with an expected typical wind velocity zoomed in on the N V resonance line. By fitting for the blue edge of the N V P-Cygni profile, the wind velocity can be recovered to within ∼ 10%; 20% for the weakest wind cases. *UVEX* will enable the accurate determination of massive star wind speeds for ∼ 100 stripped stars in the LMC and SMC.
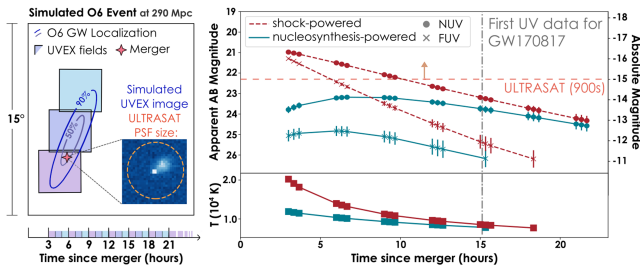
Figure 14. (Left) *UVEX* promptly localizes BNS mergers, locating counterparts within their host galaxy. (Right) Two UV bands can measure the evolution speed and peak luminosity (top) and constrain temperature (bottom), discriminating between models.

3.2.2. *A New Window on Core Collapse Supernovae*

UVEX will open a new window on stellar death and galactic chemical enrichment by massive stars by acquiring the first UV slit spectroscopy of core collapse explosions from hours to days after stellar demise. *UVEX* will address key outstanding questions, including: How do massive stars evolve in the very final stages of their lives? What is the chemical composition, ionization state, and kinematics of late-stage eruptive mass-loss events?

UVEX spectroscopic observations will provide an unprecedented view of the final years in the life of stars, the chemical composition of their winds, and ejected mass that enriches galaxies in the elements. These are among the least understood aspects of stellar evolution (Smith et al. 2011). The explosion of a massive star launches a shock into the circumstellar medium (CSM), heating the material up to 10^5 K, which subsequently radiates copious UV continuum and line emission (Figure 15). The gas rapidly expands and cools, shifting the peak of the emission towards longer wavelengths. Combined with the higher line blanketing at lower temperatures, this suppresses the UV flux within a few days. Because of its much larger velocity compared to any pre-explosion mass ejections, the SN shock acts as a time machine, and a UV spectroscopic sequence during the earliest (<2 days post-explosion) stages offers a unique opportunity to probe the mass-loss history and chemical composition of the exploding star in the last years of its evolution.

Recent observations have revealed an unexpected diversity of massive star behavior in the decades before core collapse, including enhanced and eruptive mass loss. A leading model suggests that this results from nuclear burning instabilities in the final stages of stellar evolution (Quataert & Shiode 2012; Fuller 2017). Our current knowledge of the composition, ionization stage, and kinematics of the ejected material is limited to the information from optical spectroscopy. But for young hot objects, the optical is relatively poor in bright emission

lines (Groh 2014). As a result, fundamental properties of the progenitor star and physical conditions that lead to enhanced mass loss are unconstrained. Even for the extremely well-monitored SN2013cu, with exquisite optical spectroscopy starting as early as 15.5hr after collapse (Gal-Yam et al. 2014), state-of-the art modeling cannot determine the progenitor type (Groh 2014).

Early UV spectroscopy will be transformative. Compared to the optical, UV accesses a significantly larger number of spectral transitions, adding crucial constraints to an otherwise under-constrained problem (Figure 15). Virtually all young stellar explosions have SEDs peaking in the UV, where can be found resonance lines such as CIV, HeII, and NIV that have high optical depths, enabling detection of much lower wind densities than the optical. UV also probes highly ionized Fe lines at λ 1200–1450 which can be used to directly measure the close CSM metallicity (at these high temperatures no optical Fe transition is available).

No current or planned observatory can obtain rapid-response broadband UV spectroscopic sequences. To date, the best-observed core collapse event is SN 1987A, and the best constraints come from the *International Ultraviolet Explorer (IUE)* (Pun et al. 1995). In subsequent decades, no comparable UV spectral sequence has ever been acquired. The earliest *HST* UV spectrum of a SN was 3.3 days after explosion (Tinyanont et al. 2021). The *Swift* UVOT slitless grism has rapid-response NUV capability, but limited sensitivity and low resolution, and *Swift* does not extend to the feature-rich FUV. *UVEX* will uniquely fill this observational gap.

3.2.3. *A Community Resource for Exploring the Dynamic Sky*

UVEX will open a new window on the dynamic universe by providing the first rapid (<1 day) sensitive UV spectroscopic follow-up of variable and explosive events. New Windows on the Dynamic Universe is one of three priority science areas in the Astro2020 decadal survey because of the enormous opportunities opened by facilities such as LIGO/Virgo, Rubin, the IceCube Neutrino Observatory, SKA, and many more. A wide variety of explosive phenomena have spectral energy distributions (SEDs) peaking in the UV at early times, and in many cases, spectroscopy holds the key for addressing fundamental questions. *UVEX* will play a unique and central role in this theme by providing the first sensitive, rapid response UV spectroscopic follow-up capability.

3.3. *Pillar 3: A Legacy of Deep Synoptic All-Sky Surveys*

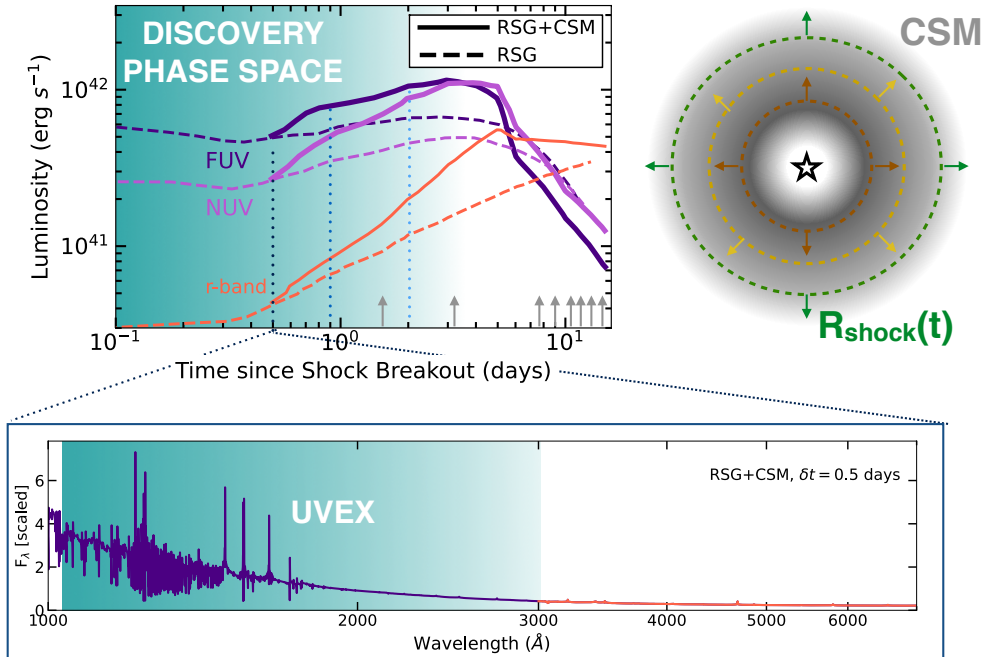The coming decade will see modern synoptic and deep wide-area sky surveys with Rubin, *Roman*, and *Euclid*,

Figure 15. The explosion of a red supergiant (RSG) star surrounded by a dense shell of CSM (grey shell in upper right) is a bright source of FUV (dark purple) and NUV emission (light purple). As the explosion's shock propagates into the CSM (dashed lines in upper right), it ionizes material that then recombines, producing a rich UV spectrum (lower panel) that carries direct information on the unknown chemical composition of this material. At early times the optical emission is significantly fainter (see r-band) and has less prominent spectral features, as shown in the lower panel (red line). Dashed lines in the upper-left panel: FUV, NUV and r-band light curves of the same RSG explosion without a thick CSM. Grey vertical arrows: epochs of acquired UV spectra of SNe, including *IUE* observations of SN 1987A and the earliest *HST* spectra of SN 2020fqv. *UVEX* will thus explore a completely pristine part of the parameter space and will provide the characterization of stellar explosions of all types in their earliest, hottest phases. Simulated spectra from Dessart et al. (2017).

for which *UVEX* will provide the crucial, deep, complementary two-band UV data. Each point on the sky will be visited a minimum of 10 times during the prime *UVEX* mission, with cadences ranging from 12 hrs to 6 months. The LMC/SMC survey will be performed through observations taken on a weekly cadence, and the deep extragalactic fields required for validating the extragalactic dwarf galaxy survey will be cadenced to provide regular instrument calibrations. The combination will provide static images and time-domain information with enormous legacy value, enabling a broad range of science limited only by the ingenuity of the community. In addition, the spectral images from *UVEX*'s long (1°), offset, varying width slit will be taken with every pointing. These will be archived, affording significant discovery space in the spectral domain. Finally, unlike *GALEX*, *UVEX* will cover the entire sky in FUV and NUV since its modern detectors need not avoid bright objects, providing the first ever deep exploration of the Milky Way in UV.

Combined, all this data will be a rich legacy for the astronomical community to address many areas of science

beyond our core mission pillars. The following Section is dedicated to exploring in more depth a selection of these important scientific questions.

4. A COMMUNITY RESOURCE: ARCHIVAL AND EXTENDED MISSION SCIENCE

In addition to the primary scientific objectives that we address with the first two pillars of our baseline mission (Section 3), *UVEX* has the capacity to address many other important areas of investigation requiring its broad UV capabilities. The extensive data provided by the legacy all-sky survey and community-driven ToO follow-up observations, as well as a GO program in an extended mission, will become the basis for transformational advancement in a wide variety of astronomical fields. In this Section, we explore a selection of areas which will benefit from the data provided by *UVEX*, including stellar astronomy (Section 4.1), galactic archaeology in the Milky Way and Magellanic Clouds (Section 4.2), galaxy formation (Section 4.3), cosmic explosions (Section 4.4, active galactic nuclei (AGN; Section 4.5), tidal disruption events (TDEs; Section 4.6),

multi-messenger astronomy (Section 4.7), and exoplanets (Section 4.8).

4.1. *Stellar Astronomy*

In the previous century, astronomers developed basic understanding of (single) star formation through stellar death and separately were able to explain how, as a result of stellar nuclear synthesis and stellar outflows from winds and explosions, the periodic table was populated with "metals" (elements other than hydrogen and helium). With the foundations thus established, in this century, astronomers are working to address the next levels of complexity due to (1) binarity and (2) metallicity. It turns out that 50–70% of stars in the Universe are in binary systems, with this fraction reaching unity for the most massive stars. For some fraction of these systems, as each of the stars evolve, mass can be lost from one star and gained by the other star. The result, in most cases, is a "common envelope event" in which one star plunges into the envelope of the other star and forms a tight binary consisting of the core of that star and the companion. The phase space determined by the masses of the two stars and the orbital parameters (separation, eccentricity, mutual inclination) is exceedingly large, and poorly understood processes such as common envelope evolution and the impact of metallicity add further complexity. In Figure 16, we display some of the key evolutionary pathways for systems with at least one white dwarf – the most common type of evolved binaries, and for which *UVEX* will provide critical observations.

Even for single stars, the evolution of a star depends on not just the mass but also its metallicity and rotation. Mass loss from stars, particularly that from massive stars, is a critical part in the evolution of a galaxy, and it is clear that mass loss is directly tied to metallicity. However, our present understanding of this important physical process is poor. Observations are needed to make further progress.

In terms of metallicity, the Sun is an average star in the Milky Way and we live in an average neighborhood. The frontier now lies in understanding star formation at low metallicities, which in turn provides insight into star formation in the young Universe. Locally, the Magellanic Clouds have metallicities of 10–20% and 40–50% relative to the Sun[2] for the SMC and LMC, respectively (e.g., McConnachie 2012). These offer convenient nearby laboratories for the study of star formation and

stellar evolution that are representative – in at least one very important aspect – of the early Universe (see Section 3.1.3).

In the following subsections, we describe further specific scientific areas for which *UVEX* will be enable significant progress in the field of stellar astronomy. First, we discuss the opportunity to probe the physics of accretion in both the context of star formation (Section 4.1.1) and in the context of outflows from accreting compact objects and classical novae (Section 4.1.2), and the most common type of evolved binaries: ones hosting at least one white dwarf (Section 4.1.3). We also discuss the ability of *UVEX* to contribute to the study of angular momentum evolution of evolved stars (Section 4.1.4), and low-metallicity stars in the Local Group (Section 4.1.5).

4.1.1. *Star Formation and Accretion*

Stars first become visible in the optical and UV during the later stages of their formation when the newly formed protostar is present, surrounded by an active accretion disk in which planets form and accrete their initial atmospheres. The stars themselves are very magnetically active, showing kilogauss level average surface magnetic fields (Johns-Krull 2007). The UV through X-ray emissions produced by the magnetic activity drives the chemistry in the atmospheres of the young planets. While the disk is still present, these high energy emissions help determine the ionization structure and chemistry in the disk, which is important in the action of both the magneto-rotational instability (MRI; e.g., Balbus & Hawley 1998) and the formation of magneto-centrifugally driven disk winds (e.g. Gressel et al. 2015), the two main candidates for producing the viscosity that leads to disk accretion onto the star. For accreting young stars, it is this accretion of disk material onto the stellar surface that is the dominant contributor to the UV and blue optical emission observed. The accretion of disk material represents the last stage in the mass assembly of newly formed stars, and generally occurs within the first 10 Myr after the star is formed (e.g., Wyatt 2008) while it is evolving along the pre-main sequence (PMS) evolutionary tracks.

The current paradigm for accretion onto young, PMS stars is magnetospheric accretion (for a recent review, see Hartmann et al. 2016), which posits that the strong magnetic fields on the surface of young stars truncate the disk near the co-rotation radius, forcing the accreting disk material to flow along the field lines such that the material impacts the stellar surface at near free-fall velocities. Theoretical work (e.g., Koenigl 1991, Shu et al. 1994, Long et al. 2005, Zanni & Ferreira 2013, Romanova et al. 2018) suggests that the coupling be-

---

[2] We list the generally accepted ranges. The exact value depends on the adopted Solar metallicity scale and abundance pattern, type of metallicity tracer (e.g., stars, nebular emission), radial variations in metallicity, etc.
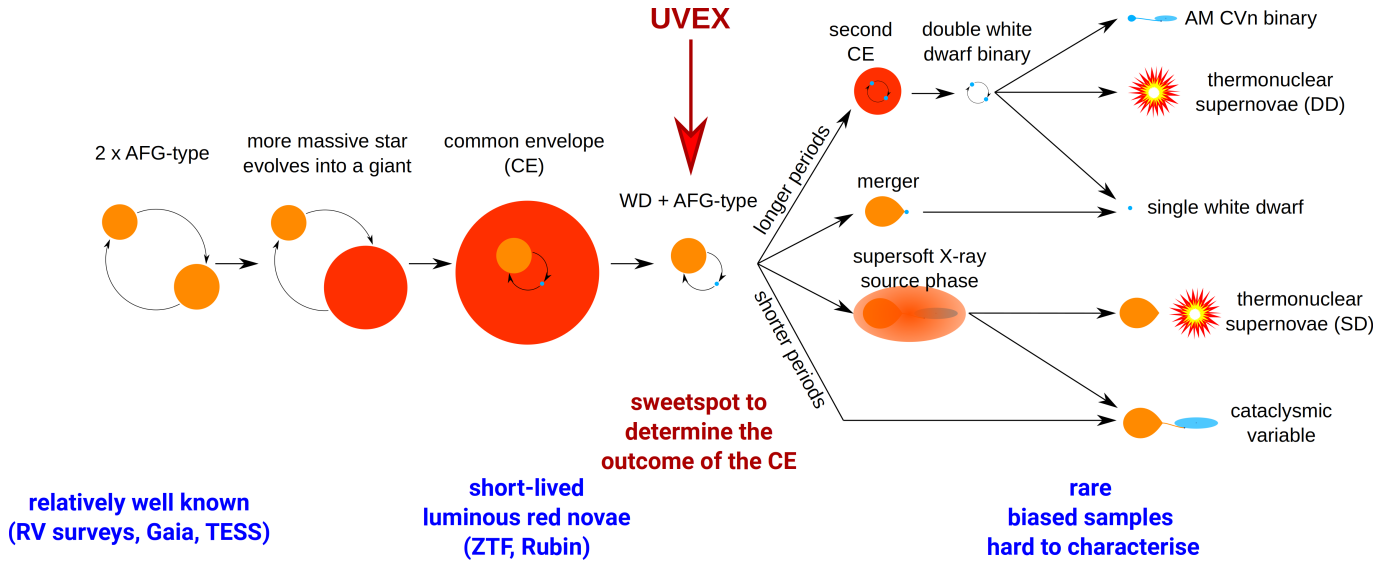
Figure 16. Schematic overview of the evolution of two AFG-type stars into a variety of compact binaries, which include low-frequency GW sources that *LISA* will detect in large numbers, and the progenitors of all types of thermonuclear SNe, including SN Ia. The stellar masses and the orbital separation of the white dwarf + AFG-type star binaries emerging from the common envelope determine the future evolution. *UVEX* will be able to deliver FUV spectroscopy of many post-common envelope white dwarf + FGK binaries, i.e., systems within a critical phase that determines their future evolution.
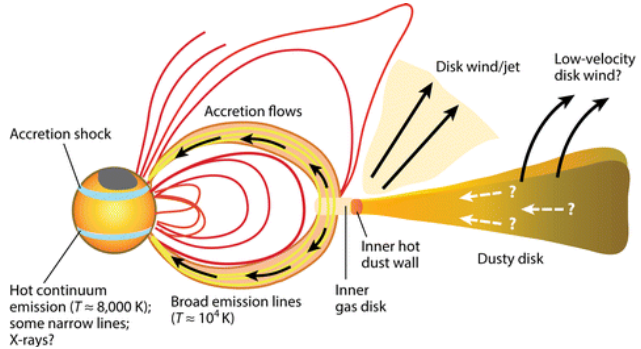
Figure 17. The close circumstellar environment of a young star (taken from Hartmann et al. 2016). Magnetospheric accretion occurs as disk material is captured by the stellar magnetic field, flowing toward the star and accreting near the stellar poles. At the base of the magnetospheric flow, the material falling at near free-fall velocities impacts the surface, creating a strong shock which produces substantial UV emission.

tween the young star's magnetosphere and its circumstellar disk is sufficient to regulate the stellar angular velocity for the lifetime of the disk. In this so-called "disk-locking" picture, angular momentum is magnetically transferred from the star to the disk and eventually ejected in a mass outflow. This picture of magnetospheric accretion and disk locking has been underpinned primarily by observations from nearby star-forming regions such as Taurus, rho Ophiuchus, the Upper Scorpius region and a handful of others. However, these regions are generally considered low density, relatively low mass star-forming regions, and have very few of the highest mass, hottest stars (O-type stars) which produce copious amounts of ionizing radiation and strong stellar winds that have important feedback effects in the star formation process (Rosen & Krumholz 2020). Studies of the Orion Nebula Cluster (ONC) have also been significant in the development of these ideas. While higher in overall mass and containing the high-mass stars of the Trapezium, this region is still not representative of the highest mass star-forming regions (Portegies Zwart et al. 2010) in which the majority of stars in our Galaxy and probably most galaxies form (see review by Portegies Zwart et al. 2010), and in which O-type stars and their feedback are expected to have a substantial impact on other stars forming there.

Taking extinction and distance into consideration, perhaps the most favorable region of massive star formation for the study of feedback processes on low-mass star formation and early stellar evolution is the Carina star forming complex. The Carina nebula complex (CNC) is located in the Carina spiral arm (e.g., Vallée 2014), and is one of the most active massive-star-forming regions in the Milky Way. Over 140 massive OB-stars (Alexander et al. 2016) and more than 1,400 young stellar objects (Povich et al. 2011; Feigelson et al. 2011) have so far been identified in the CNC, which is suggested to contain 10 times the young stellar content of the ONC (Townsley et al. 2011). The distance to the CNC, ~ 2.3 kpc, has been measured accurately using near-IR spectroscopy (e.g., Allen & Hillier 1993; Smith
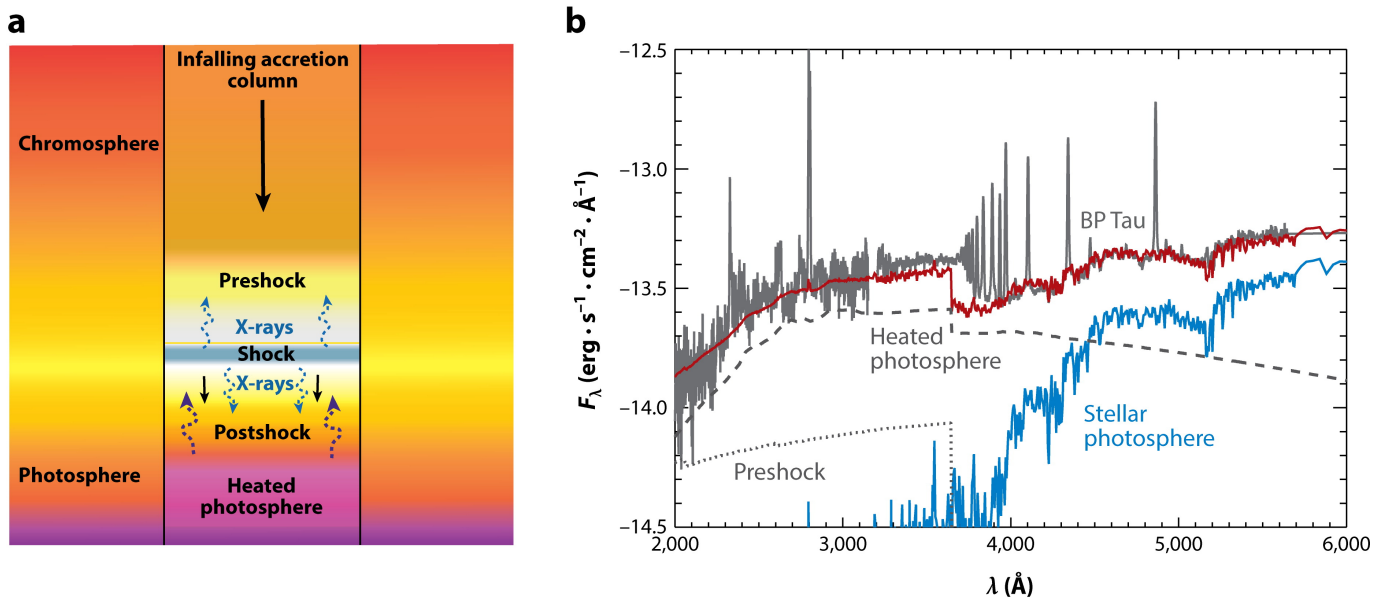
Figure 18. From Hartmann et al. (2016): (a) Schematic diagram of accretion shock structure showing the precursor or preshock region, the postshock or cooling region, and the heated photosphere below the shock. (b) Spectral energy distribution of the classical T Tauri star BP Tau (gray solid line), stellar photosphere (blue line), and accretion shock model (red line) showing contributions from the preshock (gray dotted line) and heated photosphere postshock (gray dashed line) regions.

2006). The number of O-stars in the CNC is comparable to that in other massive-star-forming regions in the Galaxy such as W43 and W51 (e.g., Blum et al. 1999; Okumura et al. 2000), but the CNC is two or three times closer than those regions. Therefore, the CNC offers an excellent opportunity to study the physics of accretion onto newly formed low-mass stars in a region that is more representative of the regions in which most stars form. Study of the low-mass stellar population and its accretion activity will provide a unique way to uncover the role of massive star feedback on the formation and early evolution of young stars.

As shown in Figure 17, when material accreting along the stellar magnetic fields reaches the star, an accretion shock is expected to form. The material impacts the star at near free-fall velocities, which is on the order of ~ 300 km s^{-1}. As a result, a strong shock forms, initially heating the material up to a temperature of $\sim 10^6$ K. As the material cools from 10^6 through 10^5 K, it emits strong lines in the X-ray and UV which in turn heat the photosphere below and immediately around the accretion shock as shown in Figure 18a. Many authors have studied the emission that results from this process (Valenti et al. 1993, Calvet & Gullbring 1998, Gullbring et al. 1998, Ingleby et al. 2013), and the accretion-related emission dominates the stellar flux in the UV (Figure 18b), making short wavelength observations the most sensitive to accretion onto young stars. For the most strongly accreting stars, the accretion luminosity

is also detected in the blue optical, but as the accretion rate falls, NUV and FUV observations are required to make reliable accretion rate estimates for young stars.

Extinction will play a role in our ability to measure mass accretion rates; however, there are at least two well-established ways to estimate the extinction from broadband colors for cool stars. In the *J-H* versus *H-K* color-color diagram, reddening and IR excess from circumstellar emission moves stars in almost orthogonal directions (e.g., Meyer et al. 1997). In addition, over the spectral type range of cool stars, these objects define a nearly horizontal line in this two-color diagram. As a result, the extinction can be reliably estimated for stellar types K-M. In addition, narrower band optical photometry can also be used to estimate the effective temperature and extinction of low mass stars (see Figure 5 of Da Rio et al. 2012 and accompanying discussion). Averaging results from these two methods will provide sufficiently accurate A_v values for the statistical nature of accretion studies that *UVEX* photometry will allow. This would require obtaining supporting ground-based observations, albeit from existing observatories.

UVEX operating with supporting ground-based facilities (e.g. Rubin) will provide the observations needed to measure accretion onto thousands of young stars in the CNC. An example of how these accretion rate determinations will be performed is shown in Figure 19 taken from Manara et al. (2012). This figure shows a two-color diagram (using colors from U to I) of young stars
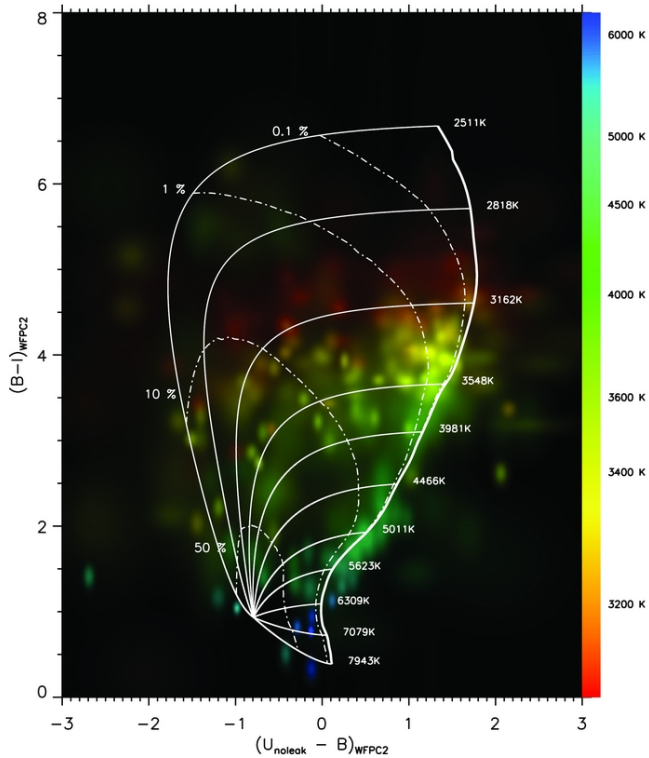
Figure 19. From Manara et al. (2012): Two-color diagram of stars in the ONC. Each source has been corrected for extinction and represented as a normalized 2D Gaussian, corresponding to the photometric errors. Sources are color-coded according to their $T_{\rm eff}$ (scale at right). The thick line represents the calibrated isochrone for no accretion; thin lines represent the simulated displacements (for different $T_{\rm eff}$) from the photospheric colors, obtained by adding an increasing amount of a model of the accretion luminosity analogous to that shown in Figure 18.

in the ONC. Red optical and near-IR colors are used to estimate spectral types and reddening for each source. Similar data for the CNC will be available from LSST (e.g., Bonito et al. 2018) and other existing or planned ground-based surveys. The nearly vertical, thick solid line shows the locus where stars without accretion fall. The thinner white lines moving to the left and down from this locus shows where stars with differing amounts of accretion land. As shown in Figure 19, many of the stars lie very close to the non-accreting locus. These stars are either not accreting at all, or accreting at levels too low to be measured using colors confined to the optical bands. Adding in FUV and NUV photometry from *UVEX* will effectively stretch this diagram out in both directions, but most importantly will stretch it in the horizontal direction, making it easier to accurately measure accretion rates and to distinguish the accretion emission from low accretion rate objects.

Fortunately, the entire CNC can fit into a single pointing of *UVEX*. A *UVEX* CNC survey could detect accreting young stars down to $\sim 0.3 M_\odot$, providing the first comprehensive study of accretion onto low-mass stars in a canonical high-mass star formation region.

GALEX did not survey this region and did not have the sensitivity to reach the required depth. *HST* is capable of making similar observations with WFC3; however, ~ 4400 pointings would be required to cover a single *UVEX* pointing. As a result, *UVEX* is the best instrument to make the requisite observations to explore the role of high mass star feedback on the accretion physics of low-mass young stars.

4.1.2. *Outflows from Accreting Compact Objects*

Accretion occurs on a wide range of physical scales, from super-massive nuclear black holes to protostars. Here, we address accretion onto compact stellar objects. Galactic accreting white dwarfs (i.e., cataclysmic variables; CVs) and stellar-mass black holes and neutron stars (i.e., X-ray binaries; XRBs) are excellent laboratories to study accretion processes and the accretion-ejection coupling mechanisms in great detail, across time scales accessible to human beings (Fender & Muñoz-Darias 2016). Moreover, accretion in these systems spans a broad range in accretion rates, from $10^{-5} - 10^2$ times the Eddington rate.

Most accreting stellar remnants spend the majority of their time in a quiescent state, punctuated by outbursts lasting a few days to months. Massive outflows are launched during those outbursts, which play an important role in the evolution of these systems. UV observations provide a unique window on these outflows. In this section, we focus on two distinct types of outbursts, each with their own phenomenology and open questions: outbursts caused by the disk instability mechanism, and classical novae.

The disk instability mechanism (DIM; for a review see Hameury 2020) occurs in a subset of CVs called dwarf novae (DNe) and in most XRBs that accrete material through Roche lobe overflow – mainly low-mass X-ray binaries (LMXBs). In these systems, mass is transferred at a relatively constant rate from a non-degenerate donor star through Roche lobe overflow onto an accretion disk around the compact object. In quiescence, the mass transfer rate through the disk onto the compact object is low, the disk itself is cold and not ionized, and the system is faint. In this state, matter builds up in the disk and the temperature rises, until a critical point is reached and an outburst starts. In outburst, the mass transfer rate through the disk is greatly increased and the disk itself is extremely bright.

Although the DIM works well in explaining the basic properties of these outbursts, it is clear that more ingredients are necessary to match the observations – most importantly, irradiation of the disk and outflows. Powerful disk winds are launched in the high state of these outbursts (Fender & Belloni 2004) and these winds carry away a significant amount of mass and angular momentum. Indeed, most of the transferred mass from the star never gets accreted onto the compact object. In this way, winds can fundamentally change the evolution of these systems.

The wind launching mechanisms for both XRBs and DNe are still very poorly understood. Line-driven winds are one of the candidates (Proga & Kallman 2002), especially for disk winds in XRBs with high mass accretion rates. Thermal winds (Begelman et al. 1983) and magnetic winds (Ferreira & Pelletier 1995; Petrucci et al. 2008; Begelman et al. 2015) likely also play a role. More observations are needed to determine which mechanism dominates in different regimes.

Outflows from accretion disks of DNe are best studied in the UV, specifically UV spectroscopy. *HST* has provided some UV spectra of LMXB outbursts and DNe, but generally only one per outburst (e.g., Sion et al. 2004; Merritt et al. 2007). In fact, due to the fact that *HST* cannot perform very fast ToOs, the DNe outbursts were only caught by accident. *UVEX*, which will be able to repoint on ∼hour timescales, will be far better able to catch these outbursts. By obtaining multiple UV spectra over the course of DN and LMXB outbursts, coordinated with multi-wavelength follow-up, we will be able to study the launching mechanism of the winds and their relation to the jet.

The second type of outburst we discuss is classical novae, outbursts driven by runaway thermonuclear burning of hydrogen accreted onto the surface of a white dwarf from a binary companion (Bode & Evans 2008, Della Valle & Izzo 2020, Chomiuk et al. 2020). Although known for centuries, our understanding of these explosions has undergone a renaissance in the last decade – beginning with the discovery of γ-ray emission (by *Fermi*, Abdo et al. 2010) and correlated optical–γ-ray variability (Li et al. 2017, Aydi et al. 2020), bright radio synchrotron emission (Weston et al. 2016a, Weston et al. 2016b), and hard X-ray emission (Nelson et al. 2019, Sokolovsky et al. 2020). Together, these observations provide evidence of internal shocks between multiple outflows that can power a substantial fraction of the optical luminosity of novae.

Although the basic picture of shocks between multiple outflows explains several multi-wavelength aspects of nova observations, a consistent picture remains elusive,

particularly as some do not exhibit correlated optical-γ-ray behavior (Li et al. 2020). However, the shock interaction region between fast polar and slower equatorial outflows may be an ideal environment for the formation of dust (Derdzinski et al. 2017). A powerful testable consequence of this scenario is the predicted i) viewing angle dependence of multi-wavelength evolution and the formation of dust in novae and ii) variations in the shock and dust formation properties as a function of the underlying white dwarf mass, which drives the amount of mass ejected and the photometric evolution of the nova (della Valle et al. 1992, Yaron et al. 2005).
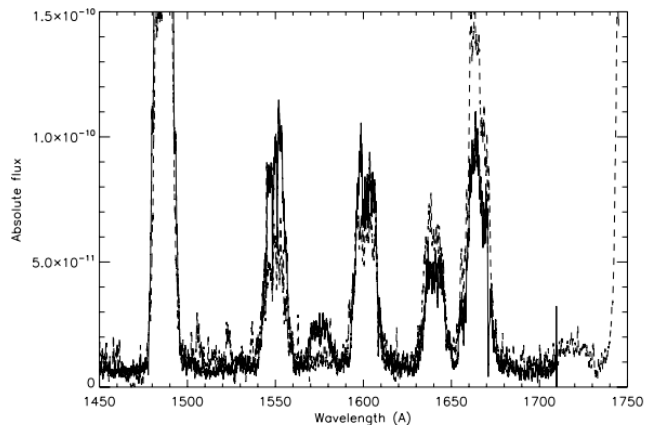
Figure 20. Comparison of the UV spectra of Nova Mon 2012 (solid) and Nova V1974 Cyg (dashed), taken from Shore et al. (2013).

UV spectroscopy is powerful in that the strongest lines of C, N, Ne, Mg that are produced in the ejecta are in that wavelength range (Shore 2012). These lines can be used to trace the ejecta density profiles, clumping, and filling factor to derive accurate ejection masses. Due to limited ToO capabilities, *HST* and *IUE* have provided a limited number of UV spectra of only the brightest and most nearby novae. Figure 20 presents two *HST* spectra of novae, showing a diversity of line profiles. The line profiles can further be used to estimate the ejecta geometry and density profiles (e.g., Shore et al. 2013). Combining the density and structure diagnostics to map out the variation in the multi-wavelength emission (radio, γ-rays) together with the ejecta dynamics/geometry and white dwarf mass of the nova. will allow us to develop a holistic picture of mass ejection in nova outbursts. Based on current estimates of the nova rate in the Milky Way (De et al. 2021) and the Magellanic Clouds (Mróz et al. 2016), a total of ∼10 novae are expected to be accessible for UV spectroscopy during the *UVEX* 2-year baseline mission (accounting for Galactic extinction).

4.1.3. *White Dwarf Companions*

Historically, identifying stellar binaries and obtaining the time series imaging and spectroscopy necessary to fully characterize these systems has been observationally taxing. However, modern all-sky imaging surveys (e.g., *Gaia*, *Kepler*, *TESS*) that provide high precision photometry and astrometry as a function of time have revolutionized our understanding of 'vanilla' low-mass binaries (e.g., two comparably low-mass main sequence stars), as well as facilitated the discovery of a small number of more exotic systems (e.g., main sequence-white dwarf binaries). Similarly, ground-based optical spectroscopy has helped to characterize a small set of these systems in the Milky Way, but numbers remain small. Concerted efforts for large-scale optical spectroscopic identification of such binaries is only getting underway (SDSS-V, DESI, WEAVE, 4MOST).

Despite progress with optical binaries in the Milky Way, there remains very little exploration of binary systems with a hot component (e.g., systems with OB stars, stripped stars, white dwarfs). In many cases the hot companion is virtually impossible to discern with optical observations. Single hot companions may not affect the optical spectra or perhaps only leave indirect trace signatures (e.g., odd optical emission line combinations) in the otherwise normal spectrum of the optically dominant star.

In other cases, even when a binary system is identified (e.g., from optical light curves or spectra), key aspects of the system (e.g., mass loss, wind speeds) or basic characteristics of the hot component (e.g., mass, temperature) are only accessible in the UV, wavelengths at which few observations exist. Thus, though we now believe some of the most influential astrophysical phenomena originate from hot star binary systems, our census and physical understanding of these systems is lacking.

In addition, binaries born as two AFG-type stars will go through a phase where the more massive star has already evolved into a white dwarf, whereas its companion is still on the main sequence. At optical wavelengths, the white dwarf is totally swamped by the companion, but it dominates the UV emission of the system.

The *UVEX* all-sky survey will identify ∼10,000 FGK-type stars that exhibit a UV excess indicating the presence of a white dwarf companion that is undetectable at optical wavelengths. Some pilot studies have been carried out with *GALEX* (Parsons et al. 2016), but many of the nearby FGK-type stars were too bright for *GALEX*. The *UVEX* detectors do not have a bright source limit. Moreover, *UVEX* will increase the FUV footprint with respect to *GALEX* by 50%. This will allow an unbiased statistical study of the population of these binaries within the Milky Way. This will both enable a full all-sky search for white dwarf + FGK binaries, as well as allow the identification of the closest systems, hence those most suitable to detailed follow-up studies.

The key parameters for the future outcome of white dwarf + FGK-type binaries are the masses of both stellar components as well as their orbital period. Whereas the mass of the main sequence star and the orbital period can be obtained from optical photometry and spectroscopy, measuring the white dwarf mass can only be done in the FUV. *HST* has observed ∼25 white dwarf + FGK binary candidates, confirming a white dwarf component in most of them. However, a population study that is sufficiently large to sample the full parameter space of stellar mass and orbital period requires a dedicated survey that is beyond the limited resources that are left to *HST*. *UVEX* will enable a population study that spans the full parameter range in stellar mass and orbital period, which is essential to establish tight observational constraints on the branching ratio of these systems with respect to their future evolution (Figure 16).

Low-resolution ($R \sim 1000$) spectroscopy covering 1150–1800Å is essential, as the Stark-broadened photospheric Lyα is sensitive to both the temperature and the surface gravity of the white dwarf, and, in conjunction with a mass-radius relation, provides a measurement of the mass. Detection of emission lines, primarily C IV 1550Å, will be a signature of ongoing mass transfer (e.g., Parsons et al. 2015). The main-sequence masses and orbital periods can be established from optical data, and hence those two components of the parameter space can be mapped out in advance of the *UVEX* survey. However, the properties of the white dwarf will be unknown prior to *UVEX* spectroscopy. A *UVEX* spectroscopic sample can then be used to extrapolate to the full, unbiased all-sky population established from the *UVEX* imaging, which in turn will put tight constraints on the low-frequency gravitational background of double-degenerates descending from white dwarf + FGK binaries, as well as on rates of the various subtypes of thermonuclear supernovae.

4.1.4. *Evolution of Angular Momentum of Stars Across the HR Diagram*

The typical story of a star's life begins with the Jeans collapse of a molecular cloud, before eventually contracting onto the Zero Age Main-Sequence (ZAMS). Conservation of angular momentum suggests that ZAMS stars have measurable rotation rates stemming from the initial angular momentum of their respective parent molecular clouds. However, observations show that there is a strong separation between fast and slow rotating stars at a temperature of $\sim 6200\ K$. This separation, com-

monly referred to as the Kraft break, represents a rough boundary between stars with radiative envelopes and stars with convective envelopes (Kraft 1967).

The Kraft break highlights the significance of convective envelopes to angular momentum evolution in stars as they are essential to powering dynamo action, which generates the self-sustaining magnetic field that steals angular momentum via interaction with stellar winds (Weber & Davis 1967). This connection ties a star's rotation to both its magnetic field and its age, both of which are notoriously difficult to characterize. In general, magnetic activity and age are quantified in terms of angular momentum using rotation-activity relations and gyro-chronology, respectively.

Empirical rotation-activity relations come in several forms, one of which is a comparison of UV emission to rotation period. Stelzer et al. (2016) attempted to derive a UV rotation-activity for M dwarfs using *GALEX* photometry and *Kepler* rotation periods to better understand fully convective dynamos, but was limited by a lack of observations and commented that follow-up UV observations would be a powerful constraint for a M dwarf rotation-activity relation. Additionally, Dixon et al. (2020) found rotation-activity relations for giants using *GALEX* and APOGEE, but also suffered from a lack of fast rotating stars.

With significantly improved angular resolution and greater sensitivity than *GALEX*, *UVEX* presents an opportunity to derive well constrained UV rotation-activity relations. This is especially true as an increasing number of stellar rotation periods are becoming available from large-scale time-series surveys. ESA's approved *PLAnetary Transits and Oscillations of stars* (*PLATO*) mission, with a targeted launch date in 2026, will support *UVEX* in this science by delivering ultra-precise optical light-curves for more than 2 million FGK dwarfs and subgiants and nearly 300,000 M dwarfs (Montalto et al. 2021).

Finally, it should be possible to associate large numbers of these stars with space-based rotation and activity measures to regions of the Galaxy with well estimated ages, including the recently identified stellar "strings" that represent coherent stellar populations spanning large regions of the Galaxy (e.g., Kounkel et al. 2020). This will allow the development of robust rotation-activity-age relations for stars across the HR diagram, and in turn allow the mapping of stellar ages across large swathes of the Milky Way.

4.1.5. *Lower-metallicity Massive Stars in the Local Group*

Despite their importance to wide-ranging next generation astrophysics (e.g., as discussed in Section 3.1.3 and illustrated in Figure 11), theoretical models for massive stars remain essentially untested below the metallicity of the SMC. The requirement of deep spectroscopy for individual resolved massive stars severely limits the environments to which this stellar calibration work can be applied. Early results from Wolf–Lundmark–Melotte and IC 1613 identified these galaxies as likely SMC-like in stellar abundances, stymieing the first attempts to measure mass-loss rates at lower metallicity (e.g., Bouret et al. 2015). While challenging at $\gtrsim 1$ Mpc, the dwarf irregulars Leo A (e.g., Cole et al. 2007), the Sagittarius Dwarf Irregular Galaxy (SagDIG; Garcia 2018), and Sextans A (Camacho et al. 2016, Garcia et al. 2019a) harbor populations of massive stars that are likely our best hope for calibrating stellar models at metallicities below the SMC. As for stars in the SMC and LMC, UV is crucial to characterizing these stars and their winds (Section 3.1.3). But while *HST* has begun the work of collecting spectra for these foundational targets, the resolution, sensitivity, and wavelength coverage are of varying utility for characterizing winds and photospheric abundances, and many other potential targets await a dedicated UV survey.

UVEX has the capabilities to fulfill the promise of these metal-poor dwarf irregular galaxies for massive star model constraints. First, all-sky photometry will immediately provide the most complete picture of unobscured sub-SMC metallicity massive stars in the Local Group, where *GALEX* is severely limited by crowding and *HST* NUV coverage is incomplete (Figure 21). Compared to previous work restricted to optical selection, deep *UVEX* imaging will substantially improve the census of luminous blue stars in these galaxies, especially very hot metal-poor stripped binary products.

UVEX spectroscopy will provide the capabilities for the first systematic investigation of stellar wind strengths at sub-SMC metallicity. Exposures of order 3–30 ks will suffice to provide detailed constraints on the resonant wind complexes and photospheric indices discussed in Section 3.1.3, enabling unique measurement of wind terminal velocities and mass loss rates unavailable from the optical, as well as quantities such as clumping filling factor, temperatures, and abundances. Approximately ten targets without UV data have already been identified with extant published optical spectroscopy (seven O to early-B giants in Sextans A from Camacho et al. 2016 and Garcia et al. 2019a; 2–3 OB stars in SagDIG from Garcia 2018). *HST* will deliver UV spectra over part of the needed wavelength range for a total of 12 OB stars below SMC metallicity (eight in Sextans A, three in Leo A, and one star in Leo P). *UVEX* will improve upon the resolution, coverage, and SNR of
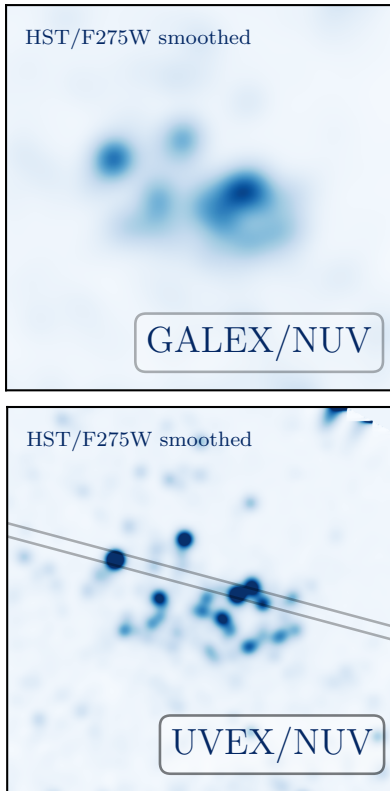
Figure 21. *UVEX* will provide access to individual massive stars in the distant, low-metallicity dwarf irregular galaxies such as Sextans A ($D \sim 1.2$ Mpc). Both full-field imaging from the all-sky survey and deep spectroscopic followup of the most UV luminous stars will yield unique constraints on young stellar populations below the metallicity of the SMC.

these spectra where they may be insufficient to measure robust wind properties (e.g., Garcia et al. 2019b). Though not part of the prime mission, a spectroscopic survey with *UVEX* would be able to, at a minimum, more than double the sample of sub-SMC massive stars with UV wind constraints.

4.2. *Galactic Archaeology*

UVEX provides a facility for mapping the Milky Way and nearby galaxies in the UV, providing insight into the distribution and physical properties of dust and precise measurements of stellar metallicity from photometry.

4.2.1. *Milky Way Dust Maps*

Many areas of extragalactic science require high-precision maps of dust extinction and reddening at high Galactic latitudes. Maps based on far-IR (FIR) dust thermal emission are widely used (e.g., Schlegel et al. 1998, Planck Collaboration et al. 2014), but suffer from a number of systematics. More concretely, these maps only trace dust extinction indirectly, and systematic er-

rors can be introduced by incorrect modeling of dust temperature, spectral index, or column density, or by variations in the ratio of dust extinction at optical wavelengths to thermal emission in the FIR. In addition, dust maps based on FIR emission are contaminated by large-scale structure (through dust emission in distant galaxies; see Chiang & Ménard 2019), which is of particular concern for cosmology.

Dust maps based on optical and near-IR stellar photometry (e.g., Marshall et al. 2006, Green et al. 2015, Juvela & Montillaud 2016) more directly measure dust extinction and reddening, and are thus less affected by these systematics. However, dust maps based on stellar photometry typically achieve lower signal-to-noise ratios than FIR emission-based maps at high Galactic latitudes, where the sky density of stars is lower and per-star extinction is lower.

At high Galactic latitudes, it is therefore critical to observe stellar photometry in the UV. The UV colors of stars are extremely sensitive to small amounts of dust, and can thus boost the SNR of per-star reddening measurements. Recent work using *GALEX* photometry in combination with LAMOST spectroscopy has mapped extinction at high Galactic latitudes (Sun et al. 2021). *UVEX* will expand the number of stars with UV photometry by a factor of ~ 5 relative to *GALEX*, enabling the creation of dust extinction maps with higher resolution and higher signal-to-noise.

4.2.1.1. *LMC and SMC*

Dust extinction laws exhibit striking variations depending on dust chemistry and the interstellar environment (Figure 22). A well-known example is variation in dust extinction curves along different sight lines in the SMC (Gordon et al. 2003).

The origin and extent of variations in dust extinction is poorly understood. This is particularly true at UV wavelengths. While the optical extinction law is well-characterized by a single parameter, $R\left(V\right)$, the UV extinction law exhibits more variability, which is only weakly correlated with $R\left(V\right)$ (Peek & Schiminovich 2013). In the UV, the NUV-band extinction is sensitive to the strength of the 2175 Å bump, thought to be carried by polycyclic aromatic hydrocarbons (PAHs) or graphite grains (Draine 2003), while the FUV-band extinction is sensitive to the slope of the far-UV rise, driven by very small grains (Mishra & Li 2015).

The gold standard for measuring dust properties is UV spectroscopy. Because shorter wavelength light is more easily scattered by dust, the amount of extinction as a function of wavelength, along with other variation (e.g., the 2175 Å bump) are the empirical anchors
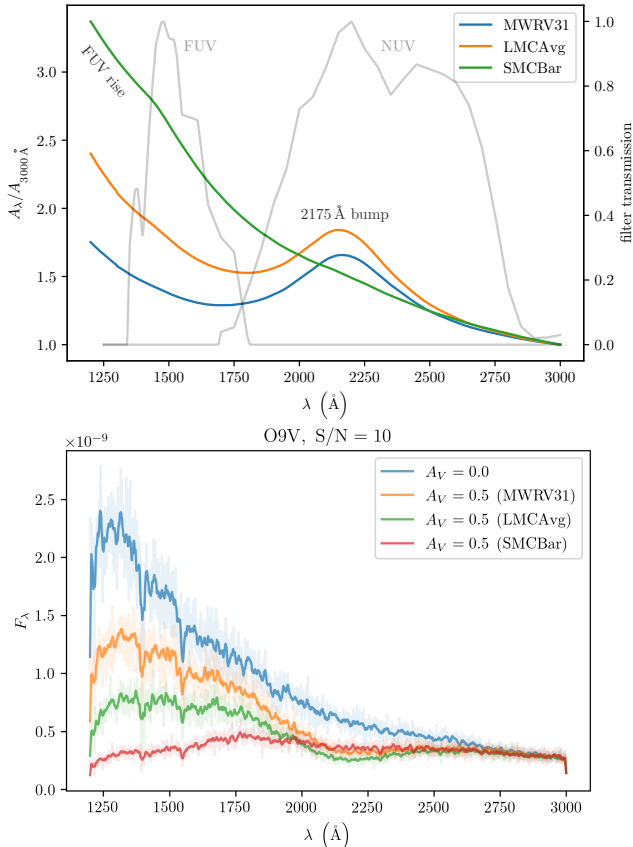
Figure 22. (Top) Three representative dust wavelength-extinction relations, from the Milky Way ($R(V) = 3.1$), the LMC, and the SMC bar. The *UVEX* NUV/FUV-band transmission curves are overplotted. Extinction in the NUV band is primarily sensitive to the strength of the 2175 Å bump, while extinction in the FUV band is primarily sensitive to the slope of the FUV rise. (Bottom) The effect of different dust extinction laws on an O9V-star spectrum, observed at a native signal-to-noise ratio of 10 (shaded curves), and then smoothed to *UVEX* resolution to show that coarse features are clearly discernible. The lack of a 2175 Å bump and strong FUV rise in the SMC bar extinction law are readily apparent.

for our knowledge of the UV extinction laws. Within the Galaxy, the UV extinction law, and its relation to dust physics, has been measured from UV spectroscopy from samples of a few hundred stars (e.g., Fitzpatrick & Massa 2007, Fitzpatrick et al. 2019, Massa et al. 2020). Far less is known about UV extinction laws at sub-Solar metallicities. The commonly used LMC and SMC dust curves are determined from averaging over a small number of sight lines, which exhibit substantial variance.

UVEX spectroscopy of 1000 hot OB type stars in the LMC and SMC will provide qualitatively new insights into the UV extinction curve at sub-Solar metallicities. For example, the average SMC UV extinction curve ex-

hibits no 2175 Å bump. However, the bump is present in a handful of sight lines with UV spectroscopy in the wing of the SMC (Cartledge et al. 2005, Li et al. 2006). The precise carrier of the 2175 Å bump has not yet been determined, though PAHs are a candidate (Li 2020). A census of the precise properties (amplitude, central wavelength and width) of this feature in a variety of interstellar environments (e.g., different metallicity and interstellar radiation field) will limit the range of possible physical models of interstellar dust at low metallicity (e.g., Draine 2003, Hensley & Draine 2021). By piggybacking off of *UVEX* spectroscopic surveys of O-stars in the LMC and SMC (see Section 3.1.3), we can expand this sample by ∼1000 stars. Because dust affects the broad UV spectrum, even fairly low-SNR (≈ 10) and moderate-resolution ($R \sim 1300$) spectra obtained by *UVEX* are well-suited for measuring variations in the UV dust extinction curve in the SMC and LMC.

4.2.2. *Metallicity Mapping in the Milky Way*

The resolved stellar populations of the Milky Way encode its formation history. The stellar halo of the Milky Way, in particular, hosts a wide variety of substructure, such as streams, globular clusters, and disrupted dwarf galaxies, accumulated through a combination of *in situ* star formation and accretion (e.g., Helmi et al. 1999; Helmi 2008; Bland-Hawthorn & Gerhard 2016). A key diagnostic for unraveling the formation history of the Milky Way is stellar metallicity since metallicities of individual stars can be used to identify substructures and infer chemical enrichment processes. Metallicities are typically derived from iron lines in optical spectroscopy, and dedicated surveys (e.g., APOGEE, LAMOST, GALAH, 4MOST, *Gaia* radial velocity survey; e.g., Deng et al. 2012, De Silva et al. 2015, Majewski et al. 2017) will provide such measurements for ∼ 30 million stars – a small fraction of the >1 billion Milky Way stars surveyed by *Gaia* given the flux limits of spectroscopic surveys.

Photometric metallicities offer access to a much larger population of stars. Measuring a photometric metallicity usually involves combining UV/u-band imaging with an optical band. UV wavelengths are particularly metallicity sensitive (capturing, e.g., the Balmer break and iron line blanketing in the mid-UV) when combined with optical imaging. For example, the UV color excess method (Carney 1979) takes advantage of the metallicity dependency of $u - g$ color at constant optical color. Using this method, SDSS mapped the metallicity of a volume-complete sample of two million F/G dwarfs in the Milky Way disk and halo, with typical uncertainties of 0.2 dex in [Fe/H] (Ivezić et al. 2008). These to-
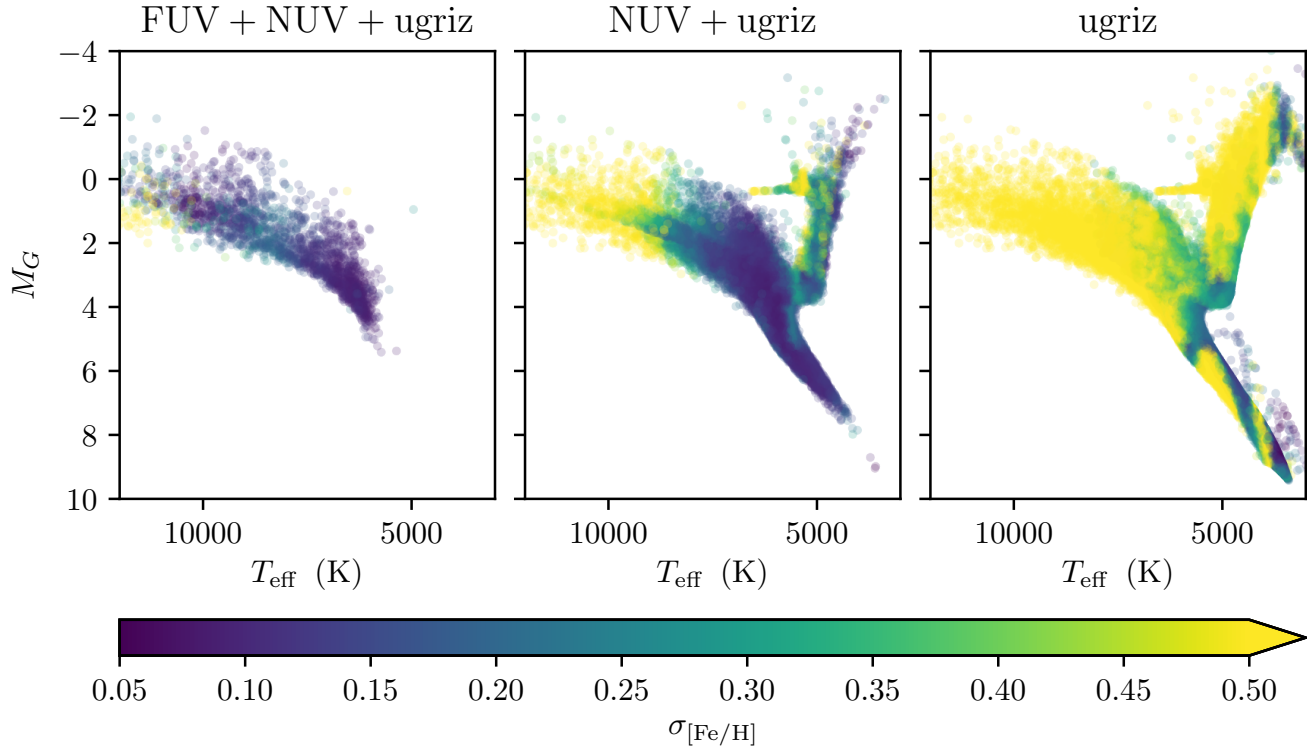
Figure 23. Cramér-Rao bounds on the uncertainties (i.e., the theoretical precision) in [Fe/H] obtained using different combinations of *UVEX* and Rubin band photometry, assuming photometric uncertainties of 0.02 mag. Though *UVEX* detects fewer low-temperature stars than Rubin, it will achieve lower uncertainties in [Fe/H], particularly for hot (and therefore preferentially young) stars.

mographic maps of Milky Way stellar metallicity were a boon to Galactic archaeology, identifying chemically distinct subcomponents within our Galaxy.

Combined with Rubin optical photometry in the Southern Hemisphere and PS1 optical photometry in the Northern Hemisphere, *UVEX* will allow an even more sensitive determination of stellar metallicity. Although FUV-NUV color alone is not sufficient to determine metallicity, the combination of *UVEX* photometry and optical colors will allow a much more sensitive determination of stellar metallicity than possible with optical data alone. Specifically, NUV$-g$ color is far more sensitive to metalicity than $u - g$ color. Because the *UVEX* all-sky survey is slightly shallower than the Rubin u-band, it will observe fewer stars than Rubin. However, *UVEX* will obtain much more precise metallicities per star, particularly for hot stars (see Figure 23). *UVEX* will obtain NUV photometry of ∼300 million Milky Way stars, probing a significant fraction of the entire Galaxy (see Figure 24).

4.3. *Galaxy Formation*

One of the primary motivators in extragalactic astronomy is to understand how galaxies form and evolve over cosmic time. This is an enormous enterprise that has spanned decades, engaged hundreds if not thousands of astronomers world-wide, and occupied major fractions of observing time on the ground and in space. While much is known, next-generation surveys could revolutionize our understanding of the field if and only if they exploit the full power of the electromagnetic spectrum. UV imaging and spectroscopic surveys are an essential component of this revolution. This is because the UV measures SFR averaged over a timescale which is matched to evolutionary changes in galaxies, ∼ 100 Myr. Optical probes such as Hα are noisy averages of only ∼ 10 Myr, while IR traces reprocessed UV radiation in massive, metal-rich galaxies. UV is uniquely sensitive to the lowest mass, lowest metallicity systems that are virtually dust-free (Fisher et al. 2014) and represent analogues to the first galaxies (Figure 25). The UV also cleanly probes small amounts of residual star formation in otherwise passively evolving galaxies, essential for understanding how and why galaxies quench individually and collectively (Figure 26). UV spectroscopy probes key elements including carbon, whose abundance is otherwise poorly constrained. UV spectroscopy also provides unique access to signatures of the circumgalactic
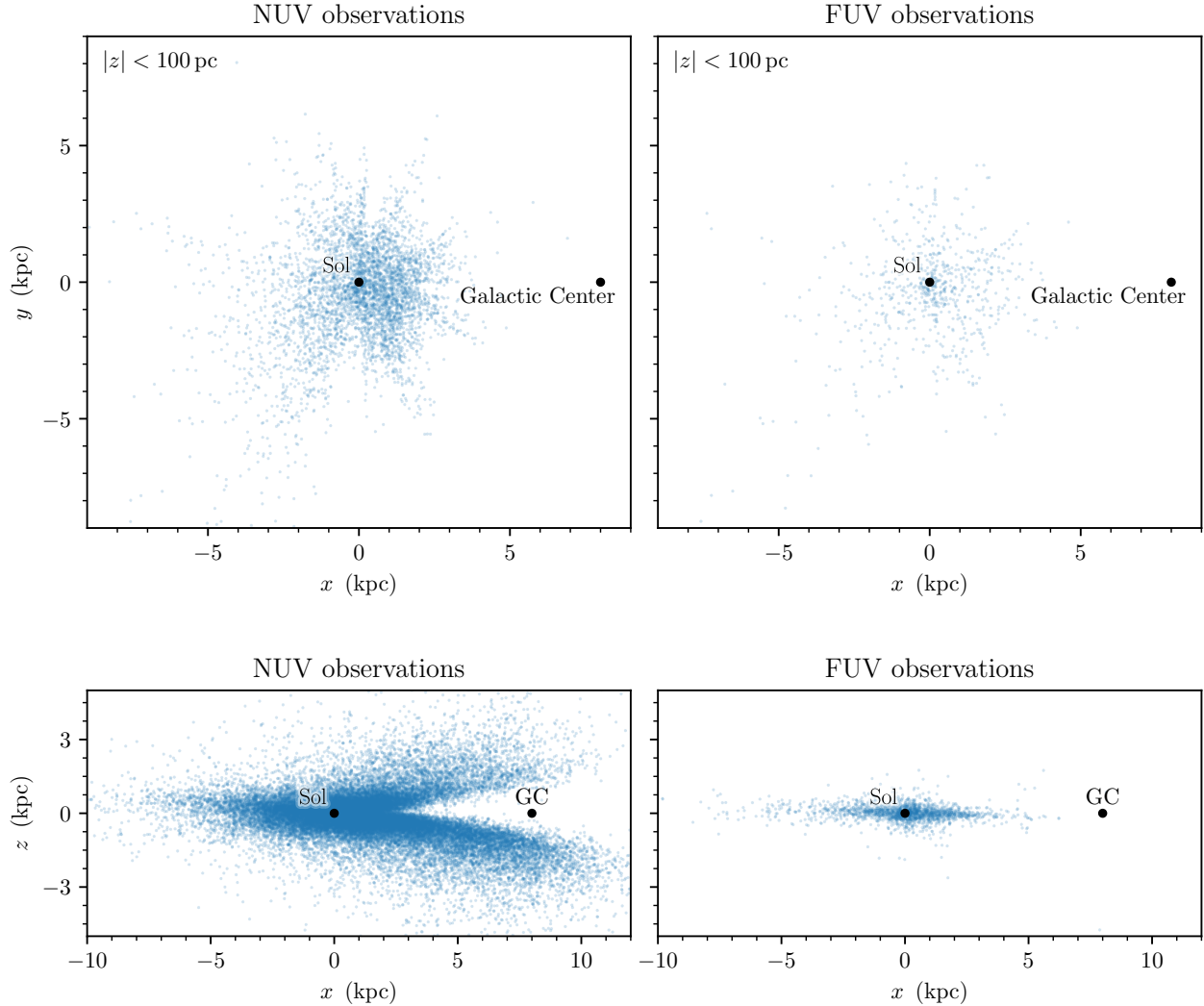
Figure 24. Expected spatial distribution of Milky Way stars observed by *UVEX*. The top panels show a bird's-eye view – centered on the Sun – of stars within 100 pc of the mid-plane of the Galaxy that would be observed in the NUV (left) and FUV (right) bands. The bottom panels show the distribution of stars that would be observed in these two bands, projected onto the (x, z)-plane (in Cartesian Galactic coordinates, centered on the Sun). As can be seen from these panels, *UVEX* will observe stars through a large volume of the Milky Way, extending several kiloparsecs along sight-lines that do not pass through the inner Galaxy.

medium (CGM) and feedback-driven outflows in nearby galaxies including through Lyα and metal absorption lines, processes which lie at the heart of our modern understanding of galaxy evolution. In this Section, we discuss the potential applications of a UV imaging and spectroscopic survey mission on Galaxy Formation, Galaxy Evolution, and Galaxy-Halo Co-evolution.

4.3.1. *The Galaxy "HR-Diagram"*

A fundamental tool for probing galaxy evolution is the UV-optical color-magnitude diagram (UVOCMD; Figure 27). The extinction-corrected UVOCMD is often viewed analogously as a galaxy "HR-diagram" (GHR),

because the optical/NIR magnitude traces stellar mass (M_*), and the UVO color (e.g., NUV-r) traces specific star formation rate (sSFR) to remarkably low levels. The long-term buildup of stars moves galaxies to the right. New star formation bursts move galaxies up, while quenching moves them down. Thus we can trace on this diagram the influence of the manifold processes driving galaxy evolution.

The *GALEX* mission and NASA Great Observatories provided a huge leap forward in our understanding of galaxy formation and evolution. We now know that the galaxy distribution can be described to first order as bimodal (i.e., either red or blue), with a population

Low Surface Brightness Gals. **Dwarfs, Low Mass Gals.** **Extended UV Disks**
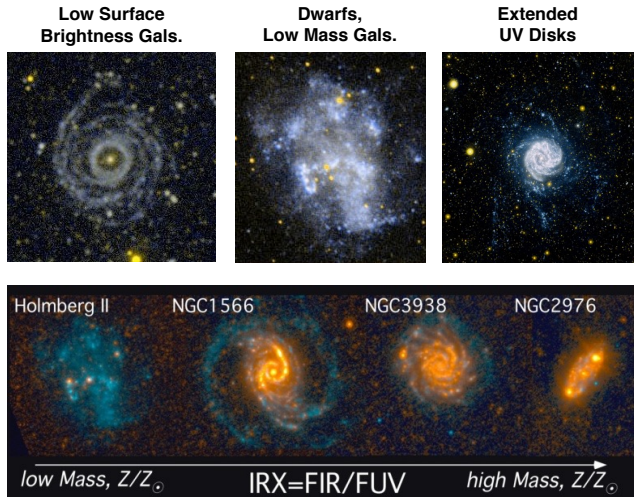
Figure 25. Low mass star forming galaxies are highly visible in the UV because their metallicity and extinction are low, and the UV sky is dark.

of transitional galaxies in the so-called "Green Valley" between the actively star-forming blue cloud galaxies and the passively evolving red sequence systems (Wyder et al. 2007; Schiminovich et al. 2007; Martin et al. 2007a; Martin et al. 2007b). The UVOCMD that first identified this bimodality and the intermediate green phase can also be extended beyond the low redshift galaxies observed by *GALEX* into higher redshift regimes to help explore evolution over time. As large populations of galaxies at higher redshifts have been added to the UVOCMD from more recent surveys (e.g., Ilbert et al. 2013), we can now state that the mass fraction of galaxies in the red sequence vs. the blue sequence has grown by a factor of at least ~ 3 since $z \sim 1$. This indicates that there is a global evolution over the last ~ 8 Gyr of cosmic time that we are only just beginning to understand and characterize. A new generation of galaxy studies anchored by the *UVEX* photometric and spectroscopic surveys would enable us to directly measure the evolution of galaxies across the GHR. These data will directly address three key questions: 1) What equilibrium processes create the star formation "main-sequence"? 2) What processes drive galaxies out of equilibrium leading to star formation "quenching"? and 3) How do galaxy halos and galaxies co-evolve, and how does this co-evolution govern galaxy evolution?

4.3.2. *The Star Formation Main Sequence*

Star forming galaxies form a tight "main sequence" with SFR proportional to stellar mass (Noeske et al. 2007; Wyder et al. 2007; Salim et al. 2007): the star formation main sequence (SFMS). To understand why,

we need to understand the processes driving a return to equilibrium when galaxies are perturbed by mergers/accretion/gas exhaustion. The responsible processes likely include galactic winds/fountains, accretion of new gas, and adjustments in the star formation efficiency in star-forming (SF) regions. Untangling these influences requires a large sample of SF galaxies that can be split into subsamples based on e.g., mass, deviation from the main sequence, and environment. The combination of FUV/NUV and optical/IR photometry and targeted spectroscopy allows determination of recent SF history, which probes deviations and returns to equilibrium.

Key to this investigation is the power of combining integral and differential constraints on evolution, which can only be accomplished with very large and homogeneous photometric samples spanning the UV/O/IR. The growth of stellar mass in galaxies is an integral constraint, while the SFR history is a differential constraint (Madau & Dickinson 2014). The UVOCMD vs. redshift is an integral constraint, while a measure of the flux of galaxies across the UVOCMD provides the next level of differential constraint (Martin et al. 2007a; Martin et al. 2017; Darvish et al. 2018; de Sá-Freitas et al. 2021). By combining GHR integral and differential constraints with galaxy-halo connection methods (e.g., the Halo Occupation Distribution [HOD]), we can take a step towards the ideal of "watching" galaxies evolve by statistically weaving together the snapshots we observe. Because stellar and dark halo mass can only increase with time, and because the integral and differential constraints are linked by a continuity equation, we can begin to assemble an ensemble of individual galaxy star formation histories, and correlate these with halo mass and environment. This approach will provide a powerful new constraint on galaxy formation and evolution models and numerical simulations.

How does this work in the case of the SFMS? The best way to diagnose equilibrium processes is to observe them out of equilibrium, where they will be maximally subject to the return-to-equilibrium processes. If we consider galaxies on, below, and above the SF main sequence, the integral constraint comes from how many galaxies are in each bin vs. redshift. The differential constraint comes from how fast galaxies are moving between these states. The distribution in bursting "Star Formation Acceleration" ($SFA \equiv d(NUV - H)/dt \sim d(sSFR)/dt > 0$) and quenching ($SFA < 0$) gives the relative fraction vs. the speed of these processes. Fast bursting could be produced by mergers, and slow bursting by changes in gas accretion. Fast quenching could be produced by galactic winds evacuating the gas, while slow quenching by starvation of gas (accretion strangulation by hot gas
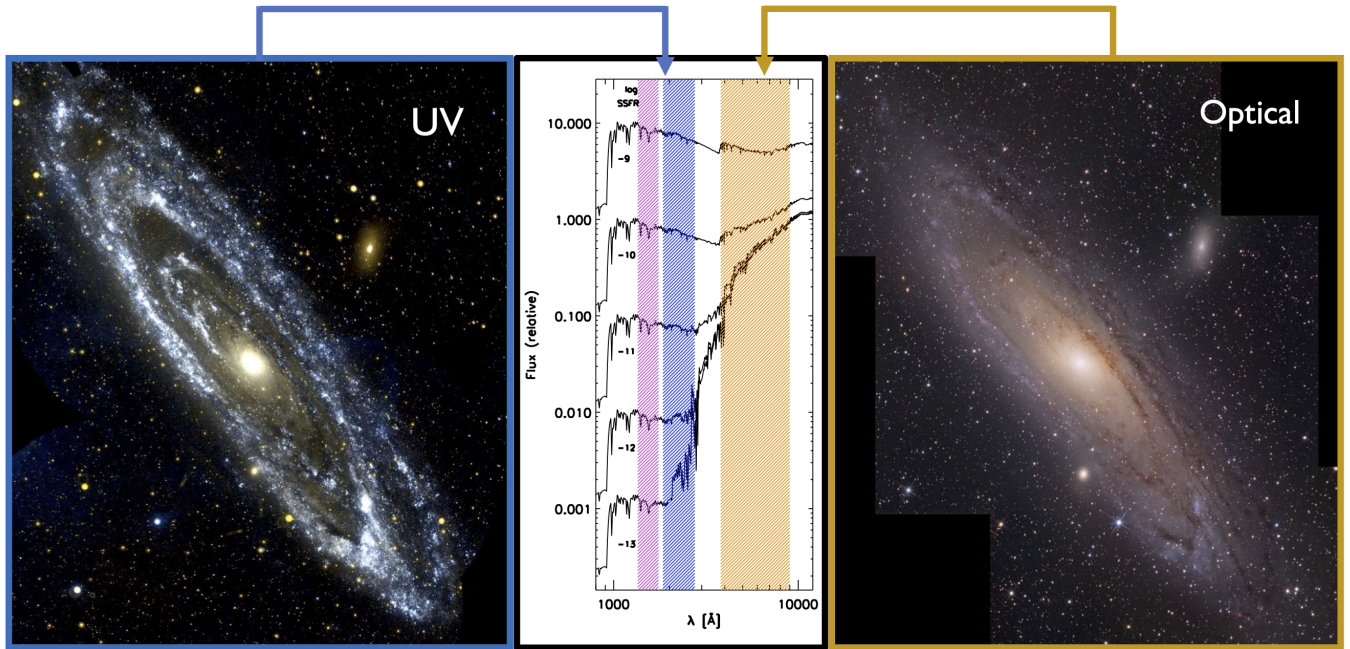
Figure 26. The optical band traces ∼ 1–5 Gyr of star formation history; UV traces 100–300 Myr, and can measure small amounts of residual star formation superimposed upon old stellar populations [image credits: M31 optical: Adam Block/NOAO/AURA/NSF; UV: *GALEX*/JPL/NASA].

or ram pressure/tidal stripping of satellites). Therefore the spread in SFR and the distribution in star formation acceleration give strong constraints on the equilibrium processes on the SFMS.

We do not know whether the lowest mass galaxies exhibit a SFMS, and what the dispersion around the relation is. It might be the case that very low mass galaxies have long periods of quiescence punctuated by SF bursts, as is suggested by resolved stellar photometry of nearby dwarf galaxies (Weisz et al. 2014a; Weisz et al. 2014b; Weisz et al. 2014c; Weisz et al. 2015). *UVEX* will supply the necessary sample to determine the star formation history in the lowest-mass galaxies in the universe. UV observations provide a direct measurement of SFR in these low mass galaxies because of their low mass, metallicity, and dust extinction.

4.3.3. *Cosmic Quenching*

Cosmic quenching has shut down star formation by more than an order of magnitude since $z \sim 2$. Quenched galaxies exist at all masses but dominate the high mass population. Yet this fundamental evolutionary process is still poorly understood. Why do most high mass galaxies quench? Why do some intermediate and low mass galaxies quench, while others do not? What are the physical processes responsible for quenching: merg-

ing, starvation/strangulation, stripping, feedback? How does quenching depend on halo mass, environment, position in the cosmic web, central/satellite identification? What causes rejuvenation in quenched galaxies?

The approach discussed in the previous section allows us to measure the flux of galaxies from the SFMS to the red sequence (quenching through the green valley, $SFA > 0$) and the flux of galaxies experiencing periods of rejuvenation (bursting, $SFA < 0$). The speed of quenching and bursting is determined by the physical processes at work, such as strangulation (slow) and mergers/AGN winds (fast). Combining the integral and differential constraints will test whether we have fully accounted for the evolutionary tracks of galaxies across the GHR. The distribution of star formation acceleration vs. position on the GHR, vs. environment (e.g., local density), AGN presence, and central/satellite status will provide powerful new constraints on models and simulations of galaxy quenching. The FUV and NUV provide the maximum leverage to study quenching because the UV traces SFR even for very low sSFR galaxies, where quenching has already begun. In other words, they magnify the green valley, where galaxies in transition reside.

4.3.4. *Galaxy-Halo Co-Evolution*
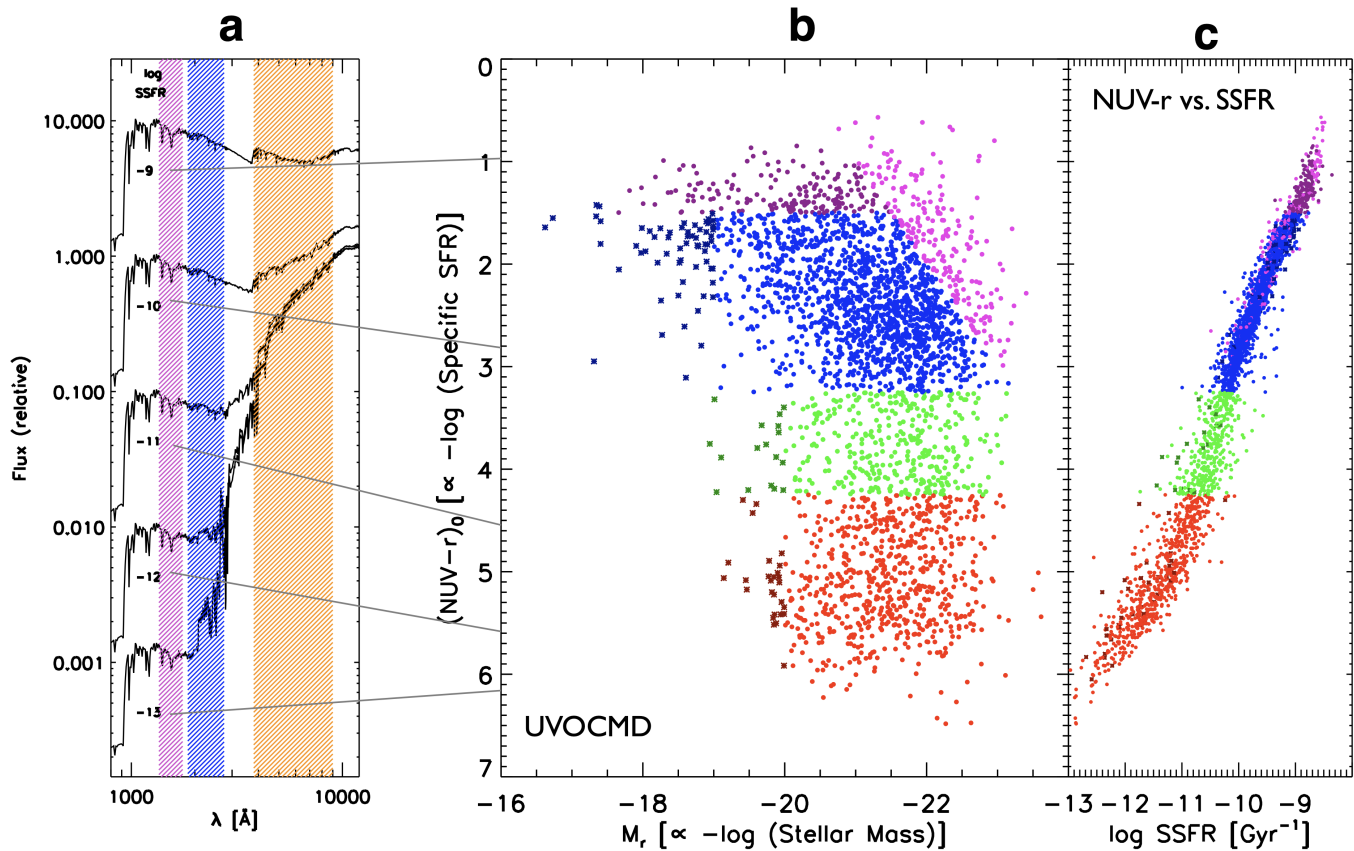
Figure 27. Galaxy HR Diagram constructed from mass-tracing optical/NIR color and FUV or NUV color. a) Old population with superimposed star-forming population with different specific star-formation rates (sSFR). b) Distribution of galaxies on the GHR showing the relation between star forming (main sequence) galaxies [blue], galaxies bursting above the SFMS [purple], transition galaxies [green], and quenched galaxies [red]. c) There is a tight correlation apparent between the extinction-corrected NUV-r color and sSFR.

Galaxy formation and evolution is governed by the flow of gas, metals, and energy into and out of the halo. Galaxy evolution is really galaxy-halo co-evolution. Most of the baryons in the universe are located in the halos and CGM of galaxies and the intergalactic medium (IGM; Tumlinson et al. 2017). The baryons required for star formation in galaxies are delivered through the halo and returned there by galactic winds. Thus, the SFMS and the causes of cosmic quenching may ultimately be tied to the flow of gas in the halo. A census of this halo gas vs. galaxy mass, star formation history, and environment is required to understand the co-evolution of galaxies and their halos.

Lyα is the most sensitive tracer of halo gas in emission. Lyα halos can be measured photometrically by stacking analysis of galaxies with redshifts that place Lyα at the peak of the FUV band (compared to neighboring redshifts). Because of its long slit and fast spectrograph design, and the fact that the spectrograph will be operating continuously during imaging exposures, *UVEX* will obtain serendipitous spectra of thousands of Lyα

galaxy halos, providing information about kinematics, inflows, and outflows. Lyα halo measurements can be stacked on galaxy properties on the GHR diagram in order to determine global scaling laws between halos and galaxies (Figure 28). The key observables are the Lyα luminosity (L_α), line profile (width, mean), and mass to light ratio (M/L_α). For example, low mass galaxies that are above and below the SFMS can be compared in M/L_α to determine the role of halo gas flows in maintaining main-sequence equilibrium. Quenching galaxies may show lower M/L_α than galaxies of the same mass on the SFMS. Metal lines (O IV, O VI, N V, C IV, C III], Si IV) may also be detected from warm baryonic halos.

4.3.5. *Tests of Fundamental Baryonic Structure Formation Processes*

In order to understand a fundamental astrophysical process such as star formation, it is critical to vary key parameters to extremes in order to explore how the process changes. In particular, the lowest mass, lowest metallicity, and lowest gas density regimes of star formation probe the impact of mass, metallicity, and density
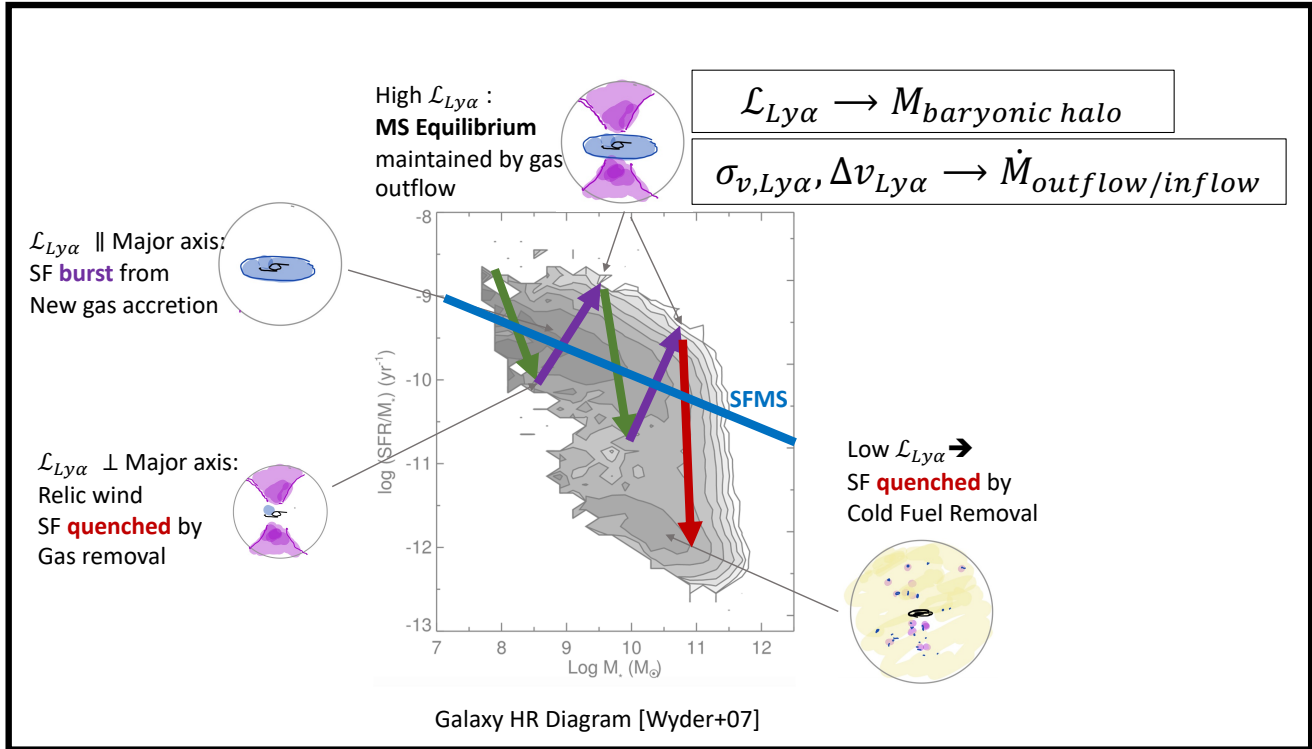
Figure 28. Galaxy HR diagram related to baryonic halo traced by Lyα . Halo Lyα luminosity gives baryonic halo mass, and line profile gives mass flux in outflows or inflows through the halo. *UVEX*-traced SFR and star formation acceleration give recent bursting/quenching history.

on this process. UV is unique in its ability to trace star formation in low mass, low metallicity, and low density regimes, providing key tests of star formation scaling laws, the IMF, and the root cause of low baryon efficiency and low metallicity in the lowest mass galaxies.

For example, *GALEX* discovered that many galaxies have "Extended UV" (XUV) disks (Thilker et al. 2005; Thilker et al. 2007; Lemonias et al. 2011), extended regions of low-density gas and star formation unlike the bulk of most disk galaxies. These extended regions may be produced by on-going accretion of gas from the IGM, and if so could be used to study the effects of IGM accretion on galaxy growth. XUV disks and low surface brightness galaxies are laboratories for studying the extreme low end of the Schmidt-Kennicutt star formation scaling law (Kennicutt 1998). *GALEX* showed that there is a sharp transition in the power-law Schmidt-Kennicutt dependence of SFR density with gas density (Wyder et al. 2009; Bigiel et al. 2008). Star formation continues, but the dependence is much steeper, suggesting a physical transition perhaps produced by the lack of dust and resulting low H_2 formation rate and H_2/H I fraction (Krumholz 2013). A deep *UVEX* survey would provide a definitive sample of low-mass galaxies and XUV disks, allowing the study of the most

extreme examples. Follow-up of these with long-slit UV spectroscopy would constrain stellar populations, star formation rate and history, metallicity, and dust content.

The IMF has been assumed to be universal based on relatively limited data. The high-mass end of the IMF may be particularly sensitive to key processes, since these low-probability objects require the most massive molecular clouds to form without the negative feedback of stellar winds. A powerful constraint on the high-mass end of the IMF comes from comparing Hα and UV luminosity, since the former traces the highest mass stars and the later traces high- to intermediate-mass stars. *GALEX* provided strong but not definitive evidence for a top-light IMF in low mass galaxies (Lee et al. 2009; Meurer et al. 2009b). The challenge in interpretation is that the burstiness of star formation history in low mass galaxies produces a noisy Hα/UV ratio which could be biased (Weisz et al. 2012). Hα and UV respond differently to dust extinction (Calzetti et al. 2000), which adds uncertainty and possible bias (Seibert et al. 2005; Johnson et al. 2007a; Johnson et al. 2007b; Salim & Narayanan 2020). However, with a large, homogeneous, multi-wavelength sample it should be possible to simultaneously solve the star formation history (SFH),
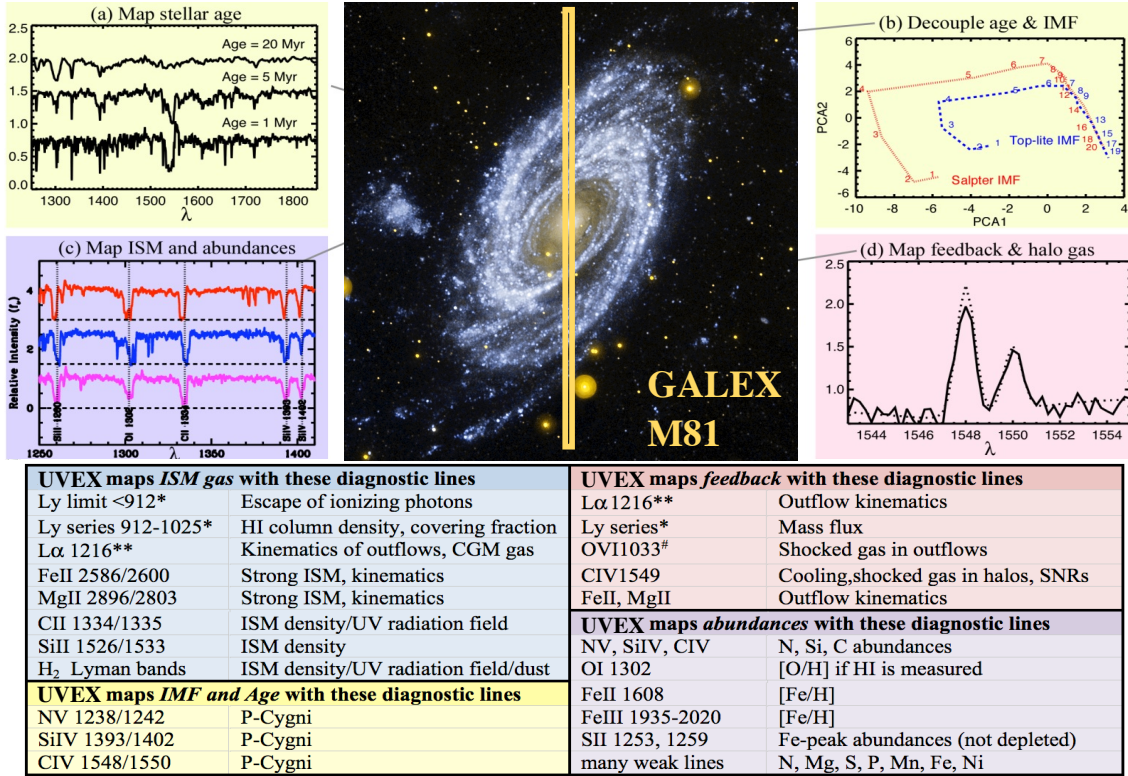
Figure 29. UV spectroscopy provides key physical diagnostics of galaxies, including metallicity (notably carbon), IMF, stellar age, and the presence of feedback. *UVEX* long-slit spectroscopy will provide exquisite spectra of nearby and distant galaxies in the FUV and NUV.

dust, and IMF problem using the connect-the-dots approach for SFH described above and recent techniques to constrain extinction and extinction laws (Salim & Narayanan 2020).

The lowest mass galaxies are also the least successful at making stars (lowest baryon-to-dark matter ratio) and at making (or keeping) metals. Since galaxies are as a whole inefficient at making stars, low mass systems are perfect laboratories for uncovering the processes which prevent efficient star formation and metal retention, determining the low-mass end of the baryon-to-dark matter efficiency relation (Moster et al. 2013) and the mass-metallicity relation (Tremonti et al. 2004). It should be possible to use a differential constraint on SFH, in combination with measurements of Lyα emission in low mass galaxy halos, to track the ebb and flow of star formation in low mass systems, and relate this to the feedback-driven outflows which are believed to be the root cause for the low baryon efficiency and metallicity of low mass galaxies.

A UV spectroscopic subsample of low mass galaxies and low density star formation regions would provide critical calibration of the photometric sample. With fast *UVEX* long-slit spectroscopy, it will be possible to measure UV spectra in low surface brightness conditions where star formation is below the canonical threshold. Spectroscopy provides critical diagnostics of stellar age, metallicity, feedback, and the IMF (Figure 29).

4.4. *Cosmic Explosions*

Supernovae (SNe; Branch & Wheeler 2017) play a major role in the structure and evolution of galactic ecology and thus constitute a vibrant research area of modern astrophysics. Stellar explosions inject energy, momentum and newly synthesized metals into the interstellar medium. With the recent discovery of kilonovae resulting from double NS coalescence (e.g., Margutti & Chornock 2020), astronomers now have a better understanding of how cosmic explosions contribute to the buildup of the periodic table.

We identify three main frontier areas in the field of stellar explosions. Firstly, massive stars that eventually undergo gravitational collapse (core collapse SNe) leave stellar residue in the form of NSs and BHs. The natal properties of neutron stars – rotation and magnetic field strength – appears to range over many orders of magnitude. Newly formed BHs can be born spinning slowly and dominated by fallback or spinning rapidly and gen-

erating tremendous amount of power via accretion of stellar debris. In either case, in some fraction of the events the central object injects power following the explosion (e.g., luminous magnetar or power generated by an accreting black hole), and the resulting supernova is distinct and bright. In fact, the spinning accreting black hole is an accepted model for GRBs (e.g., see Woosley & Bloom 2006; Hjorth & Bloom 2012; Cano et al. 2017 for reviews of GRB-SNe) and the magnetar model is a popular explanation for super-luminous SNe (SLSNe; see below) and might be behind some observational manifestations of "Fast and Blue Optical Transients" as well (FBOTs; see below).

Next, the structure and chemical composition of stars at the time of explosion, and their very recent mass-loss history in the final $\sim 0.1 - 100$ years before stellar death are among the least understood aspects of stellar evolution (e.g. Smith 2014) and have direct consequences on the explodability of a star (e.g., Janka 2017 and references therein). Specifically, a major open question is whether the physical origin of instabilities that act in the final moments of stellar life ($\delta t < 1$ yr) and that originate deep down in the stellar core (e.g., Quataert et al. 2016, Fuller & Ro 2018, Morozova et al. 2020, Leung & Fuller 2020; Wu & Fuller 2021) can trigger the most extreme episodes of mass loss in massive stars across the mass spectrum that we have just started to uncover with observations (for some examples see, e.g., Pastorello et al. 2013; Margutti et al. 2014; Smith 2014, Margutti et al. 2017, Bruch et al. 2021, Strotjohann et al. 2021; Jacobson-Galán et al. 2021). Extreme mass loss timed with core-collapse might play an important role in defining the thermal UV-optical emission of the emerging, albeit motley, class of FBOTs (Drout et al. 2014, Arcavi et al. 2016, Pursiainen et al. 2018, Ho et al. 2021a). From a different perspective, the non-thermal emission of long GRBs and FBOTs represents one of the few real-time observational manifestations of the compact object formed in core-collapse: the properties of their relativistic or sub-relativistic jets directly link back to those of the newly-formed neutron star or black hole (Margutti et al. 2019, Ho et al. 2019a, Ho et al. 2019b, Ho et al. 2020a, Coppejans et al. 2020, Perley et al. 2019, Perley et al. 2021a).

Last is our limited understanding of the progenitor star populations of several types of SNe. In particular, we lack a clear picture of the progenitors of Hydrogen-poor supernovae (which together comprise >50% of SNe by volume, Li et al. 2011), including normal core-collapse explosions and SLSNe (e.g., Quimby et al. 2013, Chomiuk et al. 2012). Similarly, a complete picture of the origin of SNe of Type Ia, which have been widely employed as cosmic distance ladders to reveal the accelerating Universe (Riess et al. 1998), continues to be shrouded (e.g., Maoz et al. 2014).

In summary, the past decade has uncovered a dizzying range of new phenomena, but our overall understanding of them is poor. This lack of understanding is significant, as it further impacts the estimates of the initial stellar mass function in galaxies and star formation through cosmic time (e.g., Smith 2014 and references therein). Stated succinctly: linking stellar progenitors to SN types and to their compact object remnants is a fundamental goal in modern astrophysics.

It is clear that further progress requires observational guidance, and indeed one of *UVEX*'s main science objectives is to perform follow-up spectroscopy of core-collapse supernovae (see Section 3.2.2). Below we outline further the ability of *UVEX* to advance our understanding of the phenomena and physics of the frontier areas discussed above. We first summarize the unique diagnostic value provided by UV spectroscopy (Section 4.4.1). We then discuss the key progress that will result from focused UV spectroscopic studies of the most common types of SNe (Section 4.4.2). We conclude with how the all-sky *UVEX* survey will naturally allow for exploration of exotica, in particular the most luminous and also the rarest events (Section 4.4.3).

4.4.1. *The Unique Role of UV Spectroscopic Observations of Cosmic Explosions*

Following a stellar explosion, the debris is very hot. The peak emission naturally cascades from high energy to low energy as time goes by. The first radiation able to escape the explosion is the shock breakout (see Waxman & Katz 2017 for a recent review), which peaks in the UV on timescales of $\approx$ hours for many extended stellar progenitors (e.g., Campana et al. 2006; Bersten et al. 2018). The next phase of UV emission can arise from two distinct phenomena: (i) the SN shock interaction with a companion star (e.g., Kasen 2010, Liu et al. 2015); (ii) the SN shock interaction with the very nearby CSM, which was sculpted by the recent mass loss by the progenitor star before stellar death (e.g., Smith 2014; Chevalier & Irwin 2011; Chevalier & Fransson 2017 and references therein). For massive stellar explosions, scenario (ii) applies. The gas then rapidly expands and cools, shifting the peak of the emission towards increasingly longer wavelengths. This combines with the higher line blanketing at lower temperatures to quickly suppress the UV flux within a few days after the end of the interaction phase. This final phase of declining UV emission (and progressively emerging optical emission) from the shock heated ejecta can thus be studied by using ground-based observations (see the temporal evolution

of the UV and r-band light-curves from a red supergiant star explosion in Figure 15).

Our focus here is on the second phase of UV emission, which probes the mass-loss history of the star. This phase is rich with diagnostics (e.g., mass and composition of the ejecta; mass and radius of the pre-explosion ejected shell or shells; etc.). The short-lived nature ($\delta t \lesssim 48$ hours) of the UV emission from the explosion's shock interaction either with the companion or with confined CSM shells deposited in the environment by the dying star in the years before explosion, coupled with the current complete lack of UV spectroscopic facilities with rapid repointing capabilities, makes this an assuredly fertile field for both detailed studies and exploration.

Obtaining rapid-response broadband UV spectroscopic sequences is beyond the capabilities of current missions (see Section 3.2.2). As we detail in the next section, at early times optical spectra are relatively featureless (see the UV-optical spectrum displayed in Figure 15), and rapid optical spectroscopy does not access enough bright emission lines to constrain parameters (see, e.g., Section 4 of Groh 2014, for the case study of SN 2013cu, a SN with arguably the best optical flash spectroscopy, and yet an unconstrained stellar progenitor type because of the lack of UV spectroscopic coverage).

UVEX, with its ToO capabilities and highly sensitive low-resolution spectrometer, is perfectly matched to realize the vision described above. *UVEX* spectroscopic observations of stellar explosions will be capable of mapping for the first time the chemical composition, kinematics, and location of the innermost layers of CSM of normal (Section 4.4.2) and exotic (Section 4.4.3) stellar explosions, providing information that would not be otherwise available. In the case of Type Ia SNe, *UVEX* observations have the potential to unveil the nature of the companion stars to exploding CO white dwarfs. Very early UV spectroscopy thus provides a direct probe of the immediate explosion's environment and progenitor system.

4.4.2. *UV Spectroscopic Studies of "Ordinary" SNe*

Recent observations of outbursting behavior in stars before core-collapse have shaken the traditional understanding of mass loss in evolved massive stars (e.g., Smith 2014 for a recent review). A combination of pre-explosion optical imaging and post-explosion optical spectroscopy have demonstrated that a large fraction of massive stars, spanning all known classes (from ordinary Type IIP SNe to rare broad-lined Type Ic SNe), undergo major instabilities in the years preceding stellar death that spew dense shells of material into the sur-

rounding environment (e.g., Ofek et al. 2010, Ofek et al. 2014, Margutti et al. 2014, Margutti et al. 2017, Milisavljevic et al. 2015, Ho et al. 2019c, Bruch et al. 2021, Tartaglia et al. 2021, Strotjohann et al. 2021). In some cases the amount of expelled matter can reach $\gtrsim 1~M_\odot$, completely changing the observable properties of the resulting transient. This was not predicted on theoretical grounds and challenges physical mechanisms that drive mass loss in evolved massive stars (Smith 2014). One leading model suggests that these mass ejections can result from nuclear burning instabilities in the final stages of stellar evolution (Quataert & Shiode 2012; Fuller & Ro 2018; Wu & Fuller 2021).

To advance our understanding of the physics behind these mass ejections it is necessary to know the chemical composition, ionization stage and kinematics of the ejected material. UV spectroscopy is crucial because: (i) compared to the optical, it accesses a significantly larger number of spectral transitions, adding crucial constraints to an otherwise under-constrained problem (Figure 15, lower panel; Figure 30); (ii) virtually all young stellar explosions are bright UV emitters, with a spectral energy distribution that peaks in the UV, and a UV flux that is several times larger than the optical flux (Figure 15, upper-left panel); (iii) UV probes resonance lines such as C IV $\lambda\lambda1548,1551$, He II $\lambda1640$, and N IV $\lambda1719$ which, given their high optical depths, are detectable at significantly lower wind densities compared to the optical and allow a much more precise determination of the wind velocity structure; and (iv) finally, UV also probes highly-ionized Fe lines at $\lambda\lambda$ 1200–1450, which can be used as direct probes of the close CSM metallicity and would otherwise be inaccessible (at these high temperatures, no Fe transition is available in the optical).

UVEX will perform dedicated follow-up of core-collapse SNe as part of its primary science objectives (see Section 3.2.2), but will also have the capacity to investigate other "ordinary" types of SN. For example, in the specific context of Type Ia SNe, a novel way to gain insight into their progenitor systems is by studying the short-lived excess of UV emission that is expected to originate from the SN shock interaction with the companion star in the first ~ 48 hrs after explosion (Kasen 2010, their Figure 3). Type Ia SNe are believed to originate from a binary system where the exploding star is a Carbon-Oxygen White Dwarf (C/O WD; e.g., Maoz et al. 2014). The nature of the companion star is a matter of intense debate, as current observations point to WDs in some cases and non-degenerate companions (e.g. main sequence stars) in others. The UV burst properties (temperature, luminosity, duration) depend on the
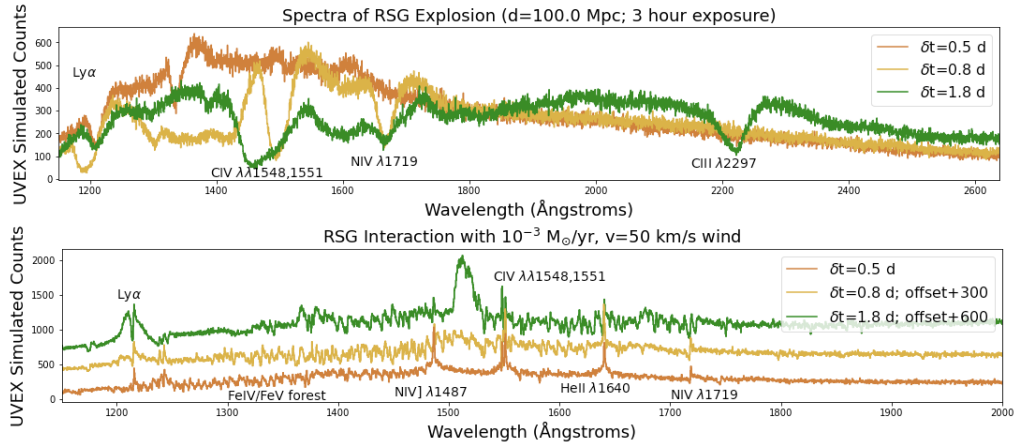
Figure 30. Simulated multi-epoch early *UVEX* spectra of the RSG explosions of Figure 15. We assume a representative distance of 100 Mpc and a *UVEX* exposure time of 3 hours. *Upper panel*: RSG explosion without CSM. *Lower panel*: RSG explosion embedded in thick CSM created by large pre-explosion mass-loss with rate of $10^{-3} \, \mathrm{M_\odot \, yr^{-1}}$ and ejected with velocity of $v_w = 50 \, \mathrm{km \, s^{-1}}$. The presence of dense CSM in the explosion's surroundings completely changes the spectroscopic appearances of the SN (and increases the fraction of flux in the UV, Fig. 15). In both cases (with or without CSM), the UV spectrum undergoes very rapid evolution during the first few days after the explosion, and allows us to constrain the kinematics, chemical composition and ionization stage of the emitting material. At these epochs the optical emission is significantly fainter. Simulated spectra taken from Gezari et al. (2008a) and Dessart et al. (2017).

properties of the companion star and thus provide direct insight into its nature (e.g., Brown et al. 2012).

UVEX has the potential to acquire the first UV spectra of Type Ia SNe at $\delta t < 48$ hrs and constrain the nature of their progenitor systems. To date, due to limitations of current observing facilities, the earliest UV spectroscopic observation of a Type Ia SN has been acquired at $\delta t \approx +5$ days with *HST* (R. J. Foley, private communication), well after the end of any emission from shock interaction with the companion.

To conclude, the acquisition of the first UV spectroscopic sequences of stellar explosions at very early times by *UVEX* will open an entirely new window of investigation on stellar death. *UVEX* will acquire rapid, high-cadence, UV spectroscopic sequences of the youngest stellar explosions identified by ground-based surveys (in 2028 we expect a large number of surveys to be operational, including ASAS-SN, BlackGEM, LS4, ATLAS, ZTF, PS-1 and 2, LAST, an upgraded EVRYSCOPE, and more) as well as SNe discovered by other spacecraft (e.g., *ULTRASAT*). Additionally, *UVEX* is equipped to discover ≈6-10 SNe within hrs of explosion through its synoptic survey over the course of two years.

4.4.3. *Probing the Exotica: the Rarest and Most UV-luminous Stellar Deaths*

In a typical core-collapse SN, the explosion is largely isotropic and the ejecta is accelerated to velocities up to about 10 percent of the speed of light – the consequence of a neutrino-mediated spherical shock produced following core bounce (e.g., Janka 2017). However, since the
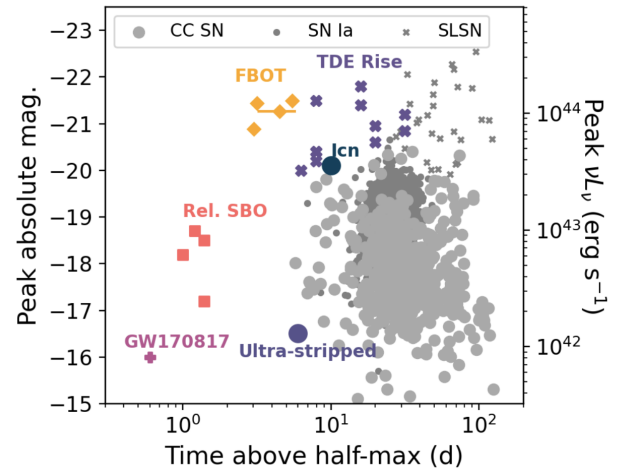
Figure 31. Luminosity vs. duration of optical transients, highlighting classes of relativistic explosions that are prime targets for *UVEX*: Fast and Blue Optical Transients ("FBOTs"; yellow diamonds), events powered by relativistic shock breakout ("Rel. SBO"; red squares), as well as ultra-stripped SNe (blue circle), counterparts to GW sources (here exemplified by GW 170817, purple plus sign), the new class of Type Icn SNe and Tidal Disruption Events ("TDEs"; purple crosses). We place these transients in the context of Ia SNe, core collapse (CC) SNe, and SLSNe from the ZTF Bright Transient Survey. References: Perley et al. (2019); Fremling et al. (2020); Margutti et al. (2019); Coppejans et al. (2020); Ho et al. (2020a); Perley et al. (2021a). Modified from Ho et al. (2021a).

late 1990s it has been realized that some massive stellar explosions are driven by a distinct mechanism involving the production of relativistic jets by a central engine: a rapidly-spinning neutron star or a black hole. The most extreme examples are long-duration gamma-ray bursts (GRBs; Piran 2004; Hjorth & Bloom 2012; Cano et al. 2017): extremely rare explosions involving ultra-relativistic (Lorentz factor $\Gamma > 100$) jets and almost exclusively discovered by high-energy satellites. However, the discovery of "low-luminosity" GRBs (or "X-ray flashes"; Galama et al. 1998; Kulkarni et al. 1998; Campana et al. 2006; Soderberg et al. 2006b; Liang et al. 2007), and observations of relativistic explosions with no associated GRB detected by wide-field surveys at other wavelengths (Soderberg et al. 2010; Cenko et al. 2013; Margutti et al. 2014; Milisavljevic et al. 2015; Ho et al. 2020b), suggest that GRBs are only the tip of the iceberg of a broader landscape of engine-driven phenomena spanning a wide variety of engine timescales, beaming angles, shock velocities, and CSM properties (Lazzati et al. 2012; Margutti et al. 2014; Milisavljevic et al. 2015; Gottlieb et al. 2021). This suggests that the role of jets in end-of-life stellar explosions may be more significant than was previously appreciated by most of the astronomical community.

Of particular importance to this mission is the population of transients sometimes termed "FBOTs" (fast blue optical transients, Figure 31) and typified by the intensely-studied event AT 2018cow (Prentice et al. 2018, Perley et al. 2019, Kuin et al. 2019, Margutti et al. 2019, Ho et al. 2019a), discovered in 2018. These events rise and fade on timescales of just a few days (an order of magnitude faster than a typical SN; Ho et al. 2021a), retain very high temperatures long after peak (Perley et al. 2019, Margutti et al. 2019), and have been shown in several cases to be accompanied by very luminous radio and sub-millimeter emission, indicating an energetic and mildly relativistic shock ($v \sim 0.1$–$0.6c$) in a very dense CSM (Margutti et al. 2019; Ho et al. 2019a; Coppejans et al. 2020; Ho et al. 2020a, 2021b; Bright et al. 2021). Hydrogen and helium were detected in the late-time spectra of AT2018cow (Perley et al. 2019, Margutti et al. 2019), indicating an important distinction from the progenitors of GRBs, which are exclusively accompanied by H/He-poor SNe.

FBOTs are fundamentally UV phenomena – the emission before, at, and (in many cases) after maximum light peaks in the UV (Drout et al. 2014; Pursiainen et al. 2018). However, they have only so far been discovered via ground-based optical surveys, and the only constraints from spectroscopy have come from the optical. The result is that even in this era of wide-field opti-cal surveys, the discovery rate is low ($\sim$1 per year), and spectroscopy has been minimally constraining. Almost all of our knowledge of this class of phenomena originates from AT2018cow itself, and there are few constraints on how these events are related to FBOTs and relativistic transients more broadly. The next ten years are unlikely to change this paradigm, since even the most powerful new time-domain facilities (e.g., the LSST carried out by the Vera C. Rubin Observatory) will not be capable of recognizing similar transients at the critical, short-lived early phases of their evolution.

A dedicated UV facility would offer several key advantages in the study of this event class. FBOTs are more luminous at UV wavelengths, the background is greatly reduced compared with the optical, and UV spectral diagnostics (with the extensive set of strong resonance lines) will be far more powerful at examining the properties of the outflow and surrounding CSM compared to what can be done with optical observations alone.

By the launch of *UVEX*, the entire sky will be surveyed in the soft X-ray bands by facilities such as Einstein-Probe (Liu 2021), transforming the study of relativistic explosions. Low-Luminosity GRBs (LL-GRBs, i.e. GRBs with significantly lower-luminosity γ-ray prompt emission) may represent phenomena intermediate to classical GRBs and ordinary SNe (Soderberg et al. 2006a, Liang et al. 2007, Nakar 2015, Cano et al. 2017). *UVEX* will obtain the first UV spectra of LLGRBs. The volumetric rate is uncertain, but could be between 0.1% and 1% of the core-collapse SN rate (Soderberg et al. 2006b, Liang et al. 2007). Their luminous UV emission is accessible to *UVEX* for spectroscopy out to $z = 0.06$, so we estimate between 6 and 60 candidates per year.

In addition, an entirely new class of strongly interacting SNe has been identified in the last few months: Type Icn SNe, i.e. SNe that show clear spectroscopic signatures of shock interaction with a He- and H-poor medium (Fraser et al. 2021; Gal-Yam et al. 2021; Perley et al. 2021b). Type Icn SNe join the groups of Type Ibn and Type IIn SNe, which show interaction with He-rich and H-rich CSM, respectively. Type Icn SNe descend from stellar progenitors that shed their envelopes at significantly earlier times before collapse, compared to their Ibn and IIn cousins. The physical nature of Type Icn SNe is unknown. These SNe are rare but UV-luminous (Figure 31), and thus detectable out to large volumes. *UVEX* has the potential to acquire the first UV spectra of a Type Icn SN and provide key information on its origin.

In summary, *UVEX* will shed exciting new light on the rarest and most mysterious cosmic explosions, trans-

forming our understanding of the many manifestations of stellar death.

4.5. *Active Galactic Nuclei*

Active galactic nuclei (AGN), corresponding to the phases in a galaxy's life when its central supermassive black hole (SMBH) is actively accreting material, are intrinsically UV phenomena. Gravitational potential energy from in-falling material becomes kinetic energy, and is then released as thermal energy from the hot accretion disk that naturally forms. Accretion disk temperature is inversely proportional to the central mass, so while emission from the accretion disks of stellar mass compact objects in the Galaxy, i.e., Galactic binaries, peak in the soft X-ray regime, emission from the accretion disks of SMBHs peak in the UV. Indeed, the first quasars were identified as unusually blue, quasi-stellar counterparts to radio sources (Schmidt 1963), and the so-called "Big Blue Bump" which dominates quasar SEDs in the spectral range from ~ 100 Å to 3000 Å is dominated by 10,000-100,000 K thermal emission from the accretion disk (Sanders et al. 1989).

Thermal UV emission from the accretion disk provides the source photons for two other distinguishing features in AGN SEDs. UV emission from the accretion disk is reradiated in the IR by dust, often assumed to be in form of a torus of material that obscures the higher energy emission along certain lines of sight (e.g., Stern et al. 2005). And UV emission is Compton up-scattered into the X-ray range by the AGN corona, creating the characteristic power-law X-ray spectrum of actively accreting, unobscured AGN.

Thus, it should come as no surprise to find that UV observations play an outsized role for AGN studies. In the following section, we consider the scientific potential of *UVEX* for AGN studies, with an emphasis on the discovery space enabled by sensitive, synoptic UV imaging, UV spectroscopy, and the $\geq 50 - 100\times$ increase in two-band UV imaging sensitivity enabled by *UVEX* relative to *GALEX*. The related phenomenon of tidal disruption events (TDEs) are discussed in the next section (Section 4.6). However, we do note that TDEs are also expected to happen in active galaxies. Ricci et al. (2021) present one dramatic candidate event, while Frederick et al. (2021) discuss optical transients in narrow-line Seyfert 1 galaxies, some of which they associate with likely TDEs. In addition, Stein et al. (2021) discuss the likely coincidence of a PeV neutrino with a TDE in an active galaxy. UV observations are a key aspect of their analysis, which shows that the EM observations can be explained with a multi-zone model: a UV-bright photosphere powering an extended synchrotron-

emitting outflow in which high-energy neutrinos are produced. Their model suggests that TDEs with mildly-relativistic outflows are likely important contributors to the cosmic neutrino flux, particularly at high energies, and also shows the key role that UV observations play in probing extreme AGN events, touching on AGN (this Section), TDEs (Section 4.6), and multimessenger astrophysics (Section 4.7). Finally, from the theoretical side, McKernan et al. (2021) and McKernan et al. (in prep.) discuss how stars embedded in AGN accretion disks can lead to TDEs.

4.5.1. *Quasar Variability*

Time domain surveys have long been recognized as important tools for studying AGN. Indeed, optical continuum variability was recognized as a common feature of quasars within a year of their initial discovery (Matthews & Sandage 1963), and was quickly exploited as a means of identifying quasars, particularly those that might be missed by the UV-excess technique due to their higher redshift (e.g., van den Bergh et al. 1973). Since then, several groups have used optical synoptic studies to construct quasar samples based on their unique optical variability, thereby avoiding the inherent biases of color selection. A non-exhaustive list of such efforts include studies of SDSS Stripe 82 (MacLeod et al. 2011), MACHO (Pichara et al. 2012), OGLE (Kozłowski et al. 2013), COSMOS (De Cicco et al. 2019), and GOODS-S (Pouliasis et al. 2019). Graham et al. (2014) show how combining optical variability from CRTS with mid-IR colors from *WISE* (e.g., Stern et al. 2012, Assef et al. 2013) improves completeness and reliability of quasar selection relative to variability or color selection alone, and optical variability selection of quasars has long been heralded as one of the many promising scientific results to come from Rubin (e.g., Ivezić et al. 2019).

UVEX will provide a powerful probe of quasar UV variability, a wavelength where quasars are $\sim 5\times$ more variable than at optical wavelengths (Gezari et al. 2013). This will be useful for a wide range of quasar studies, from simply identifying quasars, to correlating their UV light-curves with variability at other wavelengths, to mapping out the central engine and determining black hole masses, to exploring the new territory of extreme quasar variability recently opened from optical time-domain surveys. In particular, since quasar UV emission comes predominantly from the hot accretion disk, UV studies are uniquely sensitive probes of extreme events and activity close to the supermassive black hole.

By studying quasars at a wavelength where they are more variable, *UVEX* has significant promise for identifying AGN based on their variability, particularly in the

low-redshift Universe where the rest-frame UV photons are detected in the observed UV bands. Of particular interest will be identifying AGN in low-mass, low-redshift galaxies, which are predominantly star-forming (Geha et al. 2012). UV color excess techniques will therefore be somewhat compromised (e.g., Latimer et al. 2019), making UV variability a powerful tool for identifying low-luminosity AGN in dwarf galaxies. Obtaining a comprehensive census of such systems is particularly exciting as a tool to understand early BH growth and potentially answering the key open question regarding SMBH "seeds" (e.g., Reines et al. 2013): how was the universe able to create billion-solar-mass BHs in less than a Gyr (e.g., Bañados et al. 2018)? Different models for these high-redshift seeds have different predictions for the massive BH occupancy fraction in low-mass galaxies in the local universe (Reines & Comastri 2016), which *UVEX* will be well-placed to test.

4.5.2. *Reverberation Mapping*

Although the spatial structure of the AGN central engine cannot be directly resolved, the time-variable nature of AGN emission makes it possible to resolve the inner structure by correlating variability from different emitting regions and associating time delays with the light travel time (Blandford & McKee 1982, Cackett et al. 2021). This method, known as reverberation mapping, uses synoptic observations to determine the geometry of the central region; spectroscopic monitoring opens such studies up to dynamical studies as well (e.g., Pancoast et al. 2014). Reverberation mapping provides our largest sample of robust SMBH mass measurements, supplemented with a few nearby sources, such as Sgr A*, where we can kinematically resolve the central regions (e.g., Ghez et al. 2008, Cohn et al. 2021). Panda et al. (2019) discuss photometric reverberation mapping with Rubin, essentially modeling the huge sample of quasars with six-band synoptic photometry as a substitute for spectroscopic monitoring of a smaller sample, as is the current standard for reverberation campaigns (e.g., Barth et al. 2015). Providing two additional photometric bands at the wavelengths where quasars are most variable, *UVEX* will be an important supplemental dataset for photometric reverberation programs.

4.5.3. *Stellar Mass Black Hole Mergers*

One exciting, though controversial, possibility is that a significant fraction of BH-BH merger GW events occur within AGN accretion disks and are detectable in EM (e.g., Graham et al. 2020a). Stellar mass BHs are expected to be common in galactic nuclei due to mass segregation, and accretion disk gas will dissipate angular momentum, causing more massive embedded objects
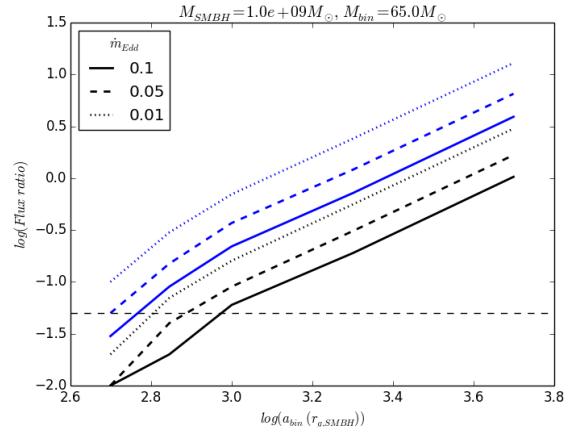
Figure 32. The merger of stellar mass BHs in an AGN accretion disk causes a bright UV flare. Plotted is the ratio of *GALEX* NUV flux (blue; similar to *UVEX* NUV) and ZTF *g*-band flux (black) from such an event relative to an unperturbed AGN disk. These curves are for a $10^9 M_\odot$ SMBH in an AGN accreting at a range of Eddington ratios: $\dot{m}_{\rm Edd} = 0.1$ (solid), 0.05 (dashed), and 0.01 (dotted), and assume that the merging BHs have a total initial mass of $65 M_\odot$, 5% of the mass is lost to GWs from the merger, and a kick velocity of $100\,{\rm km\,s^{-1}}$ for the resultant, merged BH. Ratios are plotted for a range of binary distance $a_{\rm bin}$ from the SMBH, in units of the SMBH gravitational radius, $r_{\rm g,SMBH} \equiv G\,M_{\rm SMBH}/c^2$. The horizontal dashed line corresponds to a flux increase of 5%. The flux increase is larger at shorter wavelength. From McKernan et al. (2019).

to in-spiral more rapidly than less massive ones. This provides a natural explanation for asymmetric mass mergers (McKernan et al. 2020) such as GW190814, which consisted of a $23 M_\odot$ BH coalescing with a $2.6 M_\odot$ compact object (Abbott et al. 2020b), as well as BHs more massive than 35-70 $M_\odot$, the maximum BH mass expected from a supernova (Woosley 2017), such as GW190521 which consisted of an $86 + 66 M_\odot$ BH merger (Abbott et al. 2020c). As shown by Figure 32, from McKernan et al. (2019), the disk gas provides baryons that are expected to produce a UV flare due to the merger, assuming either a short diffusion time or a thin AGN accretion disk. Jetted emission from a rapidly spinning, merged BH can also yield UV photons, implying that *UVEX* will be a powerful tool for studying counterparts not only to NS merger events (discussed in Section 3.2.1), but also to BH merger events.

4.5.4. *Supermassive Black Hole Binaries*

Time-domain surveys have recently identified a population of quasars with apparently sinusoidal, periodic light-curves (Graham et al. 2015a, Graham et al. 2015b, Charisi et al. 2016). With the important caveat that

many candidate periodic sources are claimed on the basis of problematic statistical analyses (e.g., see discussion in Vaughan et al. 2016 and Barth & Stern 2018), actual sustained periodic or quasi-periodic variability is likely a signature of a binary supermassive black hole (SMBH) system with a sub-parsec separation. For example, D'Orazio et al. (2015) showed that the periodicity of PG 1302-102 can be explained by relativistic Doppler boosting and beaming of emission from the mini-accretion disk around a secondary SMBH as it orbits a more massive primary at velocities of a few tenths the speed of light with a separation of ~ 2000 AU (i.e., ~ 0.01 pc). This model predicts a strong inverse correlation between variability amplitude and wavelength (Xin et al. 2020), which *UVEX* will test.

4.5.5. *Flaring AGN*

UVEX will also be important for studying AGN with unusual, extreme optical light-curves, such as flaring AGN. For example, Graham et al. (2017) reported on a systematic search for major flares in AGN in the Catalina Real-time Transient Survey as part of a broader study into extreme quasar variability. Requiring flares that are quantitatively stronger than normal, stochastic quasar variability, Graham et al. (2017) identified 51 extreme events from a sample of $> 900,000$ confirmed and high-probability quasar candidates. The events typically lasted 900 days, with a median peak brightening of $\Delta m = 1.25$ mag. The sample shows a range of flare morphologies, with some being more symmetric, while others evolve with a fast rise followed by a slower, exponential decay. While a subset of the sources appear consistent with microlensing (e.g., Lawrence et al. 2016) or self-lensing (e.g., D'Orazio & Di Stefano 2018), Graham et al. (2017) attribute the majority of the events to explosive stellar-related activity in the accretion disk, such as super-luminous SNe, TDEs, and mergers of stellar mass BHs. Given the range of potential phenomena, and that the flares are likely associated with events close to the central engine in the UV-luminous accretion disk, *UVEX* observations will be critical for refining our understanding of these events and ultimately using them to improve our understanding of the extreme and poorly understood physics of AGN accretion disks.

4.5.6. *Changing-Look Quasars*

UVEX will also be important for studying "changing-look quasars", quasars which rapidly rise or drop in optical brightness (e.g., LaMassa et al. 2015, Ross et al. 2018, Stern et al. 2018, Graham et al. 2020b). Though a range of selection criteria and wavelength ranges have been used to identify such sources, changes in the innermost accretion disk occurring on the thermal or cool-
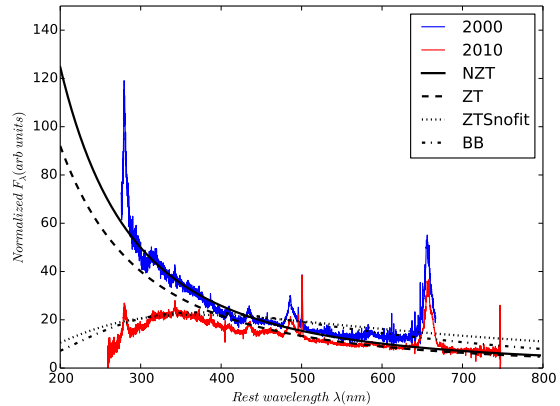
Figure 33. Example of a changing-look AGN, SDSS J110057.70-005304.5, in which the UV emission from the AGN collapsed (Ross et al. 2018). The authors explore models where the source has non-zero torque (NZT model; solid line) at the inner, stable circular orbit (ISCO; Afshordi & Paczyński 2003), and suggest that the spectrum is best explained by shutting down emission from the inner $\sim 200r_g$ of the accretion disk (ZTSnofit model; dotted line). See Ross et al. (2018) for details.

ing/heating front timescale seem to be the most plausible explanation for the year-scale variability typically observed in changing-look quasars. For example, Ross et al. (2018) present one example of a changing-look AGN where the UV emission has collapsed (Figure 33). The authors argue that the most likely explanation is that some triggering event caused the inner accretion disk to cool, and thus dim, though other models have been favored for other events (e.g., Guo et al. 2016). With few such events studied, particularly at the key UV wavelengths which likely dominate the state changes, *UVEX* will have an important role to play in determining the timescales, characteristics, and spectral changes associated with changing-look quasars.

4.6. *Tidal Disruption Events*

It is now well established that SMBHs are a ubiquitous presence in the nuclei of almost all galaxies (Magorrian et al. 1998; Kormendy & Richstone 1995; Ho 2008). In fact, the remarkably tight correlation between the masses of central SMBHs and the mass, luminosity, and structure of their host galaxies (Ferrarese & Merritt 2000; Gebhardt et al. 2000; Graham et al. 2001; Marconi & Hunt 2003) suggests coeval formation and growth over cosmic time. Despite these advancements, the formation mechanism of the primordial seeds from which SMBHs grow through accretion and mergers is yet unknown. The demographics of SMBHs in low-

mass galaxies may place the most promising constraints (Volonteri & Natarajan 2009). Unfortunately, the low-mass end of the SMBH mass function is difficult to detect, due to the smaller gravitational sphere of influence and lower Eddington luminosity of the black hole, which both scale linearly with SMBH mass. Tidal disruption events (TDEs) provide the most promising method to detect and weigh black holes below $10^8 M_\odot$, where scaling relations between black hole mass and galaxy mass are poorly constrained.

A TDE will occur when an unlucky star's orbit passes close enough to a central SMBH to be tidally ripped apart, and the resulting stellar debris is slowly consumed by the black hole, producing a luminous accretion flare. The physics of TDEs depends on the interplay of the stellar radius and the black hole tidal radius: black holes more massive than $\sim 10^8 M_\odot$ disrupt main sequence stars inside the event horizon and thus do not produce a flare, while black holes less massive than $\sim 10^{5.4} M_\odot$ do not have a tidal field sufficient to disrupt main sequence stars. Compact stars, such as white dwarfs, can be disrupted by intermediate mass black holes (IMBHs; $\sim 10^4 M_\odot$), while red giants can be disrupted by the most massive black holes known.

TDEs are not only probes of SMBH demographics. They are also an ideal laboratory to study the physics of accretion. One of the primary parameters in accretion physics is the accretion rate. The mass accretion rate in a TDE undergoes a large variation over month-to year-long timescales, starting as super-Eddington and gradually decreasing as a power-law with time. When a TDE occurs around an inactive black hole, it provides a unique opportunity to study the formation and physics of an accretion disk and its associated structure. There is increasing suspicion that TDEs are sources of very high-energy neutrinos (e.g. van Velzen et al. 2021a; see also Section 4.5). Finally, TDEs can be used to probe the occupation fraction of massive black holes in the nuclei of low-mass galaxies, which allows for the evaluation of competing models proposed to explain the surprising presence of SMBHs with masses $> 10^9 M_\odot$ in the first Gyr after the Big Bang (Bañados et al. 2018).

The census of TDE candidates has been steadily growing thanks to dedicated searches for nuclear transients from quiescent galaxies across the electromagnetic spectrum (see Gezari 2021 for a recent review).

4.6.1. *UV Properties of TDEs & Uniqueness of UVEX*

TDE candidates were first identified from the *ROSAT* X-ray All Sky Survey (Bade et al. 1996; Komossa & Bade 1999). The modest number of epochs were sufficient to establish the phenomenon from extremely soft, luminous X-ray outbursts from otherwise quiescent galaxies. The second era of TDE searches began with *GALEX*, together with joint optical observations from the ground, which led to a class of UV-selected TDEs (Gezari et al. 2008b, 2009, 2012). These TDEs are characterized by thermal emission with temperatures $T_{\rm bb} \sim (3-5) \times 10^4$ K (and radius $R_{\rm bb} \sim 10^{14}$–10^{15} cm) and emission peaking in the UV – much cooler than the original TDE candidates discovered in the soft X-rays ($T_{\rm bb} \sim 10^6$ K and $R_{\rm bb} \sim 10^{12}$ cm). Since those studies with *GALEX*, the majority of TDE discoveries have been made in the optical. ZTF is now routinely discovering 15 TDEs per year (van Velzen et al. 2021b). Follow up with the *Swift* satellite has shown that they are also very bright in the UV, with typical colors of $NUV - r < -1$ mag, and peak luminosities of $-18 < NUV < -22$ mag (Gezari 2021; see Figure 34). In fact, TDEs are some of the most luminous and long-lived UV transients in the Universe (see Figure 31).

The origin of the luminous UV-bright thermal emission from TDEs is still debated (see Section 4.6.4). Some UV and optically selected TDEs are also bright in the soft X-ray band, indicating that these are two emission components that likely co-exist in the same TDE system.

Owing to the high luminosity and long lifetime of TDEs in the UV, *UVEX* will routinely discover TDEs. However, by 2027 the TDE landscape will be quite sophisticated and the focus will be on *large and well-defined* samples of TDEs. Therefore, to illustrate *UVEX*'s capability in this field, we consider a hypothetical *UVEX* survey to discover and characterize over 1000 TDEs. The framework to compute the discovery rate of TDEs is given in Appendix D. This survey would be accompanied by a spectroscopic component to systematically probe the kinematics and structure of outflows launched by TDEs, and test competing models for the origin of the UV emission (Section 4.6.4).

The resulting data from such a survey will enable us to: (1) detect the lower energy tail of thermal emission from X-ray loud TDEs (Section 4.6.2); (2) address the "missing energy problem" for optically loud TDEs (Section 4.6.3); (3) identify the mechanisms of the UV/optical thermal emission (Section 4.6.4); and (4) probe the BH occupation fraction of low mass galaxies, and even the spin distribution of high mass BHs (Section 4.6.5).

4.6.2. *UV Detections of X-ray Loud TDEs*

The Russian-German *Spektr-RG* (*SRG*) mission is now finding TDEs at a higher rate relative to those found from optical surveys (Sazonov et al. 2021). X-ray
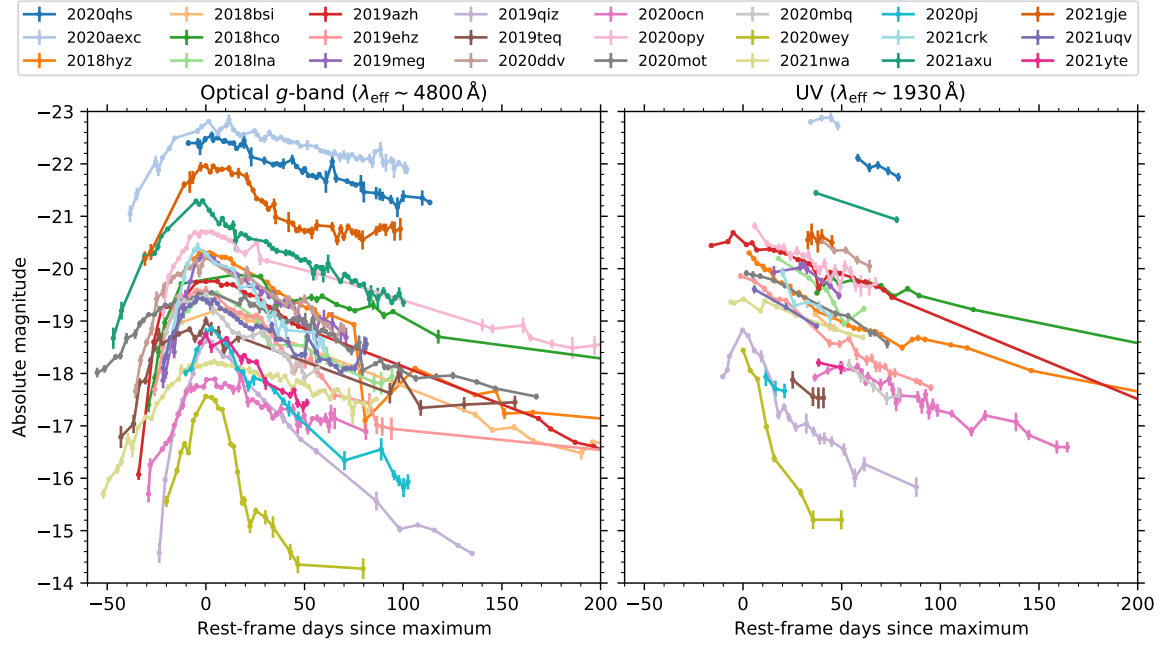
Figure 34. Optical (left panel) and UV (right panel) light curves of TDEs selected from ZTF. Since UV observations were carried out after the optical identification, only three TDEs had UV data before the peak of the light curves.
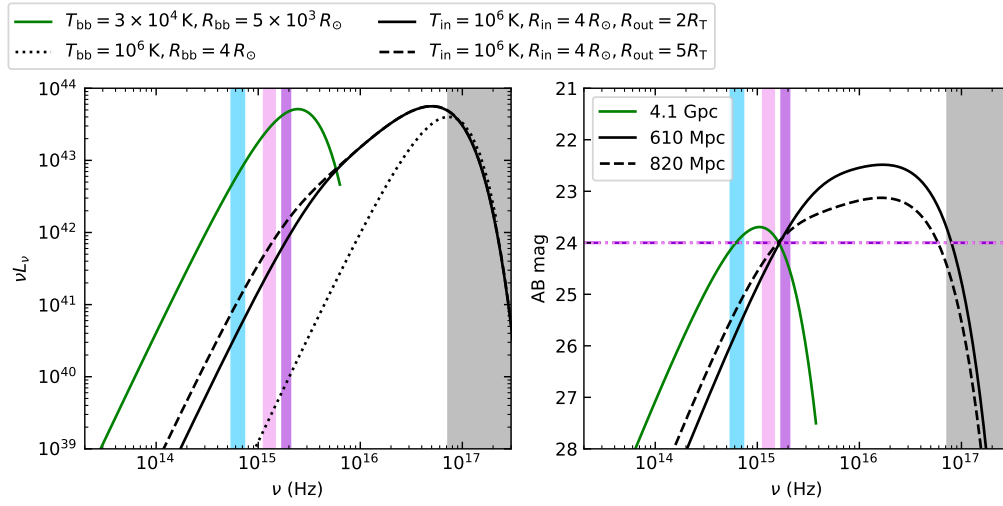
Figure 35. (Left) SEDs of typical optically-discovered (green) and X-ray-discovered (black) TDEs. Photometric bands are marked by the vertical lines in blue (g-band), light purple (NUV), deep purple (FUV), and gray (0.3–10 keV). (Right) The same SEDs are now shifted to the largest distance that still meets the *UVEX* sensitivity threshold (conservatively assumed to be 24 mag), including *K*-correction.

discovered TDEs (Saxton et al. 2020) display temperatures of $T_{\rm bb} \sim 10^6$ K and $R_{\rm bb} \sim 10^{12}$ cm, as expected from emission near the innermost stable circular orbit (ISCO) of a black hole (BH) of $M \sim 10^6 M_\odot$. The black dotted line in Figure 35 (left panel) illustrates a typical blackbody inferred from soft X-ray observations. However, from angular momentum conservation, we expect the tidal debris to circularize at a few times the tidal radius $R_{\rm T} = R_\odot (M/M_\odot)^{1/3}$ (for a solar-like star), which

means that the radius of the outer disk is of the order $R_{\rm out} \sim 10^{13}$ cm. One of the exciting capabilities of the FUV sensitivity of *UVEX* will be to detect the lower energy tail of the thermal emission of X-ray loud TDEs, even for those without the additional UV/optical component.

Multi-color disk SEDs for two different choices of $R_{\rm out} = 2R_{\rm T}$ and $5R_{\rm T}$ are shown in solid and dashed black lines in Figure 35. For a detection threshold of

24 mag, *UVEX* will be able to detect the emission from the outer accretion disk out to at least 610 Mpc.

4.6.3. *Addressing the "Missing Energy" Problem*

The total radiated energies in optically-discovered TDEs are in the range 10^{50}–10^{51} erg. This is at least one order of magnitude below the theoretically expected energy release from $0.1 M_\odot$ of accreted mass, even considering that the accretion disk may be radiatively inefficient in the super-Eddington regime (Lu & Kumar 2018). Therefore, $> 90\%$ of the expected energy released by TDEs has been missed by current observations. This is one of the major puzzles in TDEs.

A possible solution is that the majority of the disk mass is only slowly accreted onto the BH on a timescale much longer than a few years, provided that the accretion disk is very thin with a long viscous timescale. Without optically thick reprocessing gas at large distances, the disk emission is expected to be primarily in the UV and soft X-ray bands, as shown by the multicolor blackbody SED in Figure 35. This is supported by late-time (~ 5 yr) FUV/NUV observations of a handful of TDEs by *HST* after the optical emission had completely faded away (van Velzen et al. 2019). The observed FUV fluxes are in the range 23–25 mag, which are detectable either by a single *UVEX* observation or by stacking of multiple exposures. Thus, the *UVEX* all-sky survey will provide late-time FUV measurements or stringent upper limits for all $N \sim 10^3$ TDEs that will have been discovered by optical and X-ray surveys before 2028 – not feasible with individual *HST* observations for such a large number of TDEs.

4.6.4. *Confronting Observations with TDE Models*

There are two competing models for how the UV/optical emission seen in some TDEs is generated.

1. **Reprocessing of Disk Emission.** In this scenario, an optically thick gas layer (most likely in the form of an outflow) at a distance of 10^{14}–10^{15} cm absorbs the soft X-ray emission from the disk and re-emits in the UV-optical band (Metzger & Stone 2016, Roth et al. 2016, Lu & Bonnerot 2020). As the fallback rate declines with time, the density of the "reprocessing layer" drops and there is less and less absorption. Thus, the bulk of the emission is expected to shift to higher frequencies and correspondingly, $T_{\rm bb}$ **increases** and $R_{\rm bb}$ drops with time.

2. **Stream-stream Collisions.** An alternate scenario is that the bound stellar debris stream intersects itself, producing a self-crossing shock, and

the kinetic energy dissipated by the shock powers the optical emission (Piran et al. 2015, Jiang et al. 2016). In this case, $R_{\rm bb}$ is of the order of the self-crossing radius, which stays roughly unchanged over time. As the fallback rate declines with time, the shock power drops (roughly as $t^{-5/3}$) and hence the blackbody temperature $T_{\rm bb}$ is expected to **decrease** with time.

While temperature evolution is a compelling discriminator between these models, the optical band is on the Rayleigh-Jeans tail (insensitive to $T_{\rm bb}$) of the TDE thermal continuum, and UV photometry is required for a reliable measurement of the temperature evolution. However, as can be seen from Figure 34, early UV photometry is only available for a few TDEs. *UVEX* will for the first time, provide UV photometry before and after the peak, and map out the temperature evolution on timescales relevant for the circularization of the debris streams.
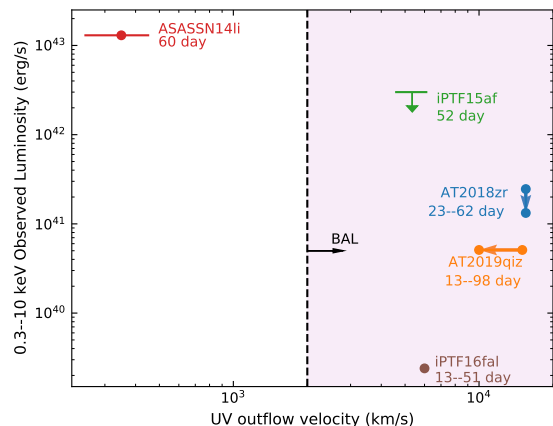
Figure 36. X-ray luminosity versus outflow velocity measured from UV spectroscopy. Among the five TDEs with published UV spectra, four exhibit broad absorption line systems (BALs; defined by $v > 2000\,{\rm km\,s^{-1}}$).

The typical ionization parameter near the optical photosphere of TDEs is $\xi \gtrsim 10^2$. This means that most atoms lose their outer-shell electrons, which are responsible for transitions in the optical band, whereas the transitions of inner-shell (K and L) electrons produce lines in the UV band. Thus, UV spectroscopy provides a unique probe of the density and velocity structures of the gas under high UV and soft X-ray fluxes.

As of late 2021 there are only five TDEs with UV spectra, ASASSN-14li (Cenko et al. 2016), iPTF16fnl (Brown et al. 2018), iPTF15af (Blagorodnova et al. 2019), AT2018zr (Hung et al. 2019), and AT2019qiz (Hung et al. 2021). Broad absorption line (BAL) systems are observed in all sources, except for ASASSN-

14li. The broad absorption/emission features are thought to arise from an outflow driven by the disk accretion or stream collision.

A direct prediction of the reprocessing scenario is that if we observe into the funnel of the disk-driven wind, more X-ray flux and less prominent UV absorption features are visible because most atoms are completely ionized by the high X-ray flux. On the other hand, if we observe from higher angles where the X-rays are obscured by the outflow, the UV absorption features should be strong. An anti-correlation between BAL presence/strength and X-ray luminosity will be a smoking gun for the reprocessing picture. The current sample of five TDEs with UV spectra so far supports this picture (see Figure 36). *UVEX* will ∼triple the sample of TDEs with UV spectra, enabling significantly more robust conclusions about such an anti-correlation.

The outflow velocity of the gas in the line formation region can be measured by the P-Cygni profiles. If the outflow is driven by disk accretion, the outflow speed should increase as the accretion rate drops at later times, because the disk-wind launching radius gets closer and closer to the innermost stable circular orbit (ISCO). In the alternative scenario, if the outflow is driven by stream collision, the outflow speed should stay roughly constant because the radius of stream self-crossing does not evolve with time (Lu & Bonnerot 2020).

In the past, the study of line-width evolution in TDEs has been stymied by the relatively late optical discovery and the latency of *HST* UV ToO triggers. Up until now, the earliest UV spectrum of a TDE only started at $\Delta t = +13\,$day (relative to the optical peak). An example *UVEX* campaign, tracking the velocity evolution of ≈ 20 TDEs with five spectroscopic observations each (from $\Delta t \sim -4\,$days to $\sim +56\,$days), will provide a unique probe of the outflow's origin. The *UVEX* spectral resolution of $R \geq 1000$ is more than adequate to measure the outflow velocity (typically $> 10^3\,\mathrm{km\,s^{-1}}$).

4.6.5. *Probing Black Hole Demographics*

The BH mass function (BHMF) below $\sim 3 \times 10^6 M_\odot$ and above $\sim 5 \times 10^8 M_\odot$ is poorly known (see Figure 37). Our goal is to use TDEs as tracers of BH demographics. Specifically, we would like to measure the BHMF at the low mass end from $10^5 M_\odot$ to $10^6 M_\odot$, and to investigate the upper bound of $M_{\rm BH}$ that can disrupt a star. The TDE rate at the low mass end is sensitive to the BH occupation fraction (Stone & Metzger 2016).

Given the relatively strong correlation between $M_{\rm BH}$ (inferred from the host galaxy central velocity dispersion) and the fallback time $t_{\rm fb}$ (derived from fitting the decay timescale of the light curve; van Velzen et al. 2020;
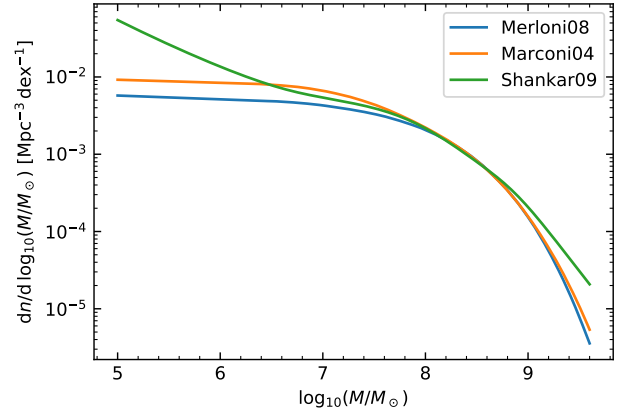
Figure 37. Three different BHMFs given in the literature (Marconi et al. 2004, Merloni & Heinz 2008, Shankar et al. 2009).

Gezari 2021; see Figure 38), one should be able to use well-sampled light curves to infer the BH mass independently of host galaxy properties. This is particularly important for IMBHs, where the scaling relations between host galaxy mass and central BH mass are poorly constrained (Greene et al. 2020). A survey cadence of $\lesssim 25$ days would be needed to track the decay of IMBH TDEs (see AT2020wey in Figure 34). Figure 39 shows that a sample of ≈ 1000 TDEs is needed to constrain the BHMF between $10^5 M_\odot$ and $10^6 M_\odot$ and to measure the shape of TDE rate suppression due to the BH event horizon.

The all-sky cadenced synoptic surveys carried out by *UVEX* will be able to build up the large sample of TDEs required to differentiate between different BHMFs, as well as to probe other questions about BH demographics that have not been possible before, such as the spin distribution of the most massive non-active BHs (Kesden 2012).

4.7. *Multi-Messenger Astronomy*

On August 17, 2017, the groundbreaking discovery of both gravitational waves and electromagnetic radiation from a neutron star merger (e.g., Abbott et al. 2017a) marked a new era in multi-messenger astrophysics (MMA). The discovery of a flaring blazar (IceCube Collaboration et al. 2018) and three tidal disruption events (Stein et al. 2021; Reusch et al. 2021; van Velzen et al. 2021b) associated with high energy neutrinos opened up yet another facet of MMA.

With planned advances in sensitivity of GW interferometers, neutrino detectors and EM surveyors, we could expect several MMA events to be discovered in the years leading to the launch of *UVEX*. However, capabilities for opening the UV window into MMA will be limited
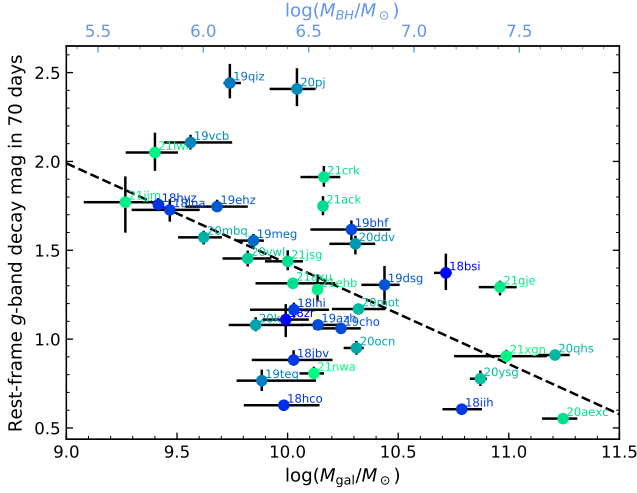
Figure 38. TDE optical decay rate as a function of host galaxy stellar mass $M_{\rm gal}$. The decay is quantified by the total magnitude the light curve fades from peak to 70 days post-peak. $M_{\rm gal}$ is measured by modeling the host galaxy UV–MIR SED following the procedures laid out in van Velzen et al. (2021b). The upper x-axis marks rough estimates of $M_{\rm BH}$ using the $M_{\rm gal}$–$M_{\rm BH}$ relation from Reines & Volonteri (2015). A statistically significant correlation was found ($p = 0.0006$ for a Kendall's Tau test), suggesting that TDEs disrupted by higher mass BHs fade slower.
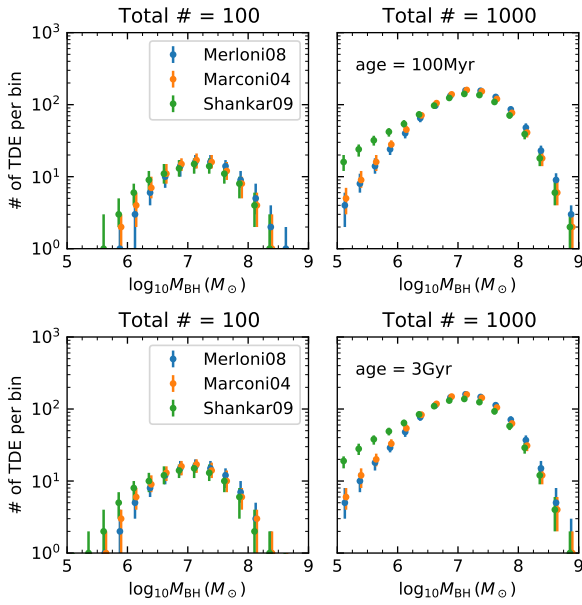
Figure 39. Observed number of TDEs as a function of $M_{\rm BH}$, under different assumptions of the total number of detected TDEs, the BHMF (Figure 37), and age of the stellar population (upper panels: 100 Myr; lower panels: 3 Gyr).

because of the combination of wide FOV, sensitivity, and rapid response time that is required. While *HST* has the sensitivity, it is neither wide-field nor does it respond fast enough. *ULTRASAT* (launch date, 2025) will have a larger FOV and rapid response, but will be much less sensitive than *UVEX* (and lacks an FUV channel), and thus will only be able to pick the lowest-hanging fruit (e.g., exceptionally nearby or bright sources). Fully realizing the potential for population studies enabled by the A+ sensitivity upgrades (e.g., H_0 constraints: Chen et al. 2018; connection to gamma-ray bursts: Abbott et al. 2017b) requires the higher sensitivity that will be provided by *UVEX*.

Opening a new region of the wavelength-depth-FOV phase space, particularly FUV imaging, *UVEX* will significantly impact the study of neutron star mergers, black hole mergers and SMBH flares. *UVEX* will tackle open questions on where the heaviest elements are synthesized and how relativistic jets are formed by identifying and characterizing the UV emission from GW and high-energy neutrino events. Neutron star mergers were discussed in Section 3.2.1, while SMBH flares and TDEs within active galaxies as potential sources of high energy neutrinos were discussed in Section 4.5. Appendix E presents the expected GW event rates and light curve models for *UVEX*.

4.8. *Exoplanets*

With thousands of discoveries at hand, the field of exoplanets is rapidly pivoting from detection to characterization. Limited thus far by the necessary advances in technology, we have nevertheless been able to explore a small number of planets in unprecedented detail. In particular, our ability to observe and understand the atmospheres of exoplanets has increased significantly over the last decade. Understanding exoplanet atmospheres, and refining how we analyze and model them, is a crucial stepping stone towards the detection and understanding of biosignatures, which are likely to be first found in exoplanet atmosphere analyses.

Transmission spectroscopy – measuring the absorbing cross section of the planet as a function of wavelength during transit – has been one of the most productive paths of atmosphere investigation. One finding is that clouds and hazes are prevalent across all types of exoplanet atmospheres (Wakeford et al. 2019, Fu et al. 2017, Iyer et al. 2016, Crossfield & Kreidberg 2017, Morley et al. 2015). Clouds and hazes can reduce the amplitude of spectral features, a reduction that can also independently be produced by high mean molecular weight atmospheres (Madhusudhan & Redfield 2015). The amplitudes of important molecular features, such as water,

vary significantly between planets in the same class – hot Jupiters (Sing et al. 2016), warm Neptunes (Crossfield & Kreidberg 2017), and super-Earths (Southworth et al. 2017) – and understanding the origin of these variations is crucial for unlocking the physical processes that dominate these atmospheres. The degeneracy between the presence of clouds and hazes and the impact of a higher mean molecular weight atmosphere has hindered further understanding of these variations.

With the launch of *JWST*, transmission spectroscopy will be substantially boosted at IR wavelengths, an important window into understanding the composition and structure of exoplanet atmospheres. However, at IR wavelengths the aforementioned aerosol/mean molecular weight degeneracy is severe. In addition, in order to holistically understand atmospheres and the physical processes that sculpt them, IR spectroscopy on its own is insufficient. We need to characterize exoplanet atmospheres over a much broader wavelength range to capture physical processes that manifest at other wavelengths and to understand the entire energy budget of the planet. We also need to characterize exoplanet atmospheres over a much larger set of exoplanet parameters than has been previously accessible, such as planet size and insolation. The upcoming ESA *Ariel* mission with the NASA/CASE contribution will fill in important gaps at optical and near-IR wavelengths for a very large number of planets, partially satisfying these needs, but there remain important atmospheric processes that are only captured in the UV. Without complementary UV observations, our ability to both plan and interpret *JWST* and *Ariel* observations will be significantly hindered. There is a broad range of atmospheric physics that can be studied with UV observations. These include Rayleigh and Mie scattering properties of cloud and haze particles (Section 4.8.1); heavy metal condensation and disequilibrium processes (Section 4.8.2); and observations of atmospheric escape in Lyman-α (e.g., Zhang et al. 2021). The former in particular presents the opportunity to identify cloudy or hazy atmospheres and break the aerosol/mean molecular weight degeneracy. Looking forward to *JWST* and *Ariel*, being able to use UV observations to predict which planets are most likely to have measurable spectral features, and to interpret the very high quality optical and IR transmission spectra that will be obtained, will be crucial for maximizing the scientific return of these missions.

In addition to atmospheric science, understanding the UV environment of exoplanets is also crucial to understanding their habitability. Much attention has turned to rocky planets orbiting in the habitable zones of M dwarfs, as they are more readily detectable and charac-

terizable than their analogs around FGK stars. Transit and radial velocity surveys, for instance, have optimized their filter bandpasses for M dwarf spectral energy distributions (e.g., Ricker et al. 2015, Addison et al. 2019). However, the UV radiation from M dwarfs is much more stochastic than that from FGK stars, with both more energetic flares and higher flare rates in general (see, e.g., Medina et al. 2020). This could have significant impact on the viability of these planets for hosting life (Estrela & Valio 2018, France et al. 2020). Understanding the UV radiation history and current insolation of rocky planets orbiting M dwarfs is another important question addressed by UV observations.

While the *HST* UV capabilities are operational, we can continue to construct and exploit multi-wavelength transmission spectroscopy and investigate the UV environment of exoplanets. However, when those capabilities are gone, we will have a large gap in our ability to constrain these phenomena. In the following sections we outline two important science cases that could be performed with an exoplanet transmission survey undertaken with a UV telescope with the capabilities of *UVEX*.

4.8.1. *Constraining Hazes in Cool Exoplanet Atmospheres*

Whereas clouds are considered to be 'grey', scattering stellar insolation roughly equally with wavelength, Rayleigh scattering of small haze particles in the upper atmospheres of exoplanets has a very strong wavelength dependence ($\propto \lambda^{-4}$). This leads to a much higher cross-section of a hazy planetary atmosphere at bluer wavelengths, and correspondingly deeper transit depths. The slope in the transmission spectrum as a function of wavelength can thus be used to measure the particle size of hazes forming high up in a planet's atmosphere. Hazes may become more significant for planets cooler than 850 K (Morley et al. 2015, Crossfield & Kreidberg 2017), which are of particular interest to the community as they approach the conditions of habitability. Significant effort and observing time will be expended by the next generation of optical and IR missions to characterize the atmospheres of cool exoplanets, and large remaining uncertainties remain about the fraction of their atmospheres that are cloudy or hazy, and the characteristics of the extant clouds and hazes. See, e.g., Figure 2 of Sing et al. (2016) for a sample of hot Jupiters with significantly varying transmission spectra between UV and IR wavelengths. Understanding how hazes manifest across a large range of atmospheric compositions, from hydrogen- and helium-dominated atmospheres to higher mean molecular atmospheres dominated by, for instance, methane or carbon dioxide, over a range of exo-

planet sizes and temperatures is crucial for breaking the aerosol/mean molecular weight degeneracy that mutes the spectral features. By measuring a large sample of UV-IR transmission spectral slopes, we can constrain trends with planet properties, which can then be compared to theoretical and experimental studies of haze production rates and compositions (e.g. Gao et al. 2017, Hörst et al. 2018, He et al. 2020).

4.8.2. *Probing Metals, Clouds, and Rainout in Hot Exoplanets*

A few low-resolution observations of ultra-hot Jupiters (>2300 K) show strong absorption at UV wavelengths which far exceeds that expected from Rayleigh scattering (e.g. Sing et al. 2013, Evans et al. 2018, von Essen et al. 2019, Fu et al. 2021). The source of the absorption is not clear, and several suggestions (photochemistry, mass loss, disequilibrium chemistry) remain under consideration. Theoretical transmission spectra of hot (>1000 K) gas giant atmospheres from Lothringer et al. (2020) show strong absorption lines from heavy metal atoms and ions at NUV wavelengths, including Fe I, Fe II, Ti I, Ni I, Ca I, and Ca II. These species had not often been included as opacity sources in transmission spectra models because of their low abundances. However, the authors show that since they have such strong absorption lines in the UV, they can significantly increase the broadband transit depths measured at these wavelengths. Indeed, evidence for heavy metal absorption has been found for some ultra-hot exoplanets at higher resolution, e.g. Fossati et al. (2010), Gibson et al. (2020), Ehrenreich et al. (2020).

Lothringer et al. (2020) demonstrate the use of a UV-optical spectral index to test whether heavy metals are indeed the mystery UV opacity source for hot exoplanets. One such index is defined in their Eq. 2: $\Delta R_{\mathrm{p,NUV-Red}} = (R_{\mathrm{p},0.2-0.3\mu m} - R_{\mathrm{p},0.6-0.7\mu m})/H_{eq}$, where $R_{\mathrm{p},0.2-0.3\mu m}$ is the radius of the planet as measured between 0.2–0.3 μm, $R_{\mathrm{p},0.6-0.7\mu m}$ is the radius of the planet as measured between 0.6–0.7 μm, and H_{eq} is the atmospheric scale height at the equilibrium temperature. If the hot atmospheres are in equilibrium, then $\Delta R_{\mathrm{p,NUV-Red}}$ should increase rapidly from 3 to 9 between 1000 and 2500 K (see their Fig. 4). Between 2500 K and 4000 K, $\Delta R_{\mathrm{p,NUV-Red}}$ will slowly decrease to 6. This predicted characteristic shape to the spectral index could be tested with a large sample of $\Delta R_{\mathrm{p,NUV-Red}}$ measurements across the 1000–4000 K temperature range measured with *UVEX*. Further, we can test if the metals are raining out after forming clouds. If this is the case, then certain metal species should have depleted abundances in the atmospheric regions probed by transmission spectroscopy. This will

lead to a shallower slope in $\Delta R_{\mathrm{p,NUV-Red}}$ between 1000 and 2500 K.

4.8.3. *A Systematic NUV/FUV Survey with UVEX*

We can address the two aforementioned questions and provide a legacy survey of UV exoplanet measurements with a *UVEX* survey spanning a broad range of both planet equilibrium temperature and radius. To construct a sample survey, we searched the NASA Exoplanet Archive for all transiting exoplanets with mass measurements, and calculated the change in transit depth of one atmospheric scale height, assuming zero albedo and a heat re-circulation factor of 0.36. We calculated the number of transit observations with *UVEX* required to reach a precision of one atmospheric scale height for each planet. This was motivated by the typical size of atmospheric features in the NUV, which are around 3–5 atmospheric scale heights (e.g. Evans et al. 2018, Wakeford et al. 2020, Lothringer et al. 2022) – thus allowing transit depth measurements with a typical precision of ~3σ. To do this, we estimated the stellar flux in the *UVEX* passbands by first searching for the exoplanet host stars in the *GALEX* database (in the *GALEX* NUV band). For systems without *GALEX* data, we estimated the NUV flux by scaling the closest stellar model from the PHOENIX grid, and summing the flux in the *GALEX* NUV passband using `Pyphot`. We then designed the sample survey of the planets most amenable to atmospheric characterization with *UVEX* (those requiring fewer transit observations to reach the required precision in transit depth). To achieve a sufficient spread in equilibrium temperature, we selected the 15 planets with the highest signal-to-noise in five temperature bins: 0–800 K, 800–1300 K, 1300–1800 K, 1800–2300 K, and >2300 K. To provide a sufficient spread in planetary radii, we additionally selected the 15 planets with the highest SNR which were smaller than Neptune (not counting duplicates from the previous step), since larger planets are over-represented when ranking by SNR. This resulted in a total sample of 81 planets ranging from V=7–17 mag, shown in Figures 40 and 41. For each transit visit of each target we estimate the total observing time as equal to the duration of two full transits (to acquire sufficient out-of-transit baseline) plus one hour of overheads. In total the proposed survey of 81 planets would take 2,230 hours to complete—approximately three months. Of these planets, 36 can be used to investigate how haze properties of exoplanet atmospheres change with size (from ~1.0–15 $R_\oplus$) and temperature (from ~200–1250 K), and 45 can be used to investigate metal rain-out in ultra-hot giant planets from ~1300–3100 K. All of our targets will

have red-optical transit depths measured by the *TESS* all-sky survey, so their $\Delta R_{\mathrm{p,NUV-Red}}$ index can be measured. Besides its use in identifying haze-formation and rainout trends, we can use this index to flag planets that exhibit large offsets, and effectively select the most favorable targets for more detailed atmosphere characterization with *JWST* and *Ariel*.

There are many critical exoplanet atmosphere processes that can only be observed in the UV. For example: the presence and composition of clouds and hazes in cool exoplanets; the rain-out of metals in hot exoplanets; atmospheric escape and mass-loss processes on highly irradiated planets; and the integrated UV radiation experienced by potentially habitable planets. The three-month survey of 81 exoplanets outlined here would directly address the first two processes. It would also provide a legacy database of spectra for additional study, and, crucially, would enable interpretation of expensive optical and IR spectra obtained by upcoming NASA investments.

5. CONCLUSION

The *UVEX* mission opens a powerful new window to simultaneously explore both the static and dynamic UV sky. With a planned launch date in the late 2020's, *UVEX* fills a critical capability gap – wide-field UV imaging – in the era when Rubin, *Roman*, and *Euclid* will be transforming our understanding of the cosmos. Here we have described just a sampling of the anticipated science yield offered by *UVEX*, which covers the gamut of modern astrophysics, including all three science goals of NASA's Astrophysics division and the Astro2020 decadal survey. As evidenced by the success of projects like the Sloan Digital Sky Survey, by providing timely and high-quality data products to the entire community, the resulting *UVEX* discoveries will be limited only by the creativity of astronomers worldwide.

REFERENCES

Abbott, B. P., Abbott, R., Abbott, T. D., et al. 2016, ApJL, 818, L22, doi: 10.3847/2041-8205/818/2/L22

—. 2017a, ApJL, 848, L12, doi: 10.3847/2041-8213/aa91c9

—. 2017b, ApJL, 848, L13, doi: 10.3847/2041-8213/aa920c

—. 2017c, Nature, 551, 85, doi: 10.1038/nature24471

—. 2020a, Living Reviews in Relativity, 23, 3, doi: 10.1007/s41114-020-00026-9

Abbott, R., Abbott, T. D., Abraham, S., et al. 2020b, ApJL, 896, L44, doi: 10.3847/2041-8213/ab960f

—. 2020c, PhRvL, 125, 101102, doi: 10.1103/PhysRevLett.125.101102

Abbott, R., Abbott, T. D., Abraham, S., et al. 2021, ApJL, 913, L7, doi: 10.3847/2041-8213/abe949

Abdo, A. A., Ackermann, M., Ajello, M., et al. 2010, Science, 329, 817, doi: 10.1126/science.1192537

Ackley, K., Amati, L., Barbieri, C., et al. 2020, A&A, 643, A113, doi: 10.1051/0004-6361/202037669

Addison, B., Wright, D. J., Wittenmyer, R. A., et al. 2019, PASP, 131, 115003, doi: 10.1088/1538-3873/ab03aa

Afshordi, N., & Paczyński, B. 2003, ApJ, 592, 354, doi: 10.1086/375559

Aggarwal, K. M. & Keenan, F. P. 1999, ApJS, 123, 311

—. 2004, PhyS, 69, 385

Alexander, M. J., Hanes, R. J., Povich, M. S., & McSwain, M. V. 2016, AJ, 152, 190, doi: 10.3847/0004-6256/152/6/190

Alexander, K. D., Berger, E., Fong, W., et al. 2017, ApJL, 848, L21, doi: 10.3847/2041-8213/aa905d

Allen, D. A., & Hillier, D. J. 1993, PASA, 10, 338

Anand, S., Coughlin, M. W., Kasliwal, M. M., et al. 2021, Nature Astronomy, 5, 46, doi: 10.1038/s41550-020-1183-3

Andreoni, I., Goldstein, D. A., Kasliwal, M. M., et al. 2020, ApJ, 890, 131, doi: 10.3847/1538-4357/ab6a1b

Arcavi, I., Hosseinzadeh, G., Howell, D. A., et al. 2017, Nature, 551, 64, doi: 10.1038/nature24291

Arcavi, I. 2018, ApJL, 855, L23, doi: 10.3847/2041-8213/aab267

Arcavi, I., Wolf, W. M., Howell, D. A., et al. 2016, ApJ, 819, 35, doi: 10.3847/0004-637X/819/1/35

Asif, A., Barschke, M., Bastian-Querner, B., et al. 2021, arXiv e-prints, arXiv:2108.01493. https://arxiv.org/abs/2108.01493

Assef, R. J., Stern, D., Kochanek, C. S., et al. 2013, ApJ, 772, 26, doi: 10.1088/0004-637X/772/1/26

Aydi, E., Sokolovsky, K. V., Chomiuk, L., et al. 2020, Nature Astronomy, 4, 776, doi: 10.1038/s41550-020-1070-y

Bañados, E., Venemans, B. P., Mazzucchelli, C., et al. 2018, Nature, 553, 473, doi: 10.1038/nature25180

Bade, N., Komossa, S., & Dahlem, M. 1996, A&A, 309, L35

Balbus, S. A., & Hawley, J. F. 1998, Reviews of Modern Physics, 70, 1, doi: 10.1103/RevModPhys.70.1

Barnes, K. L., van Zee, L., & Skillman, E. D. 2011, ApJ, 743, 137, doi: 10.1088/0004-637X/743/2/137

Baron, E., Branch, D., Hauschildt, P. H., et al. 2000, ApJ, 545, 444, doi: 10.1086/317795

Barth, A. J., & Stern, D. 2018, ApJ, 859, 10, doi: 10.3847/1538-4357/aab3c5
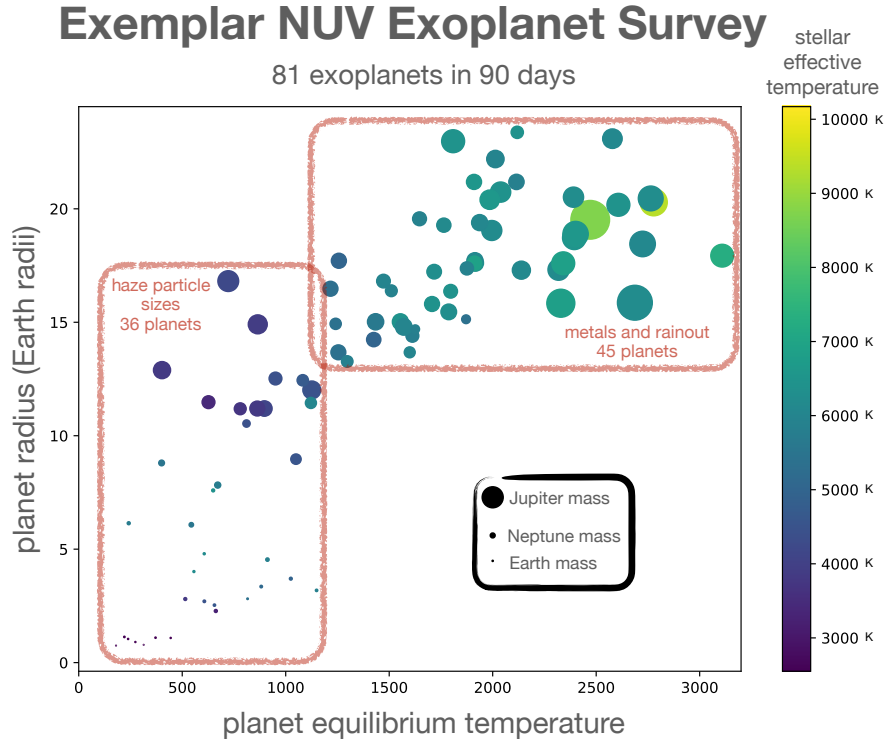
Figure 40. The planet radii and equilibrium temperatures of a sample of 81 planets that would be used to answer two critical exoplanet atmosphere questions: how haze properties of cooler exoplanets depend on planet size, equilibrium temperature, and host star properties; and the extent to which metals in ultra-hot atmospheres are raining out. The full sample would take ∼3 months to observe, and leave a legacy of FUV/NUV spectra of exoplanets that will be observed by *JWST* and *Ariel*/CASE.
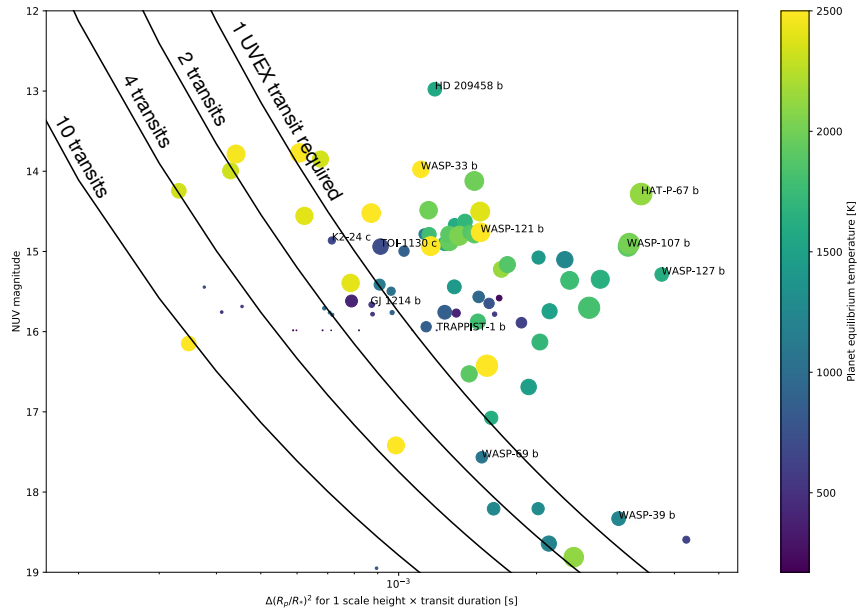
Figure 41. The observable atmospheric signal for each planet in the exemplar survey (defined as the fractional transit depth for one atmospheric scale height scaled by the transit duration), as a function of the NUV brightness of the host star. Solid lines show the number of *UVEX* transits (1, 2, 4, and 10) required to measure the transit depth to a precision of one atmospheric scale height.

Barth, A. J., Bennert, V. N., Canalizo, G., et al. 2015, ApJS, 217, 26, doi: 10.1088/0067-0049/217/2/26

Begelman, M. C., Armitage, P. J., & Reynolds, C. S. 2015, ApJ, 809, 118, doi: 10.1088/0004-637X/809/2/118

Begelman, M. C., McKee, C. F., & Shields, G. A. 1983, ApJ, 271, 70, doi: 10.1086/161178

Behroozi, P.S., et al. 2013, ApJ, 770(1), doi: 10.1088/0004-637X/770/1/57

Belczynski, K., Bulik, T., Fryer, C. L., et al. 2010, ApJ, 714, 1217, doi: 10.1088/0004-637X/714/2/1217

Ben-Ami, S., Hachinger, S., Gal-Yam, A., et al. 2015, ApJ, 803, 40, doi: 10.1088/0004-637X/803/1/40

Berg, D. A., Skillman, E. D., Henry, R. B. C., Erb, D. K., & Carigi, L. 2016, ApJ, 827, 126, doi: 10.3847/0004-637X/827/2/126

Berg D. A. et al. 2019, ApJ, doi: 10.3847/0004-637X/827/2/126

Berg, D. A., Chisholm, J., Erb, D. K., Skillman, E. D., Pogge, R. W., & Olivier, G. M. 2021, ApJ, 922, 170

Berger, E., Kulkarni, S. R., & Chevalier, R. A. 2002, ApJL, 577, L5, doi: 10.1086/344045

Berrington, K. A., Burke, P. G., Dufton, P. L., & Kingston, A. E. 1985, Atomic Data and Nuclear Data Tables, 33, 195

Bersten, M. C., Folatelli, G., García, F., et al. 2018, Nature, 554, 497, doi: 10.1038/nature25151

Bhattacharya, M., Kumar, P., & Smoot, G. 2019, MNRAS, 486, 5289, doi: 10.1093/mnras/stz1147

Bigiel, F., Leroy, A., Walter, F., et al. 2008, AJ, 136, 2846, doi: 10.1088/0004-6256/136/6/2846

Björklund, R., Sundqvist, J. O., Puls, J., & Najarro, F. 2021, Astronomy & Astrophysics, 648, A36, doi: 10.1051/0004-6361/202038384

Blagorodnova, N., Gezari, S., Hung, T., et al. 2017, ApJ, 844, 46, doi: 10.3847/1538-4357/aa7579

Blagorodnova, N., Cenko, S. B., Kulkarni, S. R., et al. 2019, ApJ, 873, 92, doi: 10.3847/1538-4357/ab04b0

Bland-Hawthorn, J., & Gerhard, O. 2016, ARA&A, 54, 529, doi: 10.1146/annurev-astro-081915-023441

Blandford, R. D., & McKee, C. F. 1982, ApJ, 255, 419, doi: 10.1086/159843

Blum, R. D., Damineli, A., & Conti, P. S. 1999, AJ, 117, 1392, doi: 10.1086/300791

Bode, M. F., & Evans, A. 2008, Classical Novae, Vol. 43 (Cambridge University Press)

Bodensteiner, J., Shenar, T., Mahy, L., et al. 2020, A&A, 641, A43, doi: 10.1051/0004-6361/202038682

Boian, I., & Groh, J. H. 2020, MNRAS, 496, 1325, doi: 10.1093/mnras/staa1540

Boksenberg, A., Evans, R. G., Fowler, R. G., et al. 1973, MNRAS, 163, 291, doi: 10.1093/mnras/163.3.291

Bolton, A. S., Schlegel, D. J., Aubourg, É., & others. 2012, AJ, 144, 144

Bonito, R., Hartigan, P., Venuti, L., et al. 2018, arXiv e-prints, arXiv:1812.03135. https://arxiv.org/abs/1812.03135

Bouret, J. C., Lanz, T., Hillier, D. J., et al. 2015, MNRAS, 449, 1545, doi: 10.1093/mnras/stv379

Branch, D., & Wheeler, J. C. 2017, Supernova Explosions (Springer-Verlag), doi: 10.1007/978-3-662-55054-0

Bright, J. S., Margutti, R., Matthews, D., et al. 2021, arXiv e-prints, arXiv:2110.05514. https://arxiv.org/abs/2110.05514

Brosch, N. 1999, Experimental Astronomy, 9, 119

Brown, J. S., Kochanek, C. S., Holoien, T. W. S., et al. 2018, MNRAS, 473, 1130, doi: 10.1093/mnras/stx2372

Brown, P. J., Dawson, K. S., de Pasquale, M., et al. 2012, ApJ, 753, 22, doi: 10.1088/0004-637X/753/1/22

—. 2021b, ApJ, 912, 46, doi: 10.3847/1538-4357/abef05

Bufano, F., Immler, S., Turatto, M., et al. 2009, ApJ, 700, 1456, doi: 10.1088/0004-637X/700/2/1456

Bulla, M., Covino, S., Kyutoku, K., et al. 2019, Nature Astronomy, 3, 99, doi: 10.1038/s41550-018-0593-y

Cackett, E. M., Bentz, M. C., & Kara, E. 2021, iScience, 24, 102557, doi: 10.1016/j.isci.2021.102557

Calvet, N., & Gullbring, E. 1998, ApJ, 509, 802, doi: 10.1086/306527

Calzetti, D., Armus, L., Bohlin, R. C., et al. 2000, ApJ, 533, 682, doi: 10.1086/308692

Camacho, I., Garcia, M., Herrero, A., & Simón-Díaz, S. 2016, A&A, 585, A82, doi: 10.1051/0004-6361/201425533

Campana, S., Mangano, V., Blustin, A. J., et al. 2006, Nature, 442, 1008, doi: 10.1038/nature04892

Cano, Z., Wang, S.-Q., Dai, Z.-G., & Wu, X.-F. 2017, Advances in Astronomy, 2017, 8929054, doi: 10.1155/2017/8929054

Cardelli, J. A., Clayton, G. C., & Mathis, J. S. 1989, ApJ, 345, 245, doi: 10.1086/167900

Carney, B. W. 1979, ApJ, 233, 211, doi: 10.1086/157383

Cartledge, S. I. B., Clayton, G. C., Gordon, K. D., et al. 2005, ApJ, 630, 355, doi: 10.1086/431922

Castor, J. I., & Lamers, H. J. G. L. M. 1979, ApJS, 39, 481, doi: 10.1086/190583

Cenko, S. B., Kulkarni, S. R., Horesh, A., et al. 2013, ApJ, 769, 130, doi: 10.1088/0004-637X/769/2/130

Cenko, S. B., Cucchiara, A., Roth, N., et al. 2016, ApJL, 818, L32, doi: 10.3847/2041-8205/818/2/L32

Charisi, M., Bartos, I., Haiman, Z., et al. 2016, MNRAS, 463, 2145, doi: 10.1093/mnras/stw1838

Chen, H.-Y., Fishbach, M., & Holz, D. E. 2018, Nature, 562, 545, doi: 10.1038/s41586-018-0606-0

Chevalier, R. A., & Fransson, C. 2006, ApJ, 651, 381, doi: 10.1086/507606

—. 2017, Thermal and Non-thermal Emission from Circumstellar Interaction, ed. A. W. Alsabti & P. Murdin (Springer), 875, doi: 10.1007/978-3-319-21846-5_34

Chevalier, R. A., & Irwin, C. M. 2011, ApJL, 729, L6, doi: 10.1088/2041-8205/729/1/L6

Chiang, Y.-K., & Ménard, B. 2019, ApJ, 870, 120, doi: 10.3847/1538-4357/aaf4f6

Chomiuk, L., Metzger, B. D., & Shen, K. J. 2020, arXiv e-prints, arXiv:2011.08751. https://arxiv.org/abs/2011.08751

Chomiuk, L., Soderberg, A. M., Moe, M., et al. 2012, ApJ, 750, 164, doi: 10.1088/0004-637X/750/2/164

Cioni, M. . R. L., Storm, J., Bell, C. P. M., et al. 2019, The Messenger, 175, 54, doi: 10.18727/0722-6691/5128

Cioni, M. R. L., Clementini, G., Girardi, L., et al. 2011, A&A, 527, A116, doi: 10.1051/0004-6361/201016137

Cohn, J. H., Walsh, J. L., Boizelle, B. D., et al. 2021, ApJ, 919, 77, doi: 10.3847/1538-4357/ac0f78

Cole, A. A., Skillman, E. D., Tolstoy, E., et al. 2007, ApJL, 659, L17, doi: 10.1086/516711

Colinda, L., et al. 1996, AJ, 112, 307m doi: 10.1086/118016

Conroy C. et al. 2015, ApJ, 805(1), doi: 10.1088/2041-8205/805/1/L2

Coppejans, D. L., & Knigge, C. 2020, NewAR, 89, 101540, doi: 10.1016/j.newar.2020.101540

Coppejans, D. L., Margutti, R., Terreran, G., et al. 2020, ApJL, 895, L23, doi: 10.3847/2041-8213/ab8cc7

Corsi, A., Gal-Yam, A., Kulkarni, S. R., et al. 2016, ApJ, 830, 42, doi: 10.3847/0004-637X/830/1/42

Crossfield, I. J. M., & Kreidberg, L. 2017, AJ, 154, 261, doi: 10.3847/1538-3881/aa9279

Crowther, P. A., Caballero-Nieves, S. M., Bostroem, K. A., et al. 2016, MNRAS, 458, 624, doi: 10.1093/mnras/stw273

Coulter, D. A., Foley, R. J., Kilpatrick, C. D., et al. 2017, Science, 358, 1556, doi: 10.1126/science.aap9811

Cowperthwaite, P. S., Berger, E., Villar, V. A., et al. 2017, ApJL, 848, L17, doi: 10.3847/2041-8213/aa8fc7

Dalcanton, J. J., Williams, B. F., Lang, D., et al. 2012, ApJS, 200, 18, doi: 10.1088/0067-0049/200/2/18

Da Rio, N., Robberto, M., Hillenbrand, L. A., Henning, T., & Stassun, K. G. 2012, ApJ, 748, 14, doi: 10.1088/0004-637X/748/1/14

Darvish, B., Martin, C., Gonçalves, T. S., et al. 2018, ApJ, 853, 155, doi: 10.3847/1538-4357/aaa5a4

De, K., Kasliwal, M. M., Hankins, M. J., et al. 2021, ApJ, 912, 19, doi: 10.3847/1538-4357/abeb75

De Cicco, D., Paolillo, M., Falocco, S., et al. 2019, A&A, 627, A33, doi: 10.1051/0004-6361/201935659

de Jager, C., Hoekstra, R., van der Hucht, K. A., et al. 1974, Ap&SS, 26, 207, doi: 10.1007/BF00642637

de Jager, C., Lamers, H. J. G. L. M., & van der Hucht, K. A. 1975, Ap&SS, 38, 313, doi: 10.1007/BF00647130

de Mink, S. E., Sana, H., Langer, N., Izzard, R. G., & Schneider, F. R. N. 2014, ApJ, 782, 7, doi: 10.1088/0004-637X/782/1/7

De Robertis, M. M., Dufour, R. J., & Hunt, R. W. 1987, JRASC, 81, 195

de Sá-Freitas, C., Gonçalves, T. S., de Carvalho, R. R., et al. 2021, MNRAS, doi: 10.1093/mnras/stab3230

De Silva, G. M., Freeman, K. C., Bland-Hawthorn, J., et al. 2015, MNRAS, 449, 2604, doi: 10.1093/mnras/stv327

della Valle, M., Bianchini, A., Livio, M., & Orio, M. 1992, A&A, 266, 232

Della Valle, M., & Izzo, L. 2020, A&A Rv, 28, 3, doi: 10.1007/s00159-020-0124-6

Deng, L.-C., Newberg, H. J., Liu, C., et al. 2012, Research in Astronomy and Astrophysics, 12, 735, doi: 10.1088/1674-4527/12/7/003

Derdzinski, A. M., Metzger, B. D., & Lazzati, D. 2017, MNRAS, 469, 1314, doi: 10.1093/mnras/stx829

—. 2017b, A&A, 605, A83, doi: 10.1051/0004-6361/201730942

Dixon, D., Tayar, J., & Stassun, K. G. 2020, AJ, 160, 12, doi: 10.3847/1538-3881/ab9080

D'Orazio, D. J., & Di Stefano, R. 2018, MNRAS, 474, 2975, doi: 10.1093/mnras/stx2936

D'Orazio, D. J., Haiman, Z., & Schiminovich, D. 2015, Nature, 525, 351, doi: 10.1038/nature15262

Donovan Meyer, J., Peek, J. E. G., Putman, M., & Grcevich, J. 2015, ApJ, 808, 136, doi: 10.1088/0004-637X/808/2/136

Draine, B. T. 2003, ARA&A, 41, 241, doi: 10.1146/annurev.astro.41.011802.094840

—. 2011, Physics of the Interstellar and Intergalactic Medium (Princeton University Press)

Drout, M. R., Chornock, R., Soderberg, A. M., et al. 2014, ApJ, 794, 23, doi: 10.1088/0004-637X/794/1/23

Drout, M. R., Piro, A. L., Shappee, B. J., et al. 2017, Science, 358, 1570, doi: 10.1126/science.aaq0049

Duez, M. D., Foucart, F., Kidder, L. E., Ott, C. D., & Teukolsky, S. A. 2010, Classical and Quantum Gravity, 27, 114106, doi: 10.1088/0264-9381/27/11/114106

Edelstein, J. Korpel, E. J., Adolfo, J., et al. 2006, ApJL, 644, L159, doi: 10.1086/505205

Ehrenreich, D., Lovis, C., Allart, R., et al. 2020, Nature, 580, 597–601, doi: 10.1038/s41586-020-2107-1

Eichler, D., Livio, M., Piran, T., et al. 1989, Nature, 340, 126, doi: 10.1038/340126a0

Elahi, P. J., Welker, C., Power, C., et al. 2018, MNRAS, 475, 5338, doi: 10.1093/mnras/sty061

Eldridge, J. J., Izzard, R. G., & Tout, C. A. 2008, MNRAS, 384, 1109, doi: 10.1111/j.1365-2966.2007.12738.x

Eldridge, J. J., & Stanway, E. R. 2009, MNRAS, 400, 1019, doi: 10.1111/j.1365-2966.2009.15514.x

Eldridge, J. J., Stanway, E. R., Xiao, L., et al. 2017, PASA, 34, e058, doi: 10.1017/pasa.2017.51

Endsley, R., Stark, D. P., Chevallard, J., & Charlot, S. 2021, MNRAS, 500, 5229, doi: 10.1093/mnras/staa3370

Estrela, R., & Valio, A. 2018, Astrobiology, 18, 1414, doi: 10.1089/ast.2017.1724

Evans, C. J., Howarth, I. D., Irwin, M. J., Burnley, A. W., & Harries, T. J. 2004, MNRAS, 353, 601, doi: 10.1111/j.1365-2966.2004.08096.x

Evans, C. J., Lennon, D. J., Smartt, S. J., & Trundle, C. 2006, A&A, 456, 623, doi: 10.1051/0004-6361:20064988

Evans, C. J., Taylor, W. D., Hénault-Brunet, V., et al. 2011, A&A, 530, A108, doi: 10.1051/0004-6361/201116782

Evans, P. A., Cenko, S. B., Kennea, J. A., et al. 2017, Science, 358, 1565, doi: 10.1126/science.aap9580

Evans, T. M., Sing, D. K., Goyal, J. M., et al. 2018, AJ, 156, 283, doi: 10.3847/1538-3881/aaebff

Feeney, S. M., Peiris, H. V., Nissanke, S. M., & Mortlock, D. J. 2021, PhRvL, 126, 171102, doi: 10.1103/PhysRevLett.126.171102

Feigelson, E. D., Getman, K. V., Townsley, L. K., et al. 2011, ApJS, 194, 9, doi: 10.1088/0067-0049/194/1/9

Fender, R., & Belloni, T. 2004, ARA&A, 42, 317, doi: 10.1146/annurev.astro.42.053102.134031

Fender, R., & Muñoz-Darias, T. 2016, The Balance of Power: Accretion and Feedback in Stellar Mass Black Holes, Vol. 905 (Springer Verlag), 65, doi: 10.1007/978-3-319-19416-5_3

Fernández, R., & Metzger, B. D. 2016, Annual Review of Nuclear and Particle Science, 66, 23, doi: 10.1146/annurev-nucl-102115-044819

Fernández, R., Tchekhovskoy, A., Quataert, E., Foucart, F., & Kasen, D. 2019, MNRAS, 482, 3373, doi: 10.1093/mnras/sty2932

Ferrarese, L., & Merritt, D. 2000, ApJL, 539, L9, doi: 10.1086/312838

Ferreira, J., & Pelletier, G. 1995, A&A, 295, 807

Findeisen, K., & Hillenbrand, L. 2010, AJ, 139, 1338, doi: 10.1088/0004-6256/139/4/1338

Fisher, D. B., Bolatto, A. D., Herrera-Camus, R., et al. 2014, Nature, 505, 186, doi: 10.1038/nature12765

Fitzpatrick, E. L., & Massa, D. 2007, ApJ, 663, 320, doi: 10.1086/518158

Fitzpatrick, E. L., Massa, D., Gordon, K. D., Bohlin, R., & Clayton, G. C. 2019, ApJ, 886, 108, doi: 10.3847/1538-4357/ab4c3a

Fossati, L., Haswell, C. A., Froning, C. S., et al. 2010, The Astrophysical Journal, 714, L222–L227, doi: 10.1088/2041-8205/714/2/l222

Foucart, F. 2012, PhRvD, 86, 124007, doi: 10.1103/PhysRevD.86.124007

France, K., Duvvuri, G., Egan, H., et al. 2020, AJ, 160, 237, doi: 10.3847/1538-3881/abb465

Franckowiak, A., Jean, P., Wood, M., Cheung, C. C., & Buson, S. 2018, A&A, 609, A120, doi: 10.1051/0004-6361/201731516

Fransson, C., Challis, P. M., Chevalier, R. A., et al. 2005, ApJ, 622, 991, doi: 10.1086/426495

Fransson, C., Ergon, M., Challis, P. J., et al. 2014, ApJ, 797, 118, doi: 10.1088/0004-637X/797/2/118

Fraser, M., Stritzinger, M. D., Brennan, S. J., et al. 2021, arXiv e-prints, arXiv:2108.07278. https://arxiv.org/abs/2108.07278

Frederick, S., Gezari, S., Graham, M. J., et al. 2021, ApJ, 920, 56, doi: 10.3847/1538-4357/ac110f

Fremling, C., Miller, A. A., Sharma, Y., et al. 2020, ApJ, 895, 32, doi: 10.3847/1538-4357/ab8943

Froese Fischer, C. & Tachiev, G. 2004, Atomic Data and Nuclear Data Tables, 87

Frost, A. J., Bodensteiner, J., Rivinius, T., et al. 2022, A&A, 659, L3, doi: 10.1051/0004-6361/202143004

Fu, G., Deming, D., Knutson, H., et al. 2017, ApJL, 847, L22, doi: 10.3847/2041-8213/aa8e40

Fu, G., Deming, D., Lothringer, J., et al. 2021, The Astronomical Journal, 162, 108, doi: 10.3847/1538-3881/ac1200

Fuller, J. 2017, MNRAS, 470, 1642, doi: 10.1093/mnras/stx1314

Fuller, J., & Ro, S. 2018, MNRAS, 476, 1853, doi: 10.1093/mnras/sty369

Gal-Yam, A., Bufano, F., Barlow, T. A., et al. 2008, ApJL, 685, L117, doi: 10.1086/592744

Gal-Yam, A., Arcavi, I., Ofek, E. O., et al. 2014, Nature, 509, 471, doi: 10.1038/nature13304

Gal-Yam, A., Bruch, R., Schulze, S., et al. 2021, arXiv e-prints, arXiv:2111.12435. https://arxiv.org/abs/2111.12435

Galama, T. J., Vreeswijk, P. M., van Paradijs, J., et al. 1998, Nature, 395, 670, doi: 10.1038/27150

Gao, P., Marley, M. S., Zahnle, K., Robinson, T. D., & Lewis, N. K. 2017, AJ, 153, 139, doi: 10.3847/1538-3881/aa5fab

Garcia, M. 2018, MNRAS, 474, L66, doi: 10.1093/mnrasl/slx194

Garcia, M., Herrero, A., Najarro, F., Camacho, I., & Lorenzo, M. 2019a, MNRAS, 484, 422, doi: 10.1093/mnras/sty3503

Garcia, M., Evans, C. J., Bestenlehner, J. M., et al. 2019b, arXiv e-prints, arXiv:1908.04687. https://arxiv.org/abs/1908.04687

Garnett, D. R. 1992, AJ, 103, 1330

Garrison-Kimmel, S., et al. 2017, MNRAS, 464, doi: 10.1093/mnras/stt2377

Gebhardt, K., Bender, R., Bower, G., et al. 2000, ApJL, 539, L13, doi: 10.1086/312840

Geha, M., Blanton, M. R., Yan, R., & Tinker, J. L. 2012, ApJ, 757, 85, doi: 10.1088/0004-637X/757/1/85

Gehrels, et al. 2004, NewAR, 48, 431, doi: 10.1016/j.newar.2003.12.055

Gezari, S. 2021, arXiv e-prints, arXiv:2104.14580. https://arxiv.org/abs/2104.14580

Gezari, S., Dessart, L., Basa, S., et al. 2008a, ApJL, 683, L131, doi: 10.1086/591647

Gezari, S., Basa, S., Martin, D. C., et al. 2008b, ApJ, 676, 944, doi: 10.1086/529008

Gezari, S., Heckman, T., Cenko, S. B., et al. 2009, ApJ, 698, 1367, doi: 10.1088/0004-637X/698/2/1367

Gezari, S., Chornock, R., Rest, A., et al. 2012, Nature, 485, 217, doi: 10.1038/nature10990

Gezari, S., Martin, D. C., Forster, K., et al. 2013, ApJ, 766, 60, doi: 10.1088/0004-637X/766/1/60

Ghez, A. M., Salim, S., Weinberg, N. N., et al. 2008, ApJ, 689, 1044, doi: 10.1086/592738

Gibson, N. P., Merritt, S., Nugroho, S. K., et al. 2020, Monthly Notices of the Royal Astronomical Society, 493, 2215–2228, doi: 10.1093/mnras/staa228

Goldstein, D. A., Veres, P., Burns, E., et al. 2017, ApJ, 848, L14, doi: 10.3847/2041-8213/aa8f41

Goldstein, D. A., Andreoni, I., Nugent, P. E., et al. 2019, ApJL, 881, L7, doi: 10.3847/2041-8213/ab3046

Gomez, S., Hosseinzadeh, G., Cowperthwaite, P. S., et al. 2019, ApJL, 884, L55, doi: 10.3847/2041-8213/ab4ad5

Gong, Y., Liu, X., Cao, Y., et al. 2019, ApJ, 883, 203, doi: 10.3847/1538-4357/ab391e

Gordon, K. D., Clayton, G. C., Misselt, K. A., Landolt, A. U., & Wolff, M. J. 2003, ApJ, 594, 279, doi: 10.1086/376774

Götberg, Y., de Mink, S. E., & Groh, J. H. 2017, A&A, 608, A11, doi: 10.1051/0004-6361/201730472

Götberg, Y., de Mink, S. E., Groh, J. H., et al. 2018, A&A, 615, A78, doi: 10.1051/0004-6361/201732274

Götberg, Y., de Mink, S. E., Groh, J. H., Leitherer, C., & Norman, C. 2019, A&A, 629, A134, doi: 10.1051/0004-6361/201834525

Götberg, Y., de Mink, S. E., McQuinn, M., et al. 2020a, A&A, 634, A134, doi: 10.1051/0004-6361/201936669

Götberg, Y., Korol, V., Lamberts, A., et al. 2020b, ApJ, 904, 56, doi: 10.3847/1538-4357/abbda5

Gottlieb, O., Lalakos, A., Bromberg, O., Liska, M., & Tchekhovskoy, A. 2021, arXiv e-prints, arXiv:2109.14619. https://arxiv.org/abs/2109.14619

Gottlieb, O., Nakar, E., & Piran, T. 2018, MNRAS, 473, 576, doi: 10.1093/mnras/stx2357

Gottlieb, O., Nakar, E., Piran, T., & Hotokezaka, K. 2018, MNRAS, 479, 588, doi: 10.1093/mnras/sty1462

Graham, A. W., Trujillo, I., & Caon, N. 2001, AJ, 122, 1707, doi: 10.1086/323090

Graham, M. J., Djorgovski, S. G., Drake, A. J., et al. 2014, MNRAS, 439, 703, doi: 10.1093/mnras/stt2499

—. 2017, MNRAS, 470, 4112, doi: 10.1093/mnras/stx1456

Graham, M. J., Djorgovski, S. G., Stern, D., et al. 2015a, Nature, 518, 74, doi: 10.1038/nature14143

—. 2015b, MNRAS, 453, 1562, doi: 10.1093/mnras/stv1726

Graham, M. J., Ford, K. E. S., McKernan, B., et al. 2020a, PhRvL, 124, 251102, doi: 10.1103/PhysRevLett.124.251102

Graham, M. J., Ross, N. P., Stern, D., et al. 2020b, MNRAS, 491, 4925, doi: 10.1093/mnras/stz3244

Green, G. M., Schlafly, E. F., Finkbeiner, D. P., et al. 2015, ApJ, 810, 25, doi: 10.1088/0004-637X/810/1/25

Greene, J. E., Strader, J., & Ho, L. C. 2020, ARA&A, 58, 257, doi: 10.1146/annurev-astro-032620-021835

Gressel, O., Turner, N. J., Nelson, R. P., & McNally, C. P. 2015, ApJ, 801, 84, doi: 10.1088/0004-637X/801/2/84

Groenewegen, M. A. T., Lamers, H. J. G. L. M., & Pauldrach, A. W. A. 1989, A&A, 221, 78

Groh, J. H. 2014, A&A, 572, L11, doi: 10.1051/0004-6361/201424852

Groh, J. H., Oliveira, A. S., & Steiner, J. E. 2008, A&A, 485, 245, doi: 10.1051/0004-6361:200809511

Gullbring, E., Hartmann, L., Briceño, C., & Calvet, N. 1998, ApJ, 492, 323, doi: 10.1086/305032

Guo, H., Malkan, M. A., Gu, M., et al. 2016, ApJ, 826, 186, doi: 10.3847/0004-637X/826/2/186

Guseva, N. G. et al 2017, *Astronomy and Astrophysics*, doi: 10.1051/0004-6361/201629181

Hagen, L. M. Z., Siegel, M. H., Hoversten, E. A., et al. 2017, MNRAS, 466, 4540, doi: 10.1093/mnras/stw2954

Haggard, D., Nynka, M., Ruan, J. J., et al. 2017, ApJL,
   848, L25, doi: 10.3847/2041-8213/aa8ede

Hallinan, G., Corsi, A., Mooley, K. P., et al. 2017, Science,
   358, 1579, doi: 10.1126/science.aap9855

Hameury, J. M. 2020, Advances in Space Research, 66,
   1004, doi: 10.1016/j.asr.2019.10.022

Han, Z., Podsiadlowski, P., & Lynas-Gray, A. E. 2007,
   MNRAS, 380, 1098,
   doi: 10.1111/j.1365-2966.2007.12151.x

Han, Z., Podsiadlowski, P., Maxted, P. F. L., Marsh, T. R.,
   & Ivanova, N. 2002, MNRAS, 336, 449,
   doi: 10.1046/j.1365-8711.2002.05752.x

Harris, J., & Zaritsky, D. 2004, AJ, 127, 1531,
   doi: 10.1086/381953

—. 2009, AJ, 138, 1243, doi: 10.1088/0004-6256/138/5/1243

Hartmann, L., Herczeg, G., & Calvet, N. 2016, ARA&A,
   54, 135, doi: 10.1146/annurev-astro-081915-023347

He, C., Horst, S. M., Lewis, N. K., et al. 2020, Haze
   Formation in Warm H2-rich Exoplanet Atmospheres.
   https://arxiv.org/abs/2008.09700

Helmi, A. 2008, A&A Rv, 15, 145,
   doi: 10.1007/s00159-008-0009-6

Helmi, A., White, S. D. M., de Zeeuw, P. T., & Zhao, H.
   1999, Nature, 402, 53, doi: 10.1038/46980

Hennessy, J., et al. 2021, Proc. SPIE 11821,
   doi: 10.1117/12.2595524

Hensley, B. S., & Draine, B. T. 2021, ApJ, 906, 73,
   doi: 10.3847/1538-4357/abc8f1

Hillier, D. J. 2020, Galaxies, 8, 60,
   doi: 10.3390/galaxies8030060

Hillier, D. J., Lanz, T., Heap, S. R., et al. 2003, ApJ, 588,
   1039, doi: 10.1086/374329

Hjorth, J., & Bloom, J. S. 2012, The Gamma-Ray Burst -
   Supernova Connection (Cambridge University Press),
   169–190

Ho, A. Y. Q., Phinney, E. S., Ravi, V., et al. 2019a, ApJ,
   871, 73, doi: 10.3847/1538-4357/aaf473

Ho, A. Y. Q., Goldstein, D. A., Schulze, S., et al. 2019b,
   arXiv e-prints, arXiv:1904.11009.
   https://arxiv.org/abs/1904.11009

—. 2019c, ApJ, 887, 169, doi: 10.3847/1538-4357/ab55ec

Ho, A. Y. Q., Perley, D. A., Kulkarni, S. R., et al. 2020a,
   arXiv e-prints, arXiv:2003.01222.
   https://arxiv.org/abs/2003.01222

Ho, A. Y. Q., Perley, D. A., Beniamini, P., et al. 2020b,
   ApJ, 905, 98, doi: 10.3847/1538-4357/abc34d

Ho, A. Y. Q., Perley, D. A., Gal-Yam, A., et al. 2021a,
   arXiv e-prints, arXiv:2105.08811.
   https://arxiv.org/abs/2105.08811

Ho, A. Y. Q., Margalit, B., Bremer, M., et al. 2021b, arXiv
   e-prints, arXiv:2110.05490.
   https://arxiv.org/abs/2110.05490

Ho, L. C. 2008, ARA&A, 46, 475,
   doi: 10.1146/annurev.astro.45.051806.110546

Hoenk, M. E. et al. 2009, Infrared Systems and
   Photoelectric Technology IV, 46, 475,
   doi: 10.1117/12.832326

Hosek, Matthew W., J., Lu, J. R., Lam, C. Y., et al. 2020,
   AJ, 160, 143, doi: 10.3847/1538-3881/aba533

Hosseinzadeh, G., Cowperthwaite, P. S., Gomez, S., et al.
   2019, ApJL, 880, L4, doi: 10.3847/2041-8213/ab271c

Hotokezaka, K., Beniamini, P., & Piran, T. 2018,
   International Journal of Modern Physics D, 27, 1842005,
   doi: 10.1142/S0218271818420051

Hotokezaka, K., & Nakar, E. 2020, The Astrophysical
   Journal, 891, 152

Humphries, C. M., Jamar, C., Malaise, D., & Wroe, H.
   1976, A&A, 49, 389

Hung, T., Cenko, S. B., Roth, N., et al. 2019, ApJ, 879,
   119, doi: 10.3847/1538-4357/ab24de

Hung, T., Foley, R. J., Veilleux, S., et al. 2021, ApJ, 917, 9,
   doi: 10.3847/1538-4357/abf4c3

Hurley, J. R., Pols, O. R., & Tout, C. A. 2000, MNRAS,
   315, 543, doi: 10.1046/j.1365-8711.2000.03426.x

Hurley, J. R., Tout, C. A., & Pols, O. R. 2002, MNRAS,
   329, 897, doi: 10.1046/j.1365-8711.2002.05038.x

Hörst, S. M., He, C., Lewis, N. K., et al. 2018, Nature
   Astronomy, 2, 303–306, doi: 10.1038/s41550-018-0397-0

IceCube Collaboration, Aartsen, M. G., Ackermann, M.,
   et al. 2018, Science, 361, eaat1378,
   doi: 10.1126/science.aat1378

Ilbert, O., McCracken, H. J., Le Fèvre, O., et al. 2013,
   A&A, 556, A55, doi: 10.1051/0004-6361/201321100

Ingleby, L., Calvet, N., Herczeg, G., et al. 2013, ApJ, 767,
   112, doi: 10.1088/0004-637X/767/2/112

Ivezić, Ž., Kahn, S. M., Tyson, J. A., et al. 2019, ApJ, 873,
   111, doi: 10.3847/1538-4357/ab042c

Ivezić, Ž., Sesar, B., Jurić, M., et al. 2008, ApJ, 684, 287,
   doi: 10.1086/589678

Iyer, A. R., Swain, M. R., Zellem, R. T., et al. 2016, ApJ,
   823, 109, doi: 10.3847/0004-637X/823/2/109

Izotov, Y. I., et al. 2019, MNRAS, 483(3),
   doi: 10.1093/mnras/sty3472

Izotov, Y. I., et al. 2019, Astronomy and Astrophysics, 623
   doi: 10.1051/0004-6361/201834768

Jacobson-Galán, W., Dessart, L., Jones, D., et al. 2021,
   arXiv e-prints, arXiv:2109.12136.
   https://arxiv.org/abs/2109.12136

Janka, H.-T. 2017, Neutrino-Driven Explosions, ed. A. W. Alsabti & P. Murdin (Springer), 1095, doi: 10.1007/978-3-319-21846-5_109

Jiang, Y.-F., Guillochon, J., & Loeb, A. 2016, ApJ, 830, 125, doi: 10.3847/0004-637X/830/2/125

Jo, Y.-S., Seon, K.-I., Min, K.-W., et al. 2017, ApJS, 231, 21, doi: 10.3847/1538-4365/aa8091

Jo, Y.-S., Seon, K.-I., Min, K.-W., et al. 2019, ApJS, 243, 9, doi: 10.3847/1538-4365/ab22ae

Johns-Krull, C. M. 2007, ApJ, 664, 975, doi: 10.1086/519017

Johnson, B. D., Schiminovich, D., Seibert, M., et al. 2007a, ApJS, 173, 392, doi: 10.1086/522960

—. 2007b, ApJS, 173, 377, doi: 10.1086/522932

Juvela, M., & Montillaud, J. 2016, A&A, 585, A38, doi: 10.1051/0004-6361/201425112

Karachentsev, I. D., & Kaisina, E. I. 2019, Astrophysical Bulletin, 74, 111, doi: 10.1134/S1990341319020019

Karachentsev, I. D. et al. 2013, AJ, 145(4), doi: 10.1088/0004-6256/145/4/101

Kasen, D. 2010, ApJ, 708, 1025, doi: 10.1088/0004-637X/708/2/1025

Kasen, D., Fernández, R., & Metzger, B. D. 2015, MNRAS, 450, 1777, doi: 10.1093/mnras/stv721

Kasen, D., Metzger, B., Barnes, J., Quataert, E., & Ramirez-Ruiz, E. 2017, Nature, 551, 80, doi: 10.1038/nature24453

Kasliwal, M. M., Nakar, E., Singer, L. P., et al. 2017, Science, 358, 1559, doi: 10.1126/science.aap9455

Kasliwal, M. M., Anand, S., Ahumada, T., et al. 2020, ApJ, 905, 145, doi: 10.3847/1538-4357/abc335

Kawaguchi, K., Kyutoku, K., Shibata, M., & Tanaka, M. 2016, ApJ, 825, 52, doi: 10.3847/0004-637X/825/1/52

Kawaguchi, K., Shibata, M., & Tanaka, M. 2020, ApJ, 889, 171, doi: 10.3847/1538-4357/ab61f6

Kennicutt, Jr., R. C. 1998, ApJ, 498, 541, doi: 10.1086/305588

Kesden, M. 2012, PhRvD, 85, 024037, doi: 10.1103/PhysRevD.85.024037

Kippenhahn, R., & Weigert, A. 1967, ZA, 65, 251

Kisielius, R., Storey, P. J., Ferland, G. J., & Keenan, F. P. 2009, MNRAS, 397, 903

Koenigl, A. 1991, ApJL, 370, L39, doi: 10.1086/185972

Komossa, S., & Bade, N. 1999, A&A, 343, 775. https://arxiv.org/abs/astro-ph/9901141

Kormendy, J., & Richstone, D. 1995, ARA&A, 33, 581, doi: 10.1146/annurev.aa.33.090195.003053

Kounkel, M., Covey, K., & Stassun, K. G. 2020, AJ, 160, 279, doi: 10.3847/1538-3881/abc0e6

Kozłowski, S., Onken, C. A., Kochanek, C. S., et al. 2013, ApJ, 775, 92, doi: 10.1088/0004-637X/775/2/92

Kraft, R. P. 1967, ApJ, 150, 551, doi: 10.1086/149359

Krüger, C. J., & Foucart, F. 2020, PhRvD, 101, 103002, doi: 10.1103/PhysRevD.101.103002

Krumholz, M. R. 2013, MNRAS, 436, 2747, doi: 10.1093/mnras/stt1780

—. 2014, PhR, 539, 49, doi: 10.1016/j.physrep.2014.02.001

Kuin, N. P. M., Wu, K., Oates, S., et al. 2019, MNRAS, 487, 2505, doi: 10.1093/mnras/stz053

Kulkarni, S. R. 2005, arXiv e-prints, astro. https://arxiv.org/abs/astro-ph/0510256

—. 2021, arXiv e-prints, arXiv:2107.09585. https://arxiv.org/abs/2107.09585

Kulkarni, S. R., Frail, D. A., Wieringa, M. H., et al. 1998, Nature, 395, 663, doi: 10.1038/27139

Lada, C. J., & Lada, E. A. 2003, ARA&A, 41, 57, doi: 10.1146/annurev.astro.41.011802.094844

LaMassa, S. M., Cales, S., Moran, E. C., et al. 2015, ApJ, 800, 144, doi: 10.1088/0004-637X/800/2/144

Latimer, C. J., Reines, A. E., Plotkin, R. M., Russell, T. D., & Condon, J. J. 2019, ApJ, 884, 78, doi: 10.3847/1538-4357/ab3289

Lawrence, A., Bruce, A. G., MacLeod, C., et al. 2016, MNRAS, 463, 296, doi: 10.1093/mnras/stw1963

Lazzati, D., Morsony, B. J., Blackwell, C. H., & Begelman, M. C. 2012, ApJ, 750, 68, doi: 10.1088/0004-637X/750/1/68

Lee, J. C., Gil de Paz, A., Tremonti, C., et al. 2009a, ApJ, 706, 599, doi: 10.1088/0004-637X/706/1/599

Lee, J. C, et al. 2011, ApJS, 192, doi: 10.1088/0067-0049/192/1/6

Lemonias, J. J., Schiminovich, D., Thilker, D., et al. 2011, ApJ, 733, 74, doi: 10.1088/0004-637X/733/2/74

Leiner, C., et al. 1998, ApJS, 127, doi: 10.1051/aas:1998105

Leung, S.-C., & Fuller, J. 2020, ApJ, 900, 99, doi: 10.3847/1538-4357/abac5d

Li, A. 2020, Nature Astronomy, 4, 339, doi: 10.1038/s41550-020-1051-1

Li, A., Misselt, K. A., & Wang, Y. J. 2006, ApJL, 640, L151, doi: 10.1086/503798

Li, K.-L., Hambsch, F.-J., Munari, U., et al. 2020, ApJ, 905, 114, doi: 10.3847/1538-4357/abc3be

Li, K.-L., Metzger, B. D., Chomiuk, L., et al. 2017, Nature Astronomy, 1, 697, doi: 10.1038/s41550-017-0222-1

Li, L.-X., & Paczyński, B. 1998, ApJL, 507, L59, doi: 10.1086/311680

Li, W., Chornock, R., Leaman, J., et al. 2011, MNRAS, 412, 1473, doi: 10.1111/j.1365-2966.2011.18162.x

Liang, E., Zhang, B., Virgili, F., & Dai, Z. G. 2007, ApJ, 662, 1111, doi: 10.1086/517959

Liu, Y. 2021, in 43rd COSPAR Scientific Assembly. Held 28 January - 4 February, Vol. 43, 1642

Liu, Z.-W., Moriya, T. J., & Stancliffe, R. J. 2015, MNRAS, 454, 1192, doi: 10.1093/mnras/stv2076

Long, M., Romanova, M. M., & Lovelace, R. V. E. 2005, ApJ, 634, 1214, doi: 10.1086/497000

Lothringer, J. D., Fu, G., Sing, D. K., & Barman, T. S. 2020, ApJL, 898, L14, doi: 10.3847/2041-8213/aba265

Lothringer, J. D., Sing, D. K., Rustamkulov, Z., et al. 2022, Nature, 604, 49, doi: 10.1038/s41586-022-04453-2

Lu, W., & Bonnerot, C. 2020, MNRAS, 492, 686, doi: 10.1093/mnras/stz3405

Lu, W., & Kumar, P. 2018, ApJ, 865, 128, doi: 10.3847/1538-4357/aad54a

Lundquist, M. J., Paterson, K., Fong, W., et al. 2019, The Astrophysical Journal, 881, L26, doi: 10.3847/2041-8213/ab32f2

Luridiana, V., Morisset, C., & Shaw, R. A. 2012, in IAU Symposium, Vol. 283, IAU Symposium, 422–423

Luridiana, V., Morisset, C., & Shaw, R. A. 2015, A&A, 573, A42

MacLeod, C. L., Brooks, K., Ivezić, Ž., et al. 2011, ApJ, 728, 26, doi: 10.1088/0004-637X/728/1/26

Madau, P., & Dickinson, M. 2014, ARA&A, 52, 415, doi: 10.1146/annurev-astro-081811-125615

Madhusudhan, N., & Redfield, S. 2015, International Journal of Astrobiology, 14, 177, doi: 10.1017/S1473550414000421

Magorrian, J., Tremaine, S., Richstone, D., et al. 1998, AJ, 115, 2285, doi: 10.1086/300353

Majewski, S. R., Schiavon, R. P., Frinchaboy, P. M., et al. 2017, AJ, 154, 94, doi: 10.3847/1538-3881/aa784d

Manara, C. F., Robberto, M., Da Rio, N., et al. 2012, ApJ, 755, 154, doi: 10.1088/0004-637X/755/2/154

Maoz, D., Mannucci, F., & Nelemans, G. 2014, ARA&A, 52, 107, doi: 10.1146/annurev-astro-082812-141031

Marconi, A., & Hunt, L. K. 2003, ApJL, 589, L21, doi: 10.1086/375804

Marconi, A., Risaliti, G., Gilli, R., et al. 2004, MNRAS, 351, 169, doi: 10.1111/j.1365-2966.2004.07765.x

Margutti, R., & Chornock, R. 2020, arXiv e-prints, arXiv:2012.04810. https://arxiv.org/abs/2012.04810

Margutti, R., Milisavljevic, D., Soderberg, A. M., et al. 2014, ApJ, 780, 21, doi: 10.1088/0004-637X/780/1/21

Margutti, R., Kamble, A., Milisavljevic, D., et al. 2017, ApJ, 835, 140, doi: 10.3847/1538-4357/835/2/140

Margutti, R., Berger, E., Fong, W., et al. 2017, ApJL, 848, L20, doi: 10.3847/2041-8213/aa9057

Margutti, R., Metzger, B. D., Chornock, R., et al. 2019, ApJ, 872, 18, doi: 10.3847/1538-4357/aafa01

Marion, G. H., Vinko, J., Kirshner, R. P., et al. 2014, ApJ, 781, 69, doi: 10.1088/0004-637X/781/2/69

Marshall, D. J., Robin, A. C., Reylé, C., Schultheis, M., & Picaud, S. 2006, A&A, 453, 635, doi: 10.1051/0004-6361:20053842

Martin, C., Hurwitz, M., & Bowyer, S. 1990, ApJ, 354, 220, doi: 10.1086/168681

Martin, D. C., Gonçalves, T. S., Darvish, B., Seibert, M., & Schiminovich, D. 2017, ApJ, 842, 20, doi: 10.3847/1538-4357/aa71a9

Martin, D. C., Wyder, T. K., Schiminovich, D., et al. 2007a, ApJS, 173, 342, doi: 10.1086/516639

Martin, D. C., Small, T., Schiminovich, D., et al. 2007b, ApJS, 173, 415, doi: 10.1086/522088

Massa, D., Fitzpatrick, E. L., & Gordon, K. D. 2020, ApJ, 891, 67, doi: 10.3847/1538-4357/ab6f01

Massey, P., & Hunter, D. A. 1998, ApJ, 493, 180, doi: 10.1086/305126

Massey, P., Neugent, K. F., & Morrell, N. 2015, ApJ, 807, 81, doi: 10.1088/0004-637X/807/1/81

—. 2017, ApJ, 837, 122, doi: 10.3847/1538-4357/aa5d17

Massey, P., Neugent, K. F., Morrell, N., & Hillier, D. J. 2014, ApJ, 788, 83, doi: 10.1088/0004-637X/788/1/83

Masuda, K., & Hotokezaka, K. 2019, ApJ, 883, 169, doi: 10.3847/1538-4357/ab3a4f

Matthews, T. A., & Sandage, A. R. 1963, ApJ, 138, 30, doi: 10.1086/147615

McConnachie, A. W. 2012, AJ, 144, 4, doi: 10.1088/0004-6256/144/1/4

McKernan, B., Ford, K. E. S., Cantiello, M., et al. 2021, arXiv e-prints, arXiv:2110.03741. https://arxiv.org/abs/2110.03741

McKernan, B., Ford, K. E. S., O'Shaugnessy, R., & Wysocki, D. 2020, MNRAS, 494, 1203, doi: 10.1093/mnras/staa740

McKernan, B., Ford, K. E. S., Bartos, I., et al. 2019, ApJL, 884, L50, doi: 10.3847/2041-8213/ab4886

Medina, A. A., Winters, J. G., Irwin, J. M., & Charbonneau, D. 2020, ApJ, 905, 107, doi: 10.3847/1538-4357/abc686

Meixner, M., Gordon, K. D., Indebetouw, R., et al. 2006, AJ, 132, 2268, doi: 10.1086/508185

Meixner, M., Panuzzo, P., Roman-Duval, J., et al. 2013, AJ, 146, 62, doi: 10.1088/0004-6256/146/3/62

Merloni, A., & Heinz, S. 2008, MNRAS, 388, 1011, doi: 10.1111/j.1365-2966.2008.13472.x

Merritt, J., Night, C., & Sion, E. M. 2007, PASP, 119, 251, doi: 10.1086/513611

Metzger, B. D., Piro, A. L., & Quataert, E. 2008, MNRAS, 390, 781, doi: 10.1111/j.1365-2966.2008.13789.x

Metzger, B. D., Bauswein, A., Goriely, S., & Kasen, D. 2015, MNRAS, 446, 1115, doi: 10.1093/mnras/stu2225

Metzger, B. D., & Stone, N. C. 2016, MNRAS, 461, 948, doi: 10.1093/mnras/stw1394

Metzger, B. D., Martínez-Pinedo, G., Darbha, S., et al. 2010, MNRAS, 406, 2650, doi: 10.1111/j.1365-2966.2010.16864.x

Meurer, G. R., Wong, O. I., Kim, J. H., et al. 2009a, in American Astronomical Society Meeting Abstracts, Vol. 213, American Astronomical Society Meeting Abstracts #213, 443.06

Meurer, G. R., Wong, O. I., Kim, J. H., et al. 2009b, ApJ, 695, 765, doi: 10.1088/0004-637X/695/1/765

Meyer, M. R., Calvet, N., & Hillenbrand, L. A. 1997, AJ, 114, 288, doi: 10.1086/118474

Milisavljevic, D., Margutti, R., Kamble, A., et al. 2015, ApJ, 815, 120, doi: 10.1088/0004-637X/815/2/120

Mishra, A., & Li, A. 2015, ApJ, 809, 120, doi: 10.1088/0004-637X/809/2/120

Moe, M., & Di Stefano, R. 2013, ApJ, 778, 95, doi: 10.1088/0004-637X/778/2/95

—. 2015, ApJ, 810, 61, doi: 10.1088/0004-637X/810/1/61

Moe, M., et al. 2019, ApJ, 875, doi: 10.3847/1538-4357/ab0d88

Montalto, M., Piotto, G., Marrese, P. M., et al. 2021, arXiv e-prints, arXiv:2108.13712. https://arxiv.org/abs/2108.13712

Mooley, K. P., Deller, A. T., Gottlieb, O., et al. 2018, Nature, 561, 355, doi: 10.1038/s41586-018-0486-3

Morley, C. V., Fortney, J. J., Marley, M. S., et al. 2015, ApJ, 815, 110, doi: 10.1088/0004-637X/815/2/110

Morozova, V., Piro, A. L., Fuller, J., & Van Dyk, S. D. 2020, ApJL, 891, L32, doi: 10.3847/2041-8213/ab77c8

Morrissey, P., Conrow, T., Barlow, T. A., et al. 2007, ApJS, 173, 682, doi: 10.1086/520512

Moster, B. P., Naab, T., & White, S. D. M. 2013, MNRAS, 428, 3121, doi: 10.1093/mnras/sts261

Mróz, P., Udalski, A., Poleski, R., et al. 2016, ApJS, 222, 9, doi: 10.3847/0067-0049/222/1/9

Muñoz-Darias, T., Casares, J., Mata Sánchez, D., et al. 2016, Nature, 534, 75, doi: 10.1038/nature17446

Murthy, J, et al. 2014, ApJS, 213(2), doi: 10.1088/0067-0049/213/2/32

Nakar, E. 2015, ApJ, 807, 172, doi: 10.1088/0004-637X/807/2/172

The National Academies Press, 2021 doi: 10.17226/26141

Nedora, V., Schianchi, F., Bernuzzi, S., et al. 2020, arXiv e-prints, arXiv:2011.11110. https://arxiv.org/abs/2011.11110

Nelemans, G., Yungelson, L. R., & Portegies Zwart, S. F. 2004, MNRAS, 349, 181, doi: 10.1111/j.1365-2966.2004.07479.x

Nelson, T., Mukai, K., Li, K.-L., et al. 2019, ApJ, 872, 86, doi: 10.3847/1538-4357/aafb6d

Nidever, D. L., Olsen, K., Walker, A. R., et al. 2017, AJ, 154, 199, doi: 10.3847/1538-3881/aa8d1c

Nikzad, S. E., et al., 1994, Instrumentation Astronomy VIII, 2198, 907-915 doi: 10.1117/12.176733

Noeske, K. G., Weiner, B. J., Faber, S. M., et al. 2007, ApJL, 660, L43, doi: 10.1086/517926

Nuza, S. E., Kitaura, F.-S., Heß, S., Libeskind, N. I., & Müller, V. 2014, MNRAS, 445, 988, doi: 10.1093/mnras/stu1746

Oates, S. R., Marshall, F. E., Breeveld, A. A., et al. 2021, MNRAS, 507, 1296, doi: 10.1093/mnras/stab2189

O'Connell, R. W. 1987, AJ, 94, 876, doi: 10.1086/114522

Ofek, E. O., Rabinak, I., Neill, J. D., et al. 2010, ApJ, 724, 1396, doi: 10.1088/0004-637X/724/2/1396

Ofek, E. O., Sullivan, M., Shaviv, N. J., et al. 2014, ApJ, 789, 104, doi: 10.1088/0004-637X/789/2/104

Okumura, S.-i., Mori, A., Nishihara, E., Watanabe, E., & Yamashita, T. 2000, ApJ, 543, 799, doi: 10.1086/317116

Özel, F., Psaltis, D., Narayan, R., & McClintock, J. E. 2010, ApJ, 725, 1918, doi: 10.1088/0004-637X/725/2/1918

Paczynski, B. 1986, ApJL, 308, L43, doi: 10.1086/184740

Pancoast, A., Brewer, B. J., Treu, T., et al. 2014, MNRAS, 445, 3073, doi: 10.1093/mnras/stu1419

Panda, S., Martínez-Aldama, M. L., & Zajaček, M. 2019, Frontiers in Astronomy and Space Sciences, 6, 75, doi: 10.3389/fspas.2019.00075

Parsons, S. G., Rebassa-Mansergas, A., Schreiber, M. R., et al. 2016, MNRAS, 463, 2125, doi: 10.1093/mnras/stw2143

Parsons, S. G., Schreiber, M. R., Gänsicke, B. T., et al. 2015, MNRAS, 452, 1754, doi: 10.1093/mnras/stv1395

Pastorello, A., Cappellaro, E., Inserra, C., et al. 2013, ApJ, 767, 1, doi: 10.1088/0004-637X/767/1/1

Paxton, B., Marchant, P., Schwab, J., et al. 2015, ApJS, 220, 15, doi: 10.1088/0067-0049/220/1/15

Peek, J. E. G., & Schiminovich, D. 2013, ApJ, 771, 68, doi: 10.1088/0004-637X/771/1/68

Perley, D. A., Mazzali, P. A., Yan, L., et al. 2019, MNRAS, 484, 1031, doi: 10.1093/mnras/sty3420

Perley, D. A., Ho, A. Y. Q., Yao, Y., et al. 2021a, arXiv e-prints, arXiv:2103.01968. https://arxiv.org/abs/2103.01968

Perley, D. A., Sollerman, J., Schulze, S., et al. 2021b, arXiv e-prints, arXiv:2111.12110. https://arxiv.org/abs/2111.12110

Peters, G. J., Gies, D. R., Grundstrom, E. D., & McSwain, M. V. 2008, ApJ, 686, 1280, doi: 10.1086/591145

Peters, G. J., Pewett, T. D., Gies, D. R., Touhami, Y. N., & Grundstrom, E. D. 2013, ApJ, 765, 2, doi: 10.1088/0004-637X/765/1/2

Petrov, P., Singer, L. P., Coughlin, M. W., et al. 2021, arXiv e-prints, arXiv:2108.07277. https://arxiv.org/abs/2108.07277

Petrucci, P.-O., Ferreira, J., Henri, G., & Pelletier, G. 2008, MNRAS, 385, L88, doi: 10.1111/j.1745-3933.2008.00439.x

Pian, E., D'Avanzo, P., Benetti, S., et al. 2017, Nature, 551, 67, doi: 10.1038/nature24298

Pichara, K., Protopapas, P., Kim, D. W., Marquette, J. B., & Tisserand, P. 2012, MNRAS, 427, 1284, doi: 10.1111/j.1365-2966.2012.22061.x

Piran, T. 2004, Reviews of Modern Physics, 76, 1143, doi: 10.1103/RevModPhys.76.1143

Piran, T., Svirski, G., Krolik, J., Cheng, R. M., & Shiokawa, H. 2015, ApJ, 806, 164, doi: 10.1088/0004-637X/806/2/164

Piro, A. L., Giacomazzo, B., & Perna, R. 2017, ApJL, 844, L19, doi: 10.3847/2041-8213/aa7f2f

Piro, A. L., & Kollmeier, J. A. 2018, The Astrophysical Journal, 855, 103

Planck Collaboration, Abergel, A., Ade, P. A. R., et al. 2014, A&A, 571, A11, doi: 10.1051/0004-6361/201323195

Ponti, G., Fender, R. P., Begelman, M. C., et al. 2012, MNRAS, 422, L11, doi: 10.1111/j.1745-3933.2012.01224.x

Portegies Zwart, S. F., McMillan, S. L. W., & Gieles, M. 2010, ARA&A, 48, 431, doi: 10.1146/annurev-astro-081309-130834

Pouliasis, E., Georgantopoulos, I., Bonanos, A. Z., et al. 2019, MNRAS, 487, 4285, doi: 10.1093/mnras/stz1483

Povich, M. S., Smith, N., Majewski, S. R., et al. 2011, ApJS, 194, 14, doi: 10.1088/0067-0049/194/1/14

Prentice, S. J., Maguire, K., Smartt, S. J., et al. 2018, ApJ, 865, L3, doi: 10.3847/2041-8213/aadd90

Prinja, R. K., Barlow, M. J., & Howarth, I. D. 1990, ApJ, 361, 607, doi: 10.1086/169224

Proga, D., & Kallman, T. R. 2002, ApJ, 565, 455, doi: 10.1086/324534

Pun, C. S. J., Kirshner, R. P., Sonneborn, G., et al. 1995, ApJS, 99, 223, doi: 10.1086/192185

Pursiainen, M., Childress, M., Smith, M., et al. 2018, MNRAS, 481, 894, doi: 10.1093/mnras/sty2309

Quataert, E., Fernández, R., Kasen, D., Klion, H., & Paxton, B. 2016, MNRAS, 458, 1214, doi: 10.1093/mnras/stw365

Quataert, E., & Shiode, J. 2012, MNRAS, 423, L92, doi: 10.1111/j.1745-3933.2012.01264.x

Quimby, R. M., Yuan, F., Akerlof, C., & Wheeler, J. C. 2013, MNRAS, 431, 912, doi: 10.1093/mnras/stt213

Ramírez-Agudelo, O. H., Simón-Díaz, S., Sana, H., et al. 2013, A&A, 560, A29, doi: 10.1051/0004-6361/201321986

Ramírez-Agudelo, O. H., Sana, H., de Mink, S. E., et al. 2015, A&A, 580, A92, doi: 10.1051/0004-6361/201425424

Ravindranath, S., Monroe, T., Jaskot, A., Ferguson, H. C., & Tumlinson, J. 2020, ApJ, 896, 170, doi: 10.3847/1538-4357/ab91a5

Reines, A. E., & Comastri, A. 2016, PASA, 33, e054, doi: 10.1017/pasa.2016.46

Reines, A. E., Greene, J. E., & Geha, M. 2013, ApJ, 775, 116, doi: 10.1088/0004-637X/775/2/116

Reines, A. E., & Volonteri, M. 2015, ApJ, 813, 82, doi: 10.1088/0004-637X/813/2/82

Reusch, S., Stein, R., Kowalski, M., et al. 2021, arXiv e-prints, arXiv:2111.09390. https://arxiv.org/abs/2111.09390

Ricci, C., Loewenstein, M., Kara, E., et al. 2021, ApJS, 255, 7, doi: 10.3847/1538-4365/abe94b

Ricker, G. R., Winn, J. N., Vanderspek, R., et al. 2015, Journal of Astronomical Telescopes, Instruments, and Systems, 1, 014003, doi: 10.1117/1.JATIS.1.1.014003

Riess, A. G., Filippenko, A. V., Challis, P., et al. 1998, AJ, 116, 1009, doi: 10.1086/300499

Robertson, B. E., Ellis, R. S., Furlanetto, S. R., & Dunlop, J. S. 2015a, ApJL, 802, L19, doi: 10.1088/2041-8205/802/2/L19

—. 2015b, ApJL, 802, L19, doi: 10.1088/2041-8205/802/2/L19

Rogerson, J. B., Spitzer, L., Drake, J. F., et al. 1973, ApJL, 181, L97, doi: 10.1086/181194

Roman-Duval, J., Proffitt, C., Monroe, T., Carlberg, J., & Taylor, J. 2020. https://www.stsci.edu/files/live/sites/www/files/home/ hst/about/space-telescope-users-committee/ presentations-and-documentation/_documents/2020_apr/ ullyses.pdf

Romanova, M. M., Blinova, A. A., Ustyugova, G. V., Koldoba, A. V., & Lovelace, R. V. E. 2018, NewA, 62, 94, doi: 10.1016/j.newast.2018.01.011

Roming, P. W. A., Kennedy, T. E., Mason, K. O., et al. 2005, SSRv, 120, 95, doi: 10.1007/s11214-005-5095-4

Rosen, A. L., & Krumholz, M. R. 2020, AJ, 160, 78,
    doi: 10.3847/1538-3881/ab9abf

Ross, N. P., Ford, K. E. S., Graham, M., et al. 2018,
    MNRAS, 480, 4468, doi: 10.1093/mnras/sty2002

Roth, N., Kasen, D., Guillochon, J., & Ramirez-Ruiz, E.
    2016, ApJ, 827, 3, doi: 10.3847/0004-637X/827/1/3

Sabbi, E., Anderson, J., Lennon, D. J., et al. 2013, AJ, 146,
    53, doi: 10.1088/0004-6256/146/3/53

Sagiv, I., Gal-Yam, A., Ofek, E. O., et al. 2014, AJ, 147,
    79, doi: 10.1088/0004-6256/147/4/79

Sahnow, D. J., Moos, H. W., Ake, T. B., et al. 2000, ApJL,
    538, L7, doi: 10.1086/312794

Salim, S., & Narayanan, D. 2020, ARA&A, 58, 529,
    doi: 10.1146/annurev-astro-032620-021933

Salim, S., Rich, R. M., Charlot, S., et al. 2007, ApJS, 173,
    267, doi: 10.1086/519218

Salim, S., Lee, J. C., Janowiecki, S., et al. 2016, ApJS, 227,
    2, doi: 10.3847/0067-0049/227/1/2

Salim, S., Boquien, M., & Lee, J. C. 2018, ApJ, 859, 11,
    doi: 10.3847/1538-4357/aabf3c

Salzer, J. J., Feddersen, J. R., Derloshon, K., et al. 2020,
    AJ, 160, 242, doi: 10.3847/1538-3881/abba11

Sana, H., & Shenar, T. 2019. https://www.eso.org/sci/
    meetings/2020/4MOST2/MultiplicityMCs4most.pdf

—. 2012b, Science, 337, 444, doi: 10.1126/science.1223344

Sana, H., et al. 2013, *Astronomy and Astrophysics*, 550,
    doi: 10.1051/0004-6361/201219621

Sanders, D. B., Phinney, E. S., Neugebauer, G., Soifer,
    B. T., & Matthews, K. 1989, ApJ, 347, 29,
    doi: 10.1086/168094

Saxton, R., Komossa, S., Auchettl, K., & Jonker, P. G.
    2020, SSRv, 216, 85, doi: 10.1007/s11214-020-00708-4

Sazonov, S., Gilfanov, M., Medvedev, P., et al. 2021,
    MNRAS, 508, 3820, doi: 10.1093/mnras/stab2843

Schiminovich, D., Wyder, T. K., Martin, D. C., et al. 2007,
    ApJS, 173, 315, doi: 10.1086/524659

Schlegel, D. J., Finkbeiner, D. P., & Davis, M. 1998, ApJ,
    500, 525, doi: 10.1086/305772

Schmidt, M. 1963, Nature, 197, 1040,
    doi: 10.1038/1971040a0

Schootemeijer, A., Götberg, Y., de Mink, S. E., Gies, D., &
    Zapartas, E. 2018, A&A, 615, A30,
    doi: 10.1051/0004-6361/201731194

Secunda, A., Cen, R., Kimm, T., Götberg, Y., & de Mink,
    S. E. 2020, ApJ, 901, 72, doi: 10.3847/1538-4357/abaefa

Seibert, M., Martin, D. C., Heckman, T. M., et al. 2005,
    ApJL, 619, L55, doi: 10.1086/427843

Sekiguchi, Y., Kiuchi, K., Kyotoku, K., & Shibata, M. 2015,
    PhRvD, 91, 064059, doi: 10.1103/PhysRevD.91.064059

Senchyna, P., Stark, D. P., Vidal-García, A., et al. 2017,
    MNRAS, 472, 2608, doi: 10.1093/mnras/stx2059

Senchyna, P., & Stark, D. P. 2019, MNRAS, 484, 1270,
    doi: 10.1093/mnras/stz058

Senchyna, P., et al. 2019, MNRAS, 488,
    doi: 10.1093/mnras/stz1907

Seon, K.-I., Edelstein, J., Korpela, E., et al. 2011, ApJS,
    196, 15, doi: 10.1088/0067-0049/196/2/15

Shankar, F., Weinberg, D. H., & Miralda-Escudé, J. 2009,
    ApJ, 690, 20, doi: 10.1088/0004-637X/690/1/20

Shappee, B. J., Simon, J. D., Drout, M. R., et al. 2017,
    Science, 358, 1574, doi: 10.1126/science.aaq0186

Shara, M. M., Crawford, S. M., Vanbeveren, D., et al. 2017,
    MNRAS, 464, 2066, doi: 10.1093/mnras/stw2450

—. 2020, MNRAS, 492, 4430, doi: 10.1093/mnras/staa038

Shenar, T., Bodensteiner, J., Abdul-Masih, M., et al. 2020,
    A&A, 639, L6, doi: 10.1051/0004-6361/202038275

Shore, S. N. 2012, Bulletin of the Astronomical Society of
    India, 40, 185.   https://arxiv.org/abs/1211.3176

Shore, S. N., De Gennaro Aquino, I., Schwarz, G. J., et al.
    2013, A&A, 553, A123,
    doi: 10.1051/0004-6361/201321095

Shu, F., Najita, J., Ostriker, E., et al. 1994, ApJ, 429, 781,
    doi: 10.1086/174363

Shustov, B., Gómez de Castro, A. I., Sachkov, M., et al.
    2018, Ap&SS, 363, 62, doi: 10.1007/s10509-018-3280-7

Simons, R., Thilker, D., Bianchi, L., & Wyder, T. 2014,
    Advances in Space Research, 53, 939,
    doi: 10.1016/j.asr.2013.07.016

Sing, D. K., Lecavelier des Etangs, A., Fortney, J. J., et al.
    2013, MNRAS, 436, 2956, doi: 10.1093/mnras/stt1782

Sing, D. K., Fortney, J. J., Nikolov, N., et al. 2016, Nature,
    529, 59, doi: 10.1038/nature16068

Sion, E. M., Cheng, F. H., Gänsicke, B. T., & Szkody, P.
    2004, ApJL, 614, L61, doi: 10.1086/425497

Smartt, S. J., Chen, T. W., Jerkstrand, A., et al. 2017,
    Nature, 551, 75, doi: 10.1038/nature24303

Smith, N. 2006, ApJ, 644, 1151, doi: 10.1086/503766

Smith, N., Li, W., Filippenko, A. V., & Chornock, R. 2011,
    MNRAS, 412, 1522,
    doi: 10.1111/j.1365-2966.2011.17229.x

—. 2014a, ARA&A, 52, 487,
    doi: 10.1146/annurev-astro-081913-040025

Smith, N., Götberg, Y., & de Mink, S. E. 2018, MNRAS,
    475, 772, doi: 10.1093/mnras/stx3181

Soderberg, A. M., Nakar, E., Berger, E., & Kulkarni, S. R.
    2006a, ApJ, 638, 930, doi: 10.1086/499121

Soderberg, A. M., Berger, E., Kasliwal, M., et al. 2006b,
    ApJ, 650, 261, doi: 10.1086/506429

Soderberg, A. M., Chakraborti, S., Pignata, G., et al. 2010, Nature, 463, 513, doi: 10.1038/nature08714

Sokolovsky, K. V., Mukai, K., Chomiuk, L., et al. 2020, MNRAS, 497, 2569, doi: 10.1093/mnras/staa2104

Southworth, J., Mancini, L., Madhusudhan, N., et al. 2017, AJ, 153, 191, doi: 10.3847/1538-3881/aa6477

Spera, M., Mapelli, M., & Bressan, A. 2015, MNRAS, 451, 4086, doi: 10.1093/mnras/stv1161

Stanway, E. R., Eldridge, J. J., & Becker, G. D. 2016, MNRAS, 456, 485, doi: 10.1093/mnras/stv2661

Stark, D. P. 2016, ARA&A, 54, 761, doi: 10.1146/annurev-astro-081915-023417

Stasińska, G., Prantzos, N., Meynet, G., et al., eds. 2012, EAS Publications Series, Vol. 54, Oxygen in the Universe

Stein, R., Velzen, S. v., Kowalski, M., et al. 2021, Nature Astronomy, 5, 510, doi: 10.1038/s41550-020-01295-8

Steiner, J. E., & Oliveira, A. S. 2005, A&A, 444, 895, doi: 10.1051/0004-6361:20052782

Stelzer, B., Damasso, M., Scholz, A., & Matt, S. P. 2016, MNRAS, 463, 1844, doi: 10.1093/mnras/stw1936

Stern, D., Eisenhardt, P., Gorjian, V., et al. 2005, ApJ, 631, 163, doi: 10.1086/432523

Stern, D., Assef, R. J., Benford, D. J., et al. 2012, ApJ, 753, 30, doi: 10.1088/0004-637X/753/1/30

Stern, D., McKernan, B., Graham, M. J., et al. 2018, ApJ, 864, 27, doi: 10.3847/1538-4357/aac726

Stone, N. C., & Metzger, B. D. 2016, MNRAS, 455, 859, doi: 10.1093/mnras/stv2281

Strotjohann, N. L., Ofek, E. O., Gal-Yam, A., et al. 2021, ApJ, 907, 99, doi: 10.3847/1538-4357/abd032

Sun, M., Jiang, B., Yuan, H., & Li, J. 2021, ApJS, 254, 38, doi: 10.3847/1538-4365/abf929

Sunyaev, R., Arefiev, V., Babyshkin, V., et al. 2021, arXiv e-prints, arXiv:2104.13267. https://arxiv.org/abs/2104.13267

Sutherland, R. S., & Dopita, M. A. 1993, ApJS, 88, 253, doi: 10.1086/191823

Tachiev, G. I. & Froese Fischer, C. 2002, A&A, 385, 716

Tanvir, N. R., Levan, A. J., González-Fernández, C., et al. 2017, ApJL, 848, L27, doi: 10.3847/2041-8213/aa90b6

Tartaglia, L., Sollerman, J., Barbarino, C., et al. 2021, A&A, 650, A174, doi: 10.1051/0004-6361/202039068

Tauris, T. M., Kramer, M., Freire, P. C. C., et al. 2017, ApJ, 846, 170, doi: 10.3847/1538-4357/aa7e89

Tayal, S. S. 2011, ApJS, 195, 12

Thaller, M. L., Bagnuolo, William G., J., Gies, D. R., & Penny, L. R. 1995, ApJ, 448, 878, doi: 10.1086/176016

The LIGO Scientific Collaboration, The Virgo Collaboration, & The KAGRA Scientific Collaboration. 2021a, arXiv e-prints, arXiv:2111.03634. https://arxiv.org/abs/2111.03634

The LIGO Scientific Collaboration, the Virgo Collaboration, Abbott, R., et al. 2021b, ApJL, 913, L7, doi: 10.3847/2041-8213/abe949

Thilker, D. A., Bianchi, L., Boissier, S., et al. 2005, ApJL, 619, L79, doi: 10.1086/425251

Thilker, D. A., Bianchi, L., Meurer, G., et al. 2007, ApJS, 173, 538, doi: 10.1086/523853

Thompson, G. I., Nandy, K., Jamar, C., et al. 1978, Catalogue of stellar ultraviolet fluxes : a compilation of absolute stellar fluxes measured by the Sky Survey Telescope (S2/68) aboard the ESRO satellite TD-1 / (The Science Research Council, UK)

Tinyanont, S., Ridden-Harper, R., Foley, R. J., et al. 2021, MNRAS, doi: 10.1093/mnras/stab2887

Townsley, L. K., Broos, P. S., Corcoran, M. F., et al. 2011, ApJS, 194, 1, doi: 10.1088/0067-0049/194/1/1

Tremonti, C. A., Heckman, T. M., Kauffmann, G., et al. 2004, ApJ, 613, 898, doi: 10.1086/423264

Tripp, T. 2019, BAAS, 51, 309

Troja, E., Piro, L., van Eerten, H., et al. 2017, Nature, 551, 71, doi: 10.1038/nature24290

Tully, R. B., Courtois, H. M., Hoffman, Y., & Pomarède, D. 2016, in The Zeldovich Universe: Genesis and Growth of the Cosmic Web, ed. R. van de Weygaert, S. Shandarin, E. Saar, & J. Einasto, Vol. 308, 305–309, doi: 10.1017/S174392131601005X

Tully, R. B., Karachentsev, I. D., Rizzi, L., & Shaya, E. J. 2019, Every Known Nearby Galaxy, HST Proposal

Tumlinson, J., Peeples, M. S., & Werk, J. K. 2017, ARA&A, 55, 389, doi: 10.1146/annurev-astro-091916-055240

Tweed, D. P., Mamon, G. A., Thuan, T. X., et al. 2018, MNRAS, 477, 1427, doi: 10.1093/mnras/sty507

Udalski, A., Szymanski, M., Kubiak, M., et al. 2000, AcA, 50, 307. https://arxiv.org/abs/astro-ph/0010150

Valenti, J. A., Basri, G., & Johns, C. M. 1993, AJ, 106, 2024, doi: 10.1086/116783

Vallée, J. P. 2014, ApJS, 215, 1, doi: 10.1088/0067-0049/215/1/1

van den Bergh, S., Herbst, E., & Pritchet, C. 1973, AJ, 78, 375, doi: 10.1086/111426

van den Heuvel, E. P. J., & De Loore, C. 1973, A&A, 25, 387

van der Hucht, K. A., Lamers, H. J. G. L. M., Faraggiana, R., Hack, M., & Stalio, R. 1976, A&AS, 25, 65

van Kerkwijk, M. H., Charles, P. A., Geballe, T. R., et al. 1992, Nature, 355, 703, doi: 10.1038/355703a0

van Velzen, S. 2018, ApJ, 852, 72, doi: 10.3847/1538-4357/aa998e

van Velzen, S., Holoien, T. W. S., Onori, F., Hung, T., & Arcavi, I. 2020, SSRv, 216, 124, doi: 10.1007/s11214-020-00753-z

van Velzen, S., Stone, N. C., Metzger, B. D., et al. 2019, ApJ, 878, 82, doi: 10.3847/1538-4357/ab1844

van Velzen, S., Stein, R., Gilfanov, M., et al. 2021a, arXiv e-prints, arXiv:2111.09391. https://arxiv.org/abs/2111.09391

van Velzen, S., Gezari, S., Hammerstein, E., et al. 2021b, ApJ, 908, 4, doi: 10.3847/1538-4357/abc258

Vaughan, S., Uttley, P., Markowitz, A. G., et al. 2016, MNRAS, 461, 3145, doi: 10.1093/mnras/stw1412

Vieira, N., Ruan, J. J., Haggard, D., et al. 2020, ApJ, 895, 96, doi: 10.3847/1538-4357/ab917d

Vigna-Gómez, A., MacLeod, M., Neijssel, C. J., et al. 2020, PASA, 37, e038, doi: 10.1017/pasa.2020.31

Villar, V. A., Guillochon, J., Berger, E., et al. 2017, ApJL, 851, L21, doi: 10.3847/2041-8213/aa9c84

Vink, J. S. 2021, arXiv e-prints, arXiv:2109.08164. https://arxiv.org/abs/2109.08164

Vink, J. S., & Sander, A. A. C. 2021, arXiv:2103.12736 [astro-ph]. https://arxiv.org/abs/2103.12736

Volonteri, M., & Natarajan, P. 2009, MNRAS, 400, 1911, doi: 10.1111/j.1365-2966.2009.15577.x

von Essen, C., Mallonn, M., Welbanks, L., et al. 2019, A&A, 622, A71, doi: 10.1051/0004-6361/201833837

Wakeford, H. R., Wilson, T. J., Stevenson, K. B., & Lewis, N. K. 2019, Research Notes of the American Astronomical Society, 3, 7, doi: 10.3847/2515-5172/aafc63

Wakeford, H. R., Sing, D. K., Stevenson, K. B., et al. 2020, AJ, 159, 204, doi: 10.3847/1538-3881/ab7b78

Walborn, N. R., Lennon, D. J., Heap, S. R., et al. 2000, PASP, 112, 1243, doi: 10.1086/316617

Wang, L., Gies, D., Peters, G., et al. 2021, in American Astronomical Society Meeting Abstracts, Vol. 53, American Astronomical Society Meeting Abstracts, 349.04

Wang, L., Gies, D. R., & Peters, G. J. 2017, ApJ, 843, 60, doi: 10.3847/1538-4357/aa740a

Waxman, E., & Katz, B. 2017, Shock Breakout Theory, ed. A. W. Alsabti & P. Murdin (Springer), 967, doi: 10.1007/978-3-319-21846-5_33

Weber, E. J., & Davis, Leverett, J. 1967, ApJ, 148, 217, doi: 10.1086/149138

Weisz, D. R., Johnson, B. D., Johnson, L. C., et al. 2012, ApJ, 744, 44, doi: 10.1088/0004-637X/744/1/44

Weisz, D. R., Dolphin, A. E., Skillman, E. D., et al. 2014a, ApJ, 789, 147, doi: 10.1088/0004-637X/789/2/147

—. 2014b, ApJ, 789, 148, doi: 10.1088/0004-637X/789/2/148

Weisz, D. R., Johnson, B. D., & Conroy, C. 2014c, ApJL, 794, L3, doi: 10.1088/2041-8205/794/1/L3

—. 2015, ApJ, 804, 136, doi: 10.1088/0004-637X/804/2/136

Weston, J. H. S., Sokoloski, J. L., Chomiuk, L., et al. 2016a, MNRAS, 460, 2687, doi: 10.1093/mnras/stw1161

Weston, J. H. S., Sokoloski, J. L., Metzger, B. D., et al. 2016b, MNRAS, 457, 887, doi: 10.1093/mnras/stv3019

Wiese, W. L., Fuhr, J. R., & Deters, T. M. 1996, Atomic transition probabilities of carbon, nitrogen, and oxygen : a critical data compilation

Williams, C. C., Curtis-Lake, E., Hainline, K. N., et al. 2018, ApJS, 236, 33, doi: 10.3847/1538-4365/aabcbb

Woosley, S. E. 2017, ApJ, 836, 244, doi: 10.3847/1538-4357/836/2/244

Woosley, S. E., & Bloom, J. S. 2006, ARA&A, 44, 507, doi: 10.1146/annurev.astro.43.072103.150558

Wu, S., & Fuller, J. 2021, ApJ, 906, 3, doi: 10.3847/1538-4357/abc87c

Wu, Y., Chen, X., Chen, H., Li, Z., & Han, Z. 2020, A&A, 634, A126, doi: 10.1051/0004-6361/201935792

Wyatt, M. C. 2008, ARA&A, 46, 339, doi: 10.1146/annurev.astro.45.051806.110525

Wyder, T. K., Martin, D. C., Schiminovich, D., et al. 2007, ApJS, 173, 293, doi: 10.1086/521402

Wyder, T. K., Martin, D. C., Barlow, T. A., et al. 2009, ApJ, 696, 1834, doi: 10.1088/0004-637X/696/2/1834

Xin, C., Charisi, M., Haiman, Z., et al. 2020, MNRAS, 496, 1683, doi: 10.1093/mnras/staa1643

Yaron, O., Prialnik, D., Shara, M. M., & Kovetz, A. 2005, ApJ, 623, 398, doi: 10.1086/428435

Ye, C. S., Fong, W.-f., Kremer, K., et al. 2020, ApJL, 888, L10, doi: 10.3847/2041-8213/ab5dc5

York, D. G., Adelman, J., Anderson, Jr., J. E., et al. 2000, AJ, 120, 1579

Zanni, C., & Ferreira, J. 2013, A&A, 550, A99, doi: 10.1051/0004-6361/201220168

Zaritsky, D., Harris, J., Thompson, I. B., & Grebel, E. K. 2004, AJ, 128, 1606, doi: 10.1086/423910

Zaritsky, D., Harris, J., Thompson, I. B., Grebel, E. K., & Massey, P. 2002, AJ, 123, 855, doi: 10.1086/338437

Zhan, H. 2018, in 42nd COSPAR Scientific Assembly, Vol. 42, E1.16–4–18

Zhang, M., Knutson, H. A., Wang, L., et al. 2021, arXiv
    e-prints, arXiv:2106.05273.
    https://arxiv.org/abs/2106.05273

Ion	Radiative Transition Probabilities	Collision Strengths
C^{+2}	Wiese et al. (1996)	Berrington et al. (1985)
C^{+3}	Wiese et al. (1996)	Aggarwal & Keenan (2004)
O^{+}	Froese Fischer & Tachiev (2004)*†	Kisielius et al. (2009)
O^{+2}	Froese Fischer & Tachiev (2004)*†	Aggarwal & Keenan (1999)

Table 2. The atomic data used with the PyNeb package to calculate ionic abundances and determine predicted emission line fluxes. Note that the O^{+2} collision strengths from Aggarwal & Keenan (1999) are calculated from a 6-level atom approximation, which is required to predict the OIII] $\lambda\lambda1661,1666$ fluxes.
* Agrees with updated values from Tayal (2011).
† Equivalent to Tachiev & Froese Fischer (2002), as recommended by Stasińska et al. (2012).

APPENDIX

A. *UVEX C/O LINE RATIO CALCULATIONS*

A primary goal of the *UVEX* metal-poor dwarf-galaxy science is to obtain new gas-phase UV observations of OIII] $\lambda\lambda1661,1666$ and CIII] $\lambda\lambda1907,1909$ in the first sample of metal-poor dwarf galaxies with young stellar populations. Using the CIII] $\lambda\lambda1907,1909$/OIII] $\lambda1666$ line ratio method benefits from the fact that C/O exhibits minimal uncertainty due to reddening, as the interstellar extinction curve is nearly flat over the wavelength range of interest ($1600-2000$ Å) and the OIII] and CIII] lines have similar excitation and ionization potentials such that their ratio has little dependence on the physical conditions of the gas (i.e., nebular T_e and ionization structure).

In order to fill in the C/O relationship with O/H in the sparsely measured metal-poor, young-age regime, we selected objects from the Sloan Digital Sky Survey (SDSS) Data Release 15 (DR15) with large equivalent widths (EWs) of emission lines (e.g., EW([OIII] $\lambda5007$)> 750 Å) and low metallicity ($12 + \log(O/H) \leq 7.45$ or $Z \leq 0.05Z_{\odot}$). High-ionization HII regions are needed given the energies required to ionize C^{+} and O^{+} are 24.8 eV and 35.1 eV respectively. High nebular electron temperatures (T_e) in low-metallicity environments allow the collisionally excited C and O transitions of interest to be observed despite their large excitation energies (6–8 eV). Below we describe the calculations that led to this selection criteria.

A.1. *Nebular Emission Line Measurements*

Each of the targets in our initial UVEX sample has been previously observed as part of the SDSS DR15. We used the publicly available SDSS data (York et al. 2000), which have been reduced with the SDSS pipeline (Bolton et al. 2012). Emission line fluxes and uncertainties were determined by Jarle Brinchmann using an upgraded pipeline similar to that of the MPA-JHU catalog, where groups of nearby lines are fit simultaneously, constrained by a single Gaussian FWHM and a single line center offset from the vacuum wavelengths (i.e., redshift).

The line measurements were corrected for Galactic plus dust extinction (a reasonable method at low redshift) using the $E(B-V)$ color excess determined from the observed-to-theoretical Hα/Hβ ratios with the Cardelli et al. (1989) reddening law. All of our targets have low extinction with $E(B-V)$ values ≤ 0.1.

A.2. *Chemical Abundances*

For all remaining calculations, we used the PyNeb package in PYTHON (Luridiana et al. 2012, 2015), assuming a five-level atom model (De Robertis et al. 1987) and default atomic data in most cases. However, our OIII] $\lambda\lambda1661,1666$ predictions require the use of a 6-level atom for which we adopt Aggarwal & Keenan (1999) who calculated the necessary collision strengths. The adopted atomic data is listed in Table 2.

A.2.1. *Temperature and Density*

We required all of the galaxies in our initial UVEX sample to have SDSS spectra with significant [OIII] $\lambda4363$ detections that allowed us to directly calculate the electron temperature, T_e, of the high-ionization gas via the OIII] I($\lambda\lambda4959,5007$)/I($\lambda4363$) ratio. The low ionization zone temperatures were then determined using the photoionization

model relationship from Garnett (1992):

$$T_e[\text{OII}] = 0.70 \times T_e[\text{OIII}] + 3000 \text{ K}, \tag{A1}$$

The [SII] $\lambda\lambda6717,6731$ ratio was used to determine the electron densities.

A.2.2. *Ionic And Total Abundances*

Ionic abundances relative to hydrogen are calculated using:

$$\frac{N(X^i)}{N(H^+)} = \frac{I_{\lambda(i)}}{I_{H\beta}} \frac{j_{H\beta}}{j_{\lambda(i)}} , \tag{A2}$$

where the emissivity coefficients, $j_{\lambda(i)}$, are functions of both temperature and density. Berg et al. (2021) demonstrated that O^+ and O^{+2} are the dominant O ions in nebular gas, while contributions from O^+ and O^{+3} (requiring an ionization potential of 54.9 eV) are negligible, even in very high-ionization galaxies. Therefore, we calculated total oxygen abundances (O/H) as

$$Z = 12 + \log(\text{O/H}) = 12 + \log(\frac{\text{O}^+}{\text{H}^+} + \frac{\text{O}^{+2}}{\text{H}^+}). \tag{A3}$$

A.3. *UV Flux Requirements*

While observed C/O abundances vary significantly amongst dwarf galaxies, the emissivity of the OIII] $\lambda1666$ line is roughly $6\times$ weaker than the emissivity of CIII] $\lambda\lambda1907,1909$, making the OIII] $\lambda1666$ line the limiting emission line of the two. We, therefore, determined the minimum flux requirement to achieve our science goals based on the predicted OIII] $\lambda1666$ fluxes of our initial metal-poor, young dwarf galaxy sample. We determined the OIII] $\lambda1666$ fluxes from the observed SDSS [OIII] $\lambda5007$ fluxes using emissivity ratios from PyNeb, assuming the high-ionization gas electron temperatures determined above. The predicted OIII] $\lambda1666$ fluxes were then reddened using the Calzetti et al. (2000) reddening law and the $E(B-V)$ color excesses determined from the Balmer decrement. This provides the minimum required observed emission line fluxes.

B. *UVEX* MAGELLANIC CLOUD SURVEY IN CONTEXT OF OTHER OBSERVATIONS

The Magellanic Clouds have long been targets of deep, wide-area, and cadenced imaging surveys in the optical and near-IR. Concerted optical and near-IR efforts have provided a detailed view of the stellar contents of the LMC and SMC (e.g., Udalski et al. 2000, Zaritsky et al. 2002, Zaritsky et al. 2004, Cioni et al. 2011, Nidever et al. 2017), while observations in the mid- and far-IR reveal much about the nature of evolved stars, dust production, and the ISM at low-metallicities (e.g., Meixner et al. 2006, Meixner et al. 2013). Upcoming surveys (e.g., Rubin, *Roman*) will provide an unprecedented deep and cadenced inventory of LMC and SMC stars in the optical and near-IR (i.e., with sub-arcsecond angular resolution and depths $m \gtrsim 25$).

Missing among these exquisite datasets is a matching, modern UV imaging survey of the LMC and SMC. Though several UV facilities have imaged the LMC and SMC, none are well-matched to properties of modern optical and near-IR datasets. *GALEX* surveyed the LMC and SMC only in the NUV band (Simons et al. 2014). Its angular resolution (5″ PSF) and limiting depth ($m_{\text{NUV}} \sim 21$) is far shallower and coarser than the optical and near-IR imaging. *Swift*/UVOT ($\sim 2.5″$) is limited to $m_{\text{UV}} \sim 19$ for point sources and only available in NUV bands (Hagen et al. 2017). *HST* has the sensitivity and angular resolution in the UV to match (or exceed) modern optical and near-IR LMC and SMC imaging (e.g., Sabbi et al. 2013), but its small FOV makes it unrealistic to survey the entirety of the LMC and SMC. Moreover, *HST* is also limited to NUV wavelengths. Other UV missions, such as *ULTRASAT* (13″ PSF), do not have characteristics that are suitable for resolved stellar populations in the LMC and SMC (e.g., Figure 9).

Spectroscopic surveys of massive stars in the LMC and SMC are far less complete and more heterogeneous than imaging surveys. The largest systematic spectroscopic survey of the LMC is the VLT/Tarantula survey which obtained multi-epoch modest resolution optical spectroscopy of $\sim$800 OB type stars in the Tarantula star-forming region of the LMC (e.g., Evans et al. 2011). Despite including only a single star-forming region and being over a decade old, this survey accounts for the majority of our knowledge of massive star properties (e.g., spectral type, binarity) in the LMC. In the SMC, combined efforts with the VLT and 2DF spectrograph have obtained optical spectra for ~ 300 massive

stars (e.g., Evans et al. 2004, Evans et al. 2006). Other optical spectroscopic efforts are generally smaller and/or focus on specific sub-classes of massive stars.

UV spectroscopy of massive stars in the LMC and SMC is essential for understanding stellar winds of massive stars at sub-Solar metallicity (see Section 3.1.3). However, compared to optical data, UV spectroscopy in the LMC and SMC is sparse. The challenge and expense of obtaining UV spectra at the distances of the LMC and SMC have limited most studies to handfuls of stars per publication. The two most prominent systematic surveys are of R136, the cluster within 30 Doradus in the LMC. Massey & Hunter (1998) acquired UV spectra of 65 stars with *HST*, while Crowther et al. (2016) obtained spectra of 57 OB stars. There are fewer UV spectra of massive stars in the SMC (e.g., Walborn et al. 2000).

Though it has taken tremendous effort to assemble the above, and other, spectroscopic datasets in the LMC and SMC, they only represent a small fraction of the entire massive star content. Estimates place the number of OB type stars in the LMC and SMC at $\sim 30,000$ (based on recent star formation rates, counting resolved stars; e.g., Harris & Zaritsky 2004, Harris & Zaritsky 2009). Of course, progress in understanding metal-poor massive star physics does not require spectra of every possible massive star. But far more are needed than are currently available.

Two ongoing and upcoming efforts stand to, at least partially, remedy the paucity of massive star spectra in the LMC and SMC. The first is from the 4MOST consortium. The 1001MC survey will target several thousand massive stars in the LMC and SMC with low-resolution optical spectroscopy (Cioni et al. 2019). Another 4MOST effort proposes to monitor $\sim 20,000$ massive stars in the LMC and SMC over the course of 5 years with medium-resolution spectroscopy, with the goal of determining binarity through radial velocity variations (Sana & Shenar 2019). 4MOST will be on sky by the mid-2020s. Multi-epoch spectral constraints on binary star characteristics from 4MOST are likely to be too late to guide substantial new *HST* UV spectra in the LMC and SMC. However, 4MOST data will be well-timed relative to *UVEX*, which will uniquely provide the stellar wind measurements.

The second effort is the *Hubble* UV Legacy Library of Young Stars as Essential Standards[3] (ULLYSES; Roman-Duval et al. 2020). This program will combine new and archival *HST* UV spectra in the LMC and SMC to form the first spectral atlas of metal-poor massive stars. This large effort is being accompanied by a VLT survey that will provide high resolution optical spectroscopy for all ULLYSES targets. ULLYSES is the first systematic program targeting UV spectra in the Magellanic Clouds. However, as we discuss in Section 3.1.3, it should be viewed as an important first step of an effort that needs more data.

In an effort to increase number statistics and homogeneity, ULLYSES is an *HST* director's discretionary program that combines new and archival STIS and COS UV spectra of ~ 300 massive stars in the LMC and SMC (Roman-Duval et al. 2020). It will create the first large UV spectral library of sub-Solar-metallicity massive stars. ULLYSES provides an important platform for improving our understanding of winds and mass loss in low-metallicity massive stars. Complementary ground-based optical spectra with the VLT will ensure an exquisite multi-wavelength dataset.

However, even with ~ 300 spectra, ULLYSES will only sparsely sample the upper HR diagram. For single stars, the mass, metallicity, rotation rate, and phase of evolution are considered primary determinants of massive star winds. ULLYSES will sample approximately ten stars for each reasonable permutation of these parameters. The dimensionality and complexity of the problem grows when binarity is included. At least 50% of massive stars are in binaries and the mass ratios and separation, in tandem with single star parameters listed above, can drive winds through mass transfer, Roche lobe overflow, and/or common envelope ejection (e.g., Sana et al. 2012). By design, ULLYSES primarily targets single stars in order to provide benchmarks in absence of additional complexity due to binarity (Roman-Duval et al. 2020).

Given the (i) large variations in wind parameters at fixed stellar property (Section 3.1.3; e.g., Crowther et al. 2016); (ii) importance of binarity to so many stellar end states (e.g., Figure 8); and (iii) the sparse (but substantially improved) sampling provided by ULLYSES, it is imperative to improve the state of UV spectra for low-metallicity massive single and binary stars.

UVEX will substantially expand on the foundation established by ULLYSES. During its two year prime mission, *UVEX* will obtain UV spectroscopy of 1000 OB stars in the LMC and SMC. The high throughput, modest spectral resolution, and broad wavelength coverage of *UVEX* are ideal for filling out areas of the HR diagram in which ULLYSES is known to be sparse, such as binary stars. *UVEX* will provide over three times as many UV spectra as ULLYSES, ensuring the robust statistics needed to quantify variations in stellar wind properties across the HR

---

[3] https://ullyses.stsci.edu

diagram and at fixed stellar parameters (e.g., luminosity, temperature, metallicity). Crucially, it will also provide the UV spectra necessary to establish the link between binary configuration and stellar winds, a connection that is known to be important, but is essentially unconstrained empirically (e.g., Crowther et al. 2016). By the time *UVEX* is on sky, 4MOST will have acquired multi-epoch optical spectral for thousands of massive stars in the LMC and SMC (e.g., Cioni et al. 2019, Sana & Shenar 2019). Spectroscopic targets for *UVEX* will be selected based on a wealth of optical spectra and time series optical and *UVEX* imaging, ensuring *UVEX* spectra covers all relevant stages of single and binary massive star evolution.

C. EXPOSURE TIME ESTIMATES FOR HOT STARS IN THE MAGELLANIC CLOUDS

Here we detail calculations for *UVEX* exposure times needed for measuring wind velocities of stripped and hot, massive stars in the Magellanic Clouds. Though we have simulated observations for a wide variety of stellar types, for brevity, we provide illustrative examples. For these examples, as assume an LMC distance of 50 kpc, the Gordon et al. (2003) extinction curve, an extinction of $E(B - V) = 0.1$ mag (typical of the LMC; Zaritsky et al. 2004), and version `0.2.dev0` of the *UVEX* exposure time calculator (ETC).

C.1. *Stripped Stars*

In order to measure the wind velocity of a stripped star in the LMC, we require SNR ≥ 10 for $F_\lambda = 6 \times 10^{-15}$ erg s^{-1} cm^{-2} Å^{-1} in 3600s at 1240 Å. This estimate is based on a stripped star with a current mass of 2.7 $M_\odot$ ($M_{\text{initial}} = 9M_\odot$) in the LMC, which corresponds to $m_v = 18.5$ mag. The model spectrum used is from the suite of stripped star models published in Götberg et al. (2018).

C.2. *Hot Massive Stars*

We compute the *UVEX* time needed to measure the terminal wind velocity of an 18 $M_\odot$ O-type main sequence star ($T_{\text{eff}} = 3 \times 10^4$ K, $\log(g) = 4.2$ dex, $m_v = 15$ mag) with a modest mass loss-rate of $\dot{M} = 1 \times 10^{-8} M_\odot$ yr^{-1} (or $v_\infty = 2900$ km s^{-1}) and the CMFGEN stellar atmospheres. To accurately recover the terminal velocity, our simulations require a SNR ≥ 10 at 1550 Å, which translates to $F_\lambda = 1.1 \times 10^{-13}$ erg s^{-1} cm^{-2} Å^{-1}. According to the ETC, this requires ~ 50 s of exposure time with *UVEX*.

D. *UVEX* TDE DISCOVERY RATE

Here we calculate the *UVEX* TDE discovery rate. At a typical temperature of 3×10^4 K, we have $L_{\text{UV}}/L_g = 6.0$ in the FUV band which we focus on in the following calculations. Based on the g-band luminosity function measured by van Velzen (2018), we infer the volumetric rate of TDE as a function of UV luminosity L:

$$\frac{d\dot{N}}{dL} = \frac{\dot{N}_0}{L_0} \left(\frac{L}{L_0} \right)^\alpha \tag{D4}$$

where $L_0 = 10^{43}$ erg s^{-1}, $\alpha \approx -2.5$, and $\dot{N}_0 = \frac{\dot{N}_{0,g}}{\ln(10)} \times 6.0^{-(\alpha+1)} \approx 1.2 \times 10^{-6}$ Mpc^{-3} yr^{-1}. The number of detected events per year will be

$$\mathcal{R} = \int_0^{D_{\text{max}}} \Omega D^2 dD \int_{L_{\text{min}}}^{L_{\text{max}}} \frac{dN}{dL_{\text{UV}}} dL_{\text{UV}} \tag{D5a}$$

$$= \frac{\Omega}{3} \frac{\dot{N}_0}{L_0} \int_{L_{\text{min}}}^{L_{\text{max}}} D_{\text{max}}^3 \left(\frac{L}{L_0} \right)^\alpha dL \tag{D5b}$$

where Ω is the solid angle of the surveyed area.

We note that the sample of luminous TDEs is currently poorly characterized – among the 13 TDEs used by van Velzen (2018), only ASASSN-15lh peaked at $> 10^{44}$ erg s^{-1}, and it has distinct spectral properties compared with other events. The shape of the luminosity function at the high end is poorly explored. Therefore, to be conservative, hereafter we only consider the rate of TDEs peaking below 10^{44} erg s^{-1}.

For each L, there is a maximum distance out to which the UV rise of a TDE can be characterized (not just simply detected). We have $4\pi D_{\text{max}}^2 f_{\text{thre}} = L$. Note that the threshold flux, f_{thre}, does not correspond to $f_0 \equiv 0.56 \times 10^{-14}$ erg s^{-1} cm^{-2} at 25 mag (limit magnitude with a 900 s dwell). Instead, we require $f_{\text{thre}} = 10f_0$ to ensure

that the TDEs peak at least 2.5 mag above the survey threshold, such that the light curve UV rise and decay can be well measured. Hence, we have,

$$\mathcal{R} = \frac{\Omega}{3} \frac{\dot{N}_0}{L_0} \int_{L_{\min}}^{10^{44} \, \mathrm{erg \, s}^{-1}} \left(\frac{L}{4\pi f_0 \times 10} \right)^{3/2} \left(\frac{L}{L_0} \right)^{-2.5} \mathrm{d}L \tag{D6}$$

We define a new parameter $x \equiv L/L_0$.

$$\mathcal{R} = \frac{\Omega}{3} \dot{N}_0 \int_{x_{\min}}^{10} \left(\frac{L_0}{4\pi f_0 \times 10} \right)^{3/2} x^{-1} \mathrm{d}x \tag{D7a}$$

$$= \frac{\Omega}{3} \dot{N}_0 (1216 \, \mathrm{Mpc})^3 \times \ln \left(\frac{10}{x_{\min}} \right) \tag{D7b}$$

$$= 2531 \Omega \tag{D7c}$$

where we have assumed $x_{\min} = 10^{42.5} \, \mathrm{erg \, s}^{-1}$ (iPTF16fnl is the faintest and fastest TDE ever discovered, see Blagorodnova et al. 2017). Note that $\mathcal{R}$ does not strongly depend upon $x_{\min}$.

We assume a mission lifetime of 2 years and require that TDEs peak after the first 2 months and before the last 2 months (such that both the rise and decay can be characterized). Therefore, the effective survey period is 1.67 yr. In order to characterize 1000 TDEs (see requirement justified in Section 4.6.5), using Eq. (D7), we have

$$2531 \times \Omega \, \mathrm{yr}^{-1} \times (1.67) \, \mathrm{yr} = 1000 \tag{D8}$$

$$\Omega = 0.24 \mathrm{ster} \tag{D9}$$

The observed fields should be selected to avoid low Galactic latitude, low declination, and regions of high Galactic extinction. The total number of visits per band per field will be $365 \times 2 \times 0.7/25 = 20.5$. The proposed exposure time per dwell is 900 s (simultaneously in FUV and NUV). We assume that a given field is visible to *UVEX* for 70% of the survey time (due to Sun constraint, etc). Thus, the surveyed solid angle should be $0.24/0.7 = 0.34$ ster, corresponding to $1200 \, \mathrm{deg}^2$ (≈ 110 *UVEX* fields). Taken together, such an imaging survey would cost 3–4% of the total *UVEX* baseline mission time.

E. *UVEX* GW EVENT RATES AND LIGHT CURVE MODELS

E.1. *Event Rates*

Currently, the LIGO-Virgo-KAGRA GW interferometers are fully funded for a fifth observing run (O5) in 2025–2026 (Abbott et al. 2020a). The sixth observing run (O6) is expected to be 18–24 months in duration in the years 2028–2029, and will overlap with *UVEX*. In addition to LIGO Hanford, LIGO Livingston, Virgo and KAGRA, the LIGO India interferometer is also expected to join the O6 run (Abbott et al. 2020a).

We undertake a detailed end-to-end simulation of the GW network performance to quantify *UVEX* measurement requirements. Our simulation assumes that all five interferometers are active in O6, but only at the funded A+ sensitivity, each with a duty cycle of 70%. The methodology is similar to that described in Petrov et al. 2021, updated to reflect population modeling results from the most recent GW transient catalog through the end of O3, GWTC-3. Fig. 7 of the GWTC-3 paper (The LIGO Scientific Collaboration et al. 2021a) shows that the data currently support a fairly broad and flat NS mass distribution. Therefore, we adopted a distribution that is uniform from 1 to 2 $M_\odot$. We use the GWTC-2 rate estimate of $R_{\mathrm{BNS}} = 320^{+490}_{-240} \, \mathrm{Gpc}^{-3} \mathrm{yr}^{-1}$ (The LIGO Scientific Collaboration et al. 2021b) as it is quoted for a uniform mass distribution consistent with what we learned from GWTC-3.

From this sample of simulated BNS mergers in O6, we select only those targets that are localized to better than $100 \, \mathrm{deg}^2$. We then determine the necessary exposure times and tiling scheme to map 90% of the enclosed probability while meeting our astrophysical requirements. Our goal is to achieve the depth necessary to detect and characterize a kilonova regardless of which model is dominant (see Section E.2 below). Thus we choose a conservative peak FUV absolute magnitude of –12.1 mag, which corresponds to an apparent magnitude of 24.4 mag at 200 Mpc (Figure 43). We use the *UVEX* ETC to estimate the required exposure time for each event depending on the distance to the source and the UV background at that simulated location. For the selected events, the estimated required exposure time varied between 500 s and 5,250 s (with a median of 1080 s).

GW events are selected as observable by *UVEX* if their entire 90% localization region can be observed to the required depth within 10 ks (Figure 42). As a result of this analysis, $\sim 2.8\%$ of the events satisfy the localization, tiling, and exposure time criteria. Of these, 53% are fully within the *UVEX* field-of-regard (accounting for sun exclusion). We conclude that 35 ToO triggers are expected to pass our selection criterion during the 18 months of the GW O6 run (20 ToO triggers would pass our selection criterion using the O5 configuration).

E.2. *Light Curve Models*

Early kilonova data do not yet exist in the UV, hence we calculate light curves for a GW170817-like event for three possible models powering the UV transient at early times.

1. The first is a semi-analytical, nucleosynthesis-powered model (Hotokezaka & Nakar 2020; also, Li & Paczyński 1998, Metzger et al. 2010), where the radiation is purely generated by radioactive decay of r-process nuclei. The model is described by 7 parameters: the mass of the ejecta (M_{ej}), the minimum and maximum velocity of the ejected material (v_{min}, v_{max}), the transition velocity between low and high opacity κ (v_{κ}), the effective grey opacity for $v \leq v_{\kappa}$ and $v > v_{\kappa}$ (κ_{low}, κ_{high}), and the power law index of the velocity distribution across the mass space (n).

2. The second model is a shock-powered analytical prescription (Piro & Kollmeier 2018), where the kilonova is powered through shock-cooling of material surrounding the merger remnant, that has been heated by a jet depositing energy into the material. It is described by four parameters, the mass of the shock-heated material (M_{sh}), the minimum velocity of the material (v_{sh}), the initial radius of the material (R_0) and the opacity of the material (κ_{sh}).

3. For the third model we use predictions that, on top of the nucleosynthesis-powered model, there is additional radiation coming from the β-decay of free neutrons that have not been captured by nuclei through r-process (Metzger et al. 2015), with a total mass of $M_{\mathrm{fn}} = 10^{-4} M_{\odot}$. This model is only considered in combination with the nucleosynthesis-powered model, and only affects the very early behavior of the light curve ($t \leq 6$h).

In Table 3 we summarize the parameters for the models, and indicate the ranges within which these parameters can vary, noting that the free neutron model is fixed. Within these ranges, 90% of the peak absolute magnitude lies between $[-15.6, -12.4]$ ($[-14.5, -10.2]$) for the nucleosynthesis powered model and $[-17.8, -15.3]$ ($[-17.9, -15.0]$) for the shock-powered model in the NUV (FUV) band. In Figure 43 we show the apparent AB magnitude of all three models in the two *UVEX* filter bands, for a GW170817-like event at a distance of 200 Mpc, calculated with the fiducial model parameters from Table 3. The cadence, 10,000 seconds, is determined by the amount of tiles needed to map the localization area as estimated from the GW analysis, for which we take a fiducial value of $100 \deg^2$, and a 1,000s exposure time.

Based on the model light curves, especially the fast fading shock-model and neutron-precursor model, our goal is for *UVEX* to respond within 3 hours on average for BNS/NS–BH events. Once *UVEX* is on target, it will map the localization area and repeat the sequence for 24 hours. The median number of tiles per event will be 5. Thus, a median of 17 epochs in the *UVEX* light curve is expected.

These results demonstrate that *UVEX* will generate high-SNR, well-sampled light curves in both FUV and NUV bands for all selected events in the O6 simulation, even in the more pessimistic case where the early UV emission is powered entirely by heavy-element nucleosynthesis.
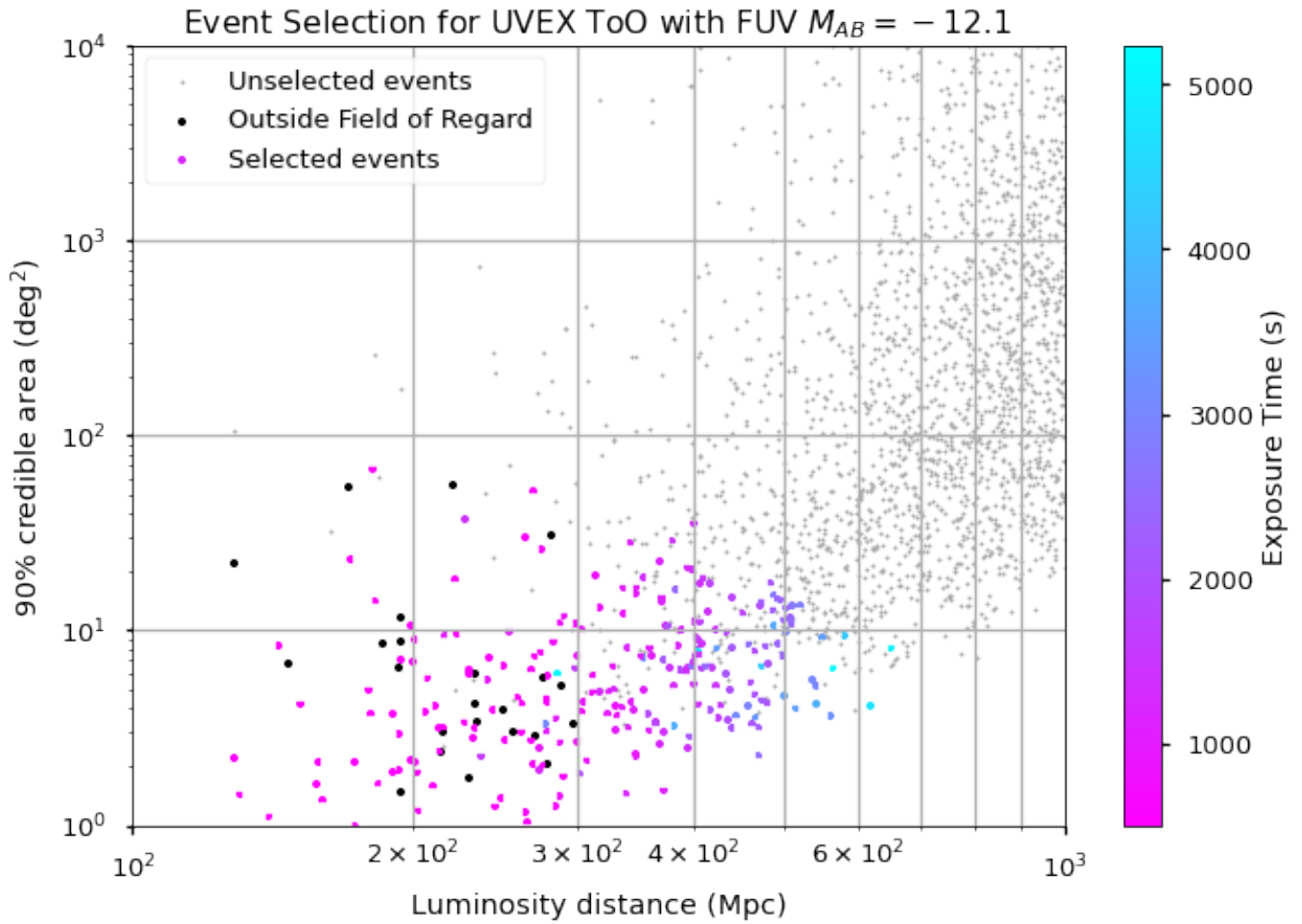
Figure 42. Simulation of GW triggers in the LIGO-Virgo-KAGRA sixth observing run (O6). The y-axis shows the 90% credible area and the x-axis shows the luminosity distance. Only those events with a credible area $<100 \, \mathrm{deg}^2$ and distance such that a depth of -12.1 mag can be achieved in each pointing will be selected; selected events are color-coded by the optimal exposure time per the *UVEX* ETC. Events that fall outside the *UVEX* field of regard are excluded and denoted as black points. (Note that the number of points in the simulation shown above is proportional to the number of predicted events in O6 but this scaling is not 1:1.)
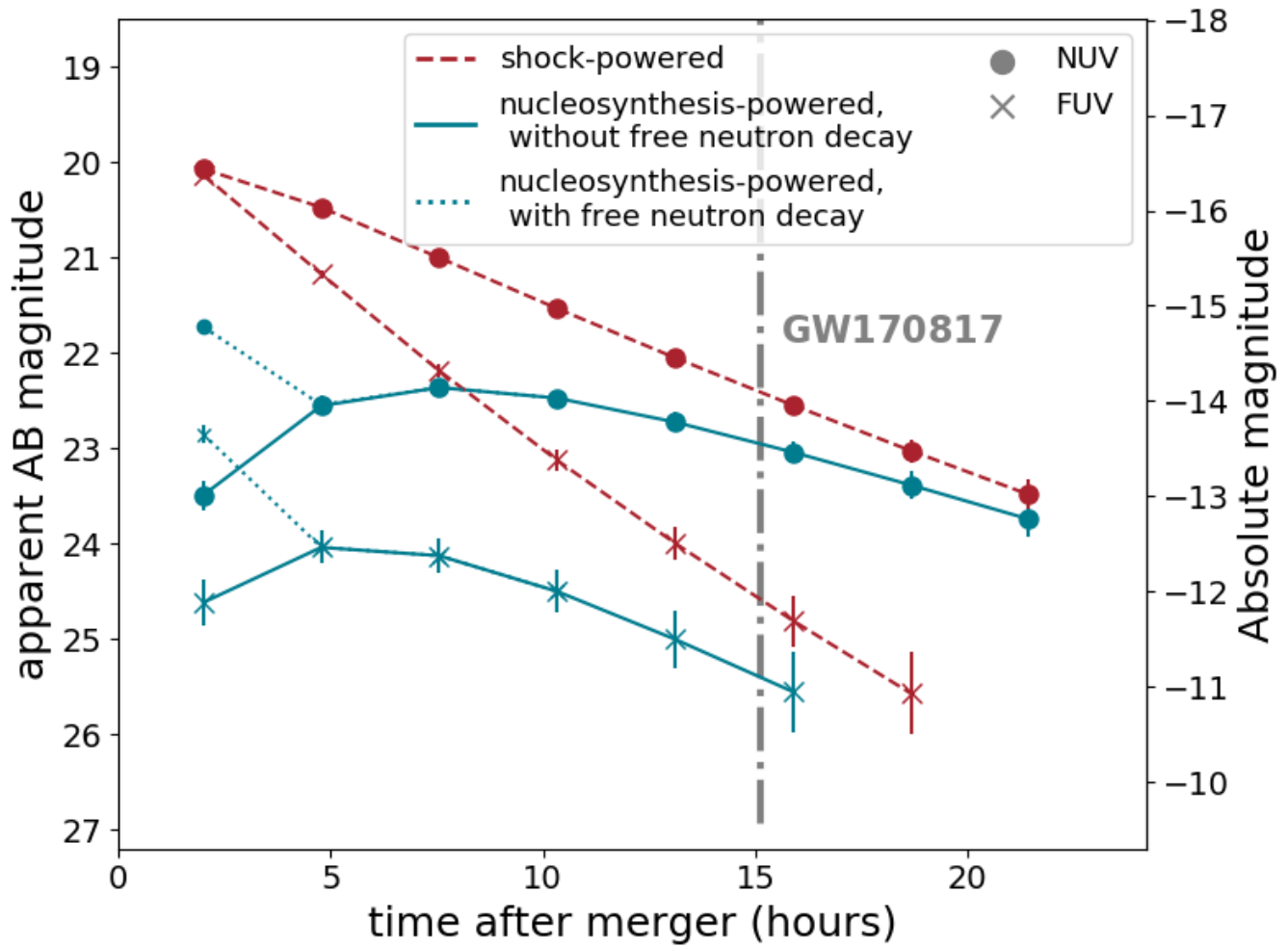
Figure 43. UV light curve predictions for a shock-powered model (dashed), and a nucleosynthesis-powered model with (dotted) and without (solid) a free neutron decay component. This light curve assumes a distance of 200 Mpc, exposure time of 1000 s and cadence of 10,000 s (due to ten tiles needed to map the localization area). Note that 24.4 mag at 200 Mpc corresponds to an absolute magnitude of -12.1 mag, which means that the targeted *UVEX* depth of -12.1 mag is sensitive to all models in both filters.

Table 3. The parameters describing the nucleosynthesis-powered and shock-powered models in neutron star mergers, with the allowed ranges within each parameter can vary. The fiducial values are the values used to generate the data in Figure 43.

Parameter (Unit)	Description	Range	Fiducial value
Nucleosynthesis Powered Model			
M_{ej} ($M_{\odot}$)	Ejecta mass	(0.01, 0.1)	0.05
v_{min} (c)	Minimum ejecta velocity	(0.05, 0.2)	0.1
v_{max} (c)	Maximum ejecta velocity	(0.3, 0.8)	0.4
n_{ej}	Power law index of ejecta density distribution	(3.5, 5)	4.5
v_{κ} (c)	Transition velocity between high and low κ	(v_{min}, v_{max})	0.2
κ_{high} (cm^2 g^{-1})	Effective grey opacity for $v \leq v_{\kappa}$	(1, 10)	3
κ_{low} (cm^2 g^{-1})	Effective grey opacity for $v \geq v_{\kappa}$	(0.1, 1)	0.5
M_{fn} ($M_{\odot}$)	Free neutron mass	-	10^{-4}
Shock Interaction Powered Model			
M_{sh} ($M_{\odot}$)	Shocked ejecta mass	(0.005, 0.05)	0.01
v_{sh}(c)	Shocked ejecta velocity	(0.1, 0.3)	0.2
R_0 (10^{10} cm)	Initial shock radius	(1, 10)	5
κ_{sh} (cm^2 g^{-1})	Effective grey opacity of shocked ejecta	(0.1, 1)	0.5